CRANFIELD UNIVERSITY

YIFEI ZHAO

A CNC MACHINE GUIDERAIL WEAR IN-PROCESS MONITORING SYSTEM

SCHOOL OF AEROSPACE, TRANSPORT AND MANUFACTURING

MSc by Research

MSc THESIS

Academic Year: 2015-2016

Supervisor: Dr Jörn Mehnen, Dr Konstantinos Salonitis

September 2016

CRANFIELD UNIVERSITY

SCHOOL OF AEROSPACE, TRANSPORT AND MANUFACTURING
MSc by Research

MSc THESIS

Academic Year 2015 -2016

YIFEI ZHAO

A CNC MACHINE GUIDERAIL WEAR IN-PROCESS MONITORING SYSTEM

Supervisor: Dr Jörn Mehnen, Dr Konstantinos Salonitis
September 2016

This thesis is submitted in partial fulfilment of the requirements for the degree of Master of Science

ABSTRACT

This research investigates and establishes a system for monitoring the guiderail wear on medium size CNC machines. The system possesses the function of measuring the wear state on guiderails in an in-process way, which is more functional and efficient than the traditional method.

In this research, two different types of sensors for monitoring each particular friction wear feature have been implemented. Calculations to complete designing of a physical experimental rig and the realisation of in-process monitoring are also discussed in detail.

The first type sensor adopted in the experiment is the accelerometer, used for monitoring the vibration caused by the wear on bearings and the increasing roughness on the guiderail surface. The second sensor is the capacitance probe mounted on the table and against a straight edge, searching the deviation signal of the moving table while rolling on the guiderail surface with wear.

The novelty of this thesis covering an in-process monitoring approach has been tested based on a physical experimental rig. The data calculation illustrates how the noise and other disturbances are filtered and data analysed to determine the state of wear. This system utilises an indirect solution to wear monitoring with less cost while delivering convincing reliability according to the experiment result. The thesis shows the possibility to acquire CNC machine guiderail wear data through an in-process monitoring system.

Keywords:

CNC machine, guiderail, friction fatigue wear, in-process, sensor, experiment rig, acceleration, vibration, noise.

ACKNOWLEDGEMENTS

I would like to express my gratitude to my supervisors, Dr Jörn Mehnen and Dr Konstantinos Salonitis, for their diligent guidance all through the year. I am also very grateful to my subject advisor Dr Andrew Starr for his valuable suggestions and support during the research.

Thanks to the staff in Tes Studio Laboratory, Luke Okay, Stefano Tedeschi and Pavan Addepalli who support my preparation of the experiment, especially Dr Cristobal who wholeheartedly help me with the system building up. Also thanks to the staff in Precision Machining Centre, Paul Morantz, Dr Paul Comley, Dr Xavier Tonnellier Dr Jonathan Abir and Dr Nan Yu who help me with the experiment design and implementation in the thermostatic laboratory. Thanks to my colleagues Mr Yu Zhuang, Mr Dingjie Duan and Mr Tao Lei from COMAC, with their support and great patient. Meanwhile, thanks to Gabrijel Persin's valuable suggestions while I was stocked in the middle and Dr Qi Zhang's great help in the critical moment of my final review.

Furthermore, I would like to thank Mr Gao, the senior engineer in AVIC and Professor Zhang in Bristol University, also Dr Ning Fang in GE, USA. Their valuable suggestions were a great help to my project.

I am also grateful to my English teacher Joanne Holden for her precious suggestions in writing skills.

Special thanks should go to my sponsor, Commercial Aircraft Corporation of China (COMAC) and China Scholarship Council for their financial support.

TABLE OF CONTENTS

ABSTRACT i
ACKNOWLEDGEMENTS 3
LIST OF FIGURES 7
LIST OF TABLES 12
1 INTRODUCTION 13
2 LITERATURE REVIEW 16
2.1 CNC Machine 16
2.1.1 Fundamental Structure of CNC Machine 16
2.1.2 Coordinate System of CNC Machine 17
2.1.3 CNC Machine Categorisation 18
2.2 Guiderail Categorisation 22
2.2.1 Categorisation of the Guiderail by Tribological Mechanism on Friction Surface 22
2.2.2 Categorisation of the Guiderail by Cross-section Shapes 25
2.3 Guiderail Accuracy 27
2.4 Wear categorisation 31
2.5 Friction Fatigue Wear 35
2.5.1 Tribological Mechanism and Properties 35
2.5.2 Static/Kinetic Friction and the Friction Coefficient 36
2.5.3 Effects of Friction Wear 37
2.6 Monitoring Solutions 38
2.6.1 Interferometer 39
2.6.2 Cylindrical Square and Dial Gauge 40
2.6.3 Dial Gauge with Digital Data Output 40
2.6.4 Laser Tracker 41
2.6.5 Gradienter 41
2.6.6 Optical Autocollimator 42
2.6.7 Capacitance Probe 42
2.7 In-process Monitoring Solution 43
2.7.1 Definition of In-process Monitoring 43
2.7.2 State-of-art of the In-process Monitoring Technology 43
2.7.3 Guiderail Wear In-process Applicable Solutions Study 45
2.8 Geometrical error budget 45
2.9 Summary 47
2.9.1 Study Object Selection 47
2.9.2 Research Approach Discussion 49
2.9.3 Requirement 50
3 AIM AND OBJECTIVES 53
3.1 Aim 53

3.2 Objectives 53
4 METHODOLOGY 54
5 DESIGN OF THE EXPERIMENT 58
5.1 Introduction 58
5.2 Monitoring Objects and Approaches Settling 59
5.2.1 Friction Wear Symptoms 59
5.2.2 Corresponding monitoring solution 60
5.3 Physical Experiment Rig Design and Build up 61
5.3.1 Guiderail, Ball Bearing and Ball Screw 61
5.3.2 Drive System 67
5.3.3 Linear Position Monitoring System 73
5.3.4 Wear Monitoring System 78
5.4 In-process Monitoring realisation 88
5.4.1 Design Consideration 88
5.4.2 Data Acquisition and Analysis 88
5.4.3 System Component Parameters 90
5.5 Experiment & Validation 90
5.5.1 Error Budget 90
5.5.2 Experiment Plan 93
6 VALIDATION RESULT DISCUSSION 120
6.1 Original Data Processing and Analysis 120
6.2 System Repeatability Test 121
6.2.1 Vibration Monitoring Repeatability Test 121
6.2.2 Smooth Curve Monitoring Repeatability Test 123
6.2.3 Conclusion of Repeatability Test 126
6.3 Wear In-process Monitoring Test 127
6.3.1 Synchronising In-process Test 128
6.3.2 Wear Symptom (1): Non-smooth Behaviour Monitoring Test 129
6.3.3 Wear Symptom (2): Smooth Curve Increase Monitoring Test 131
6.3.4 Wear Symptom (3): Small Range Vibration Monitoring Test 133
6.3.5 In-process Monitoring Performance Conclusion 133
7 CONCLUSION 136
7.1 The Categorisation to the CNC Machine Guiderail wear 136
7.2 Requirement of the Project 136
7.3 Designing of the Rig and the Experiment Process 136
7.4 Contribution to New Knowledge: In-process Monitoring Approach 136
8 DIRECTION OF FUTURE WORK 138
8.1 Improvement of Repeatability 138
8.2 Test of Reproducibility 138
8.3 Improvement to the range of application 138
8.3.1 Applicability to different types of CNC machine 139
8.3.2 Applicability to different types of guiderail 139

8.3.3 Applicability to other types of machine wear 139
REFERENCES 141

LIST OF FIGURES

Figure 2-1 CNC Machine Inner Structure (Leonardo et al., 2010) 17

Figure 2-2 Coordinate system of a CNC mill (Leonardo et al., 2010) 18

Figure 2-3 Coordinate system (with 6 degrees of freedom) (Leonardo et al., 2010) 18

Figure 2-4 Typical gantry manufactured by FERMAT Company (Besharati, et al., 2016). 19

Figure 2-5 Typical knee milling machine manufactured by Atrump (Danford, Matthew, 2007) 20

Figure 2-6 C-frame CNC machine manufactured by HURON (Technical documentation, 2010) 21

Figure 2-7 Turret milling machine manufactured by Star CNC machine tool Corp (Star, 2011) 22

Figure 2-8 Typical structure of the aerostatic guiderails (Sutar, 2013). 23

Figure 2-9 Typical structure of the hydrostatic guiderail and oil pump (Sutar, 2013). 24

Figure 2-10 Typical structure of the rolling guiderail with rolling balls in between the slide and support to reduce friction (Sutar, 2013). 24

Figure 2-11 Circular Guiderail (Wei, 2010) 26

Figure 2-12 Triangle Guiderail (Wei, 2010) 26

Figure 2-13 Rectangular Guiderail (Wei, 2010) 26

Figure 2-14 Dovetail Guiderail (Wei, 2010) 26

Figure 2-15 Multiplex Guiderail (Wei, 2010) 27

Figure 2-16 Guide way configuration (bottom side); (a) detailed model, (b) simplified model, and (c) model FEM (Majda, 2012) 29

Figure 2-17 Characteristics of joint kinematic errors variant (FEM calculation) (Majda, 2012) 30

Figure 2-18 Friction fatigue wear on the round guiderail (Bremer, 2014) .. 31

Figure 2-19 View of grinding abrasive wear (Fitch, 2013) 32

Figure 2-20 Corrosive wear on the shaft surface (Waterhouse, 1972) 33

Figure 2-21 The fretting wear on the guide rail surface (Brosend, 2012) .. 34

Figure 2-22 Scanning electron micrograph of fretting damage on the aluminium X54 (Brosend, 2012) 34

Figure 2-23 Module of rolling friction (Yanqing, 2015). 37

Figure 2-24 Optical mechanism of interferometer (Leach, Flack, Hughes, & Jones, 2009) 39

Figure 2-25 Laser tracker with a platform (Kong, 2012) 41

Figure 2-26 Typical Optical autocollimator (the reflection part) (Mross, 2015) 42

Figure 2-27 Applying a voltage to conductive objects (Lion, 2015) 43

Figure 2-28 Geometrical principle of the in-situ measuring mechanism (Bosetti and Bruschi, 2010) 44

Figure 2-29 Demonstration of pin chasing grinding in an oscillating grinding machine (Bosetti and Bruschi, 2010) 44

Figure 2-30 The deviant motions of a guiderail (**Kong, 2012**) 46

Figure 2-31 CNC machine categorisation 47

Figure 2-32 CNC machine guiderail categorisation 48

Figure 4-1 Research methodology 54

Figure 4-2 Mind map of the Project 56

Figure 5-1 The structure of the experiment design and validation 58

Figure 5-2 The symptoms caused by friction wear 60

Figure 5-3 Configuration of the guiderail and ball screw 62

Figure 5-4 Configuration of the ball bearings 63

Figure 5-5 The deviation to the parallelism of the guiderail shafts and the ball screw 63

Figure 5-6 The frame built up for the rolling system 64

Figure 5-7 The cross section of the frame material (aluminium) 64

Figure 5-8 The frame and the rolling system equipped part 1 65

Figure 5-9 The frame and the rolling system equipped part 2 65

Figure 5-10 Top View of the Rig with Stepper Motor 69

Figure 5-11 Side View of the Rig with Stepper Motor 70

Figure 5-12 Wiring Graph of the Motor Controller 72

Figure 5-13 Mechanism of the Inductive sensor (Hydraulics & Pneumatics, 2012) 74

Figure 5-14 Mechanism of LVDTs (Hydraulics & Pneumatics, 2012) 74

Figure 5-15 Mechanism of Resistive sensor (Hydraulics & Pneumatics, 2012) 75
Figure 5-16 Three behaviour modes of the rolling table (Kong, 2012)..... 80
Figure 5-17 Rolling behavior of the Capacitance and Stand Arm 81
Figure 5-18 Angle and Height of the Deviation 81
Figure 5-19 Data transferring sequence 82
Figure 5-20 LABVIEW Data Acquisition Sequence..... 83
Figure 5-21 "π" shape stand arm FEM simulation result 85
Figure 5-22 "L" shape stand arm FEM simulation result..... 85
Figure 5-23 "T" shape stand arm FEM simulation result..... 85
Figure 5-24 Side look of the capacitance probe and the straight edge (1) 87
Figure 5-25 Side look of the capacitance probe and the straight edge (1) 87
Figure 5-26 The 2D drawing of the experiment rig 89
Figure 5-27 In-process data processing sequence 89
Figure 5-28 Experiment Structure..... 94
Figure 5-29 The Rig Base..... 95
Figure 5-30 Top view of the rig..... 96
Figure 5-31 Side view on X direction 96
Figure 5-32 Side view on Y direction 97
Figure 5-33 Upward view of the rig 97
Figure 5-34 Assembly of Stepper Motor..... 98
Figure 5-35 Assembly of Linear Sensor 98
Figure 5-36 Assembly of Straight Edge..... 99
Figure 5-37 Relative Position of Straight and the Rig 99
Figure 5-38 Assembly of Capacitance Probes and Stand Arms 100
Figure 5-39 Assembly of Accelerometer 100
Figure 5-40 Relative Positions of sensors and the Rig 101
Figure 5-41 Angle of the arm on YZ plane..... 102
Figure 5-42 Angle of the arm on XY plane..... 102
Figure 5-43 Relative Moving Direction of the Straight Edge and Sensor 103

Figure 5-44 Relative Deviation of the Straight Edge 103

Figure 5-45 Assembly Points of the Linear Position Sensor 105

Figure 5-46 Assembly of Accelerometers 106

Figure 5-47 Complete Experimental Rig 107

Figure 5-48 Complete Experimental Rig 2 108

Figure 5-49 Complete Experimental Rig (with Sensors and the Straight Edge) 108

Figure 5-50 Striking Point to the Rig 110

Figure 5-51 Striking Point to the Rig 2 111

Figure 5-52 Relative Position of Components (with wear on) 113

Figure 5-53 Relative Position of Components (with wear on) 2 113

Figure 5-54 Marking the Wear Position 114

Figure 5-55 Side View of the Smooth Curve Wear 115

Figure 5-56 Guide rail and Ball Bearing Cross-section Figure 115

Figure 5-57 Approach to the Wear of Balls 116

Figure 5-58 Capacitance Sensor No.1 and No.2 118

Figure 5-59 The whole rig system after completing the assembly 119

Figure 5-60 Shafts from No.1 to Nop.4 as the test examples 119

Figure 6-1 The experimental group 120

Figure 6-2 The original data whole length 121

Figure 6-3 Accelerometer Dynamic, Static and the Difference Signals ... 122

Figure 6-4 Result of the Difference on Average 122

Figure 6-5 Percentage of Difference between di and av 123

Figure 6-6 The signal of two capacitance probe sensors and the difference (Unit of the X axis is mm, unit to the Y axis is Voltage) 124

Figure 6-7 Average of difference 125

Figure 6-8 difference to the average 126

Figure 6-9 Signals from two sensors in the same sampling frequency .. 128

Figure 6-10 Percentage of the static and dynamic sensors' difference .. 129

Figure 6-11 Wear Changes $Uwc2$ 130

Figure 6-12 Wear Changes Uwc3 131
Figure 6-13 Wear Changes Uwp2 132
Figure 6-14 Wear Changes Uwp3 132
Figure 6-15 Wear Changes Uwp4 133

LIST OF TABLES

Table 2-1 Comparative characteristics of Rolling and Sliding Guideway (Sutar, 2013) 25

Table 2-2 Effect of Wear to each Component 49

Table 2-3 Requirement of the Project 51

Table 5-1 Effects and Symptoms 59

Table 5-2 Parameters of the components 62

Table 5-3 Comparison Result 69

Table 5-4 Selection to the 1D positioning sensor with requirement 76

Table 5-5 Parameters of the potentiometer 77

Table 5-6 Accelerometer Parameters 83

Table 5-7 Capacitance Probe Parameters 84

Table 5-8 Error Budget 90

Table 5-9 List of Components 95

Table 5-10 Emery Paper Parameters 112

Table 5-11 Data Acquisition Process 118

1 INTRODUCTION

The initial aim of the project is to establish a novel monitoring system to measure the wear state of guiderail in an in-process manner. Over the last decade, several measuring systems to assess the wear of different components of CNC machine have been developed (Tan, Zhang, & Hu, 2015). The further facility performance improvement has taken advantage from the monitoring systems. In this study, the feature of the system is high resolution (reaches to micrometre level, which is correspondent to the manufacturing accuracy of the widely utilised CNC machine types, for example, turret mill and knee/knee-and-column) and with an efficient method of monitoring the guiderail on CNC machine without dismantling any device component.

Presently, the widely applied CNC machine guiderail wear measuring solution in the manufacturing industry is regular inspection. The most common maintenance periods presently adopted in the manufacturing industry is six months or 12 months (Giourntas, Hodgkiess, & Galloway, 2015). The length of this maintenance period is arranged by CNC machine suppliers with the summary of long-term hands-on experience. The major solutions utilised in the wear inspection to the straightness of machine components are: using optical equipment, a gradienter or a dial gauge (Leach, Flack, Hughes, & Jones, 2009).

The optical instrument usually uses laser tracker, an optical autocollimator and an interferometer. These apparatus come with high resolution and accuracy, also with strict assembly design and fast responding speed to signal. However, since the typical optical equipment contains two main parts which are laser ejector and reflector, the equipment is with high cost and large scale. Also, if applying the optical instrument into in-process or dynamic monitoring system, the fallacy of insufficient resistance to outside disturbance would be obvious (Kong, 2012). For instance, particles or spraying of coolant would affect the performance of optical instruments.

The gradienter is attached to a transit's telescope which allows the angle of inclined measuring via deviance of a bubble. This instrument features flexibility

and convenience but low resolution. Firstly, the resolution of the equipment (on millimetre level) does not fit the requirement of CNC machine monitoring which involves a micrometre level. Secondly, the recording to the data of deviance is difficult to the user.

The dial gauge is one of the most common tools in every industry. It has the resolution of micrometre level and is easy to be equipped. The cost is relatively low compared to optical instruments. Therefore, with proper design, the monitoring system which with dial gauges would meet the requirement of static measurement.

The main restriction of current wear monitoring systems is that they can be used only during the idle time of the CNC machine. This method needs the disassembly of the machine to its components and the avoiding of outer disturbance as preconditions. After that, the further reassembly and calibrating work are involved after the inspection is finished.

Those systems considering in-process monitoring and analysis to the data are still lacking investigation. In this case, comparing with traditional monitoring methods, the in-process monitoring solution is with significant advantages on convenience and cost saving. The aim of this research is to develop a quick, easy-to-use and cost-efficient method to assess the wear of CNC machine guiderails.

To realise the in-process monitoring function, realising measurement without suffering interruptions from the running of the machine is of importance. Thus, an idea from electronic signal processing is brought in. It is adopting the signal of disturbance and realising the offset to the data of wear monitoring. To achieve this goal, the traditional high-resolution gauging equipment, dial gauge, has been adopted in order to meet the requirement of micrometre level resolution. However, the common mechanical dial gauge has the disadvantage of not being able to transmit and transfer the digital signals. Therefore, a new type of dial gauge with the function of a digital data output is applied.

The CNC machine tool is widely utilised in the precision machining industry. The guiderail is a crucial and fundamental component of a machine tool and the wear of it can have a significant impact on the precision. In this study, the circular guiderail with rolling bearing is selected as the study object. Comparing with sliding guiderail, the rolling guiderail also has better tribology properties and causes less wear. With such reason, the type of guiderail represents the mainstream of the CNC machine guiderail configuration. (Besharati, et al., 2016)

According to the literature study of typical CNC machine guiderail wear and the state-of-the-art to the metallic material tribological characteristics study, the majority of wear on rolling guiderail is friction fatigue wear (Sutar, 2013). Thus in this research, the mechanism, effects and symptoms brought by the wear would be studied and taken as the measuring object.

The aim of the thesis is developing an in-process monitoring method to improve the CNC machine guiderail wear monitoring approach, which with systematic verification process. Comparing with the present method utilised in manufacturing industry, implementation of such advanced method suggests a promising future of efficient monitoring method improving.

2 LITERATURE REVIEW

A literature review is presented for the purpose of investigating the state-of-the-art for wear monitoring in CNC machine tools, particular on the critical component – the guide rail. The literature review includes types of guiderails which are widely implemented, major degradation which impacts the performance of CNC machines in processing and the applicable solutions to achieve monitoring the wear effectively. The scope of the study, the rationale for choices to further research and requirement are illustrated and analysed in the summary of the literature review.

2.1 CNC Machine

The Computer Numerical Control (CNC) machine is the type of instrument whose operations are numerically directed by the computer control system, taking advantage of command instructions in a specifically created program. The instructions for commanded operations are written in the program in the form of alphanumerical symbols. The program is given for the direction of the force components of a machine and it ensures the process of making parts (Leonardo et al., 2010). Comparing with traditional manual milling machine, CNC machine operation requires higher level technique to operators. However, utilising the CNC machine in the manufacturing industry may bring high resolution and accuracy. High precision CNC machines can reach the precision of several nano-metre levels (BSI, 2014).

2.1.1 Fundamental Structure of CNC Machine

The typical structure of a CNC machine acquires three main blocks as can be seen in **Figure 2-1**:

(1) Computer Control System: It contains an operation system and application NC program producing software. The input of the program can be multiple, making the program in advance and transferring it to the control system of the CNC machine is applicable. The computing system unit follows by controlling circuits, which directly control the components of the CNC machine through converted high-tension electrical signals.

(2) Adjusting Circuit: the adjusting circuit is used to guarantee the correct position of each crucial working component.

(3) Implementation of components: within the processing, the workpiece is mainly operated by the machine tools mounted on a spindle, clamps on the moving table used to firmly hold the workpiece and the guiderail in multiple directions to precisely allocate the workpiece.

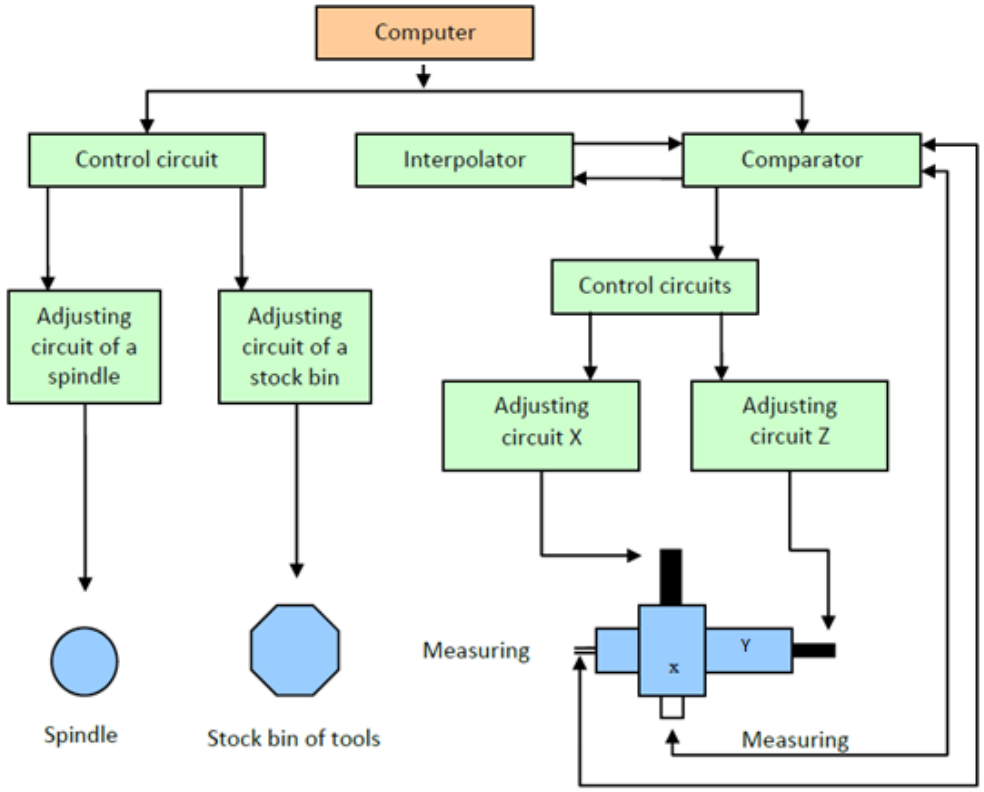

Figure 2-1 CNC Machine Internal Structure (Leonardo et al., 2010)

2.1.2 Coordinate System of CNC Machine

Theoretically, there are six degrees of freedom to the motions of CNC machine (as can be seen in **Figure 2-2** and **Figure 2-3**). Those are three linear axes (X, Y and Z) and three rotational axes (A, B and C) (Nanfara et al., 2002).

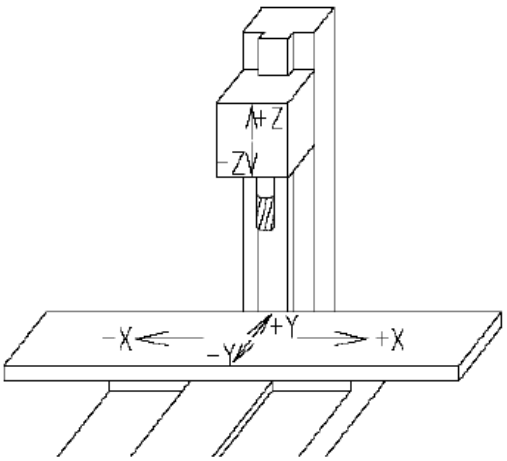

Figure 2-2 Coordinate system of a CNC mill (Leonardo et al., 2010)

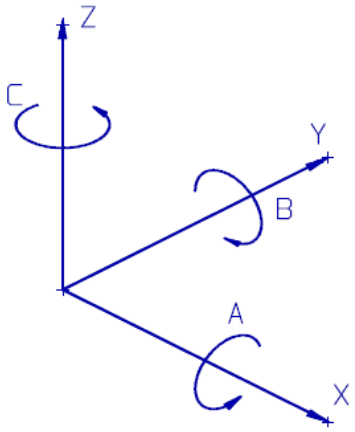

Figure 2-3 Coordinate system (with 6 degrees of freedom) (Leonardo et al., 2010)

2.1.3 CNC Machine Categorisation

Since the CNC machine has developed, there are many types of CNC machines present in the industries for parts manufacture. Presently, a large number of CNC machine tools are used for multiple operations simultaneously. There are also other types of CNC machines invented for the special purposes.

The categorisation of machine tools is necessary to narrow down the research area. According to the machine size and the field applied, the typical types of CNC machine tools are the following:

2.1.3.1 Gantry Milling Machine

The configuration of the gantry milling machine can be a spanning framework with various shapes. It is a structure that bridges over the working table with several cranes (Besharati, et al., 2016). The gantry milling machine can be very large (**Figure 2-4**) and is mainly utilised in rough milling.

Figure 2-4 Typical gantry manufactured by FERMAT Company (Besharati, et al., 2016).

2.1.3.2 Knee Mill/Knee-and-Column Milling Machine

A knee-and-column milling machine can be used for a wide range of milling operations. Such type of milling machines are one of the most common milling machines, as shown in **Figure 2-5**. The spindle and the milling cutter could be either horizontal (slab milling) or vertical (face and end milling) (Danford, Matthew, 2007).

Figure 2-5 Typical knee milling machine manufactured by Atrump (Danford, Matthew, 2007)

2.1.3.3 Floor Milling Machine

The floor milling machine is the super-heavy-duty CNC floor type boring-milling machine. It is assumed as a general machine tool for large part machining (Wu, 2012). It has been widely applied in fields such as aviation, aerospace, energy, metallurgy, transportation and ship.

2.1.3.4 C-frame Milling Machine

The CNC C-frame milling machine is the middle-size to gigantic size machine with relatively high horse power. Comparing with other types of CNC machine, the “C” structure of the machine (as can be seen in **Figure 2-6**) has the advantage of rigidity and stability since closed structural loops can bring more stiffness and accuracy than Long-open structural loops (Slocum, 2012).

Figure 2-6 C-frame CNC machine manufactured by HURON (Technical documentation, 2010)

2.1.3.5 Box Milling Machine

Box milling machines are with rigid and space saving structure that used for milling small size work piece. The type of machine majorly utilised in small work piece manufacturing or hobby workshop.

2.1.3.6 Turret Milling Machine

The CNC turret machine can be applied to different manufacturing areas. It is one type of the medium-size CNC machine (as can be seen in **Figure 2-7**) with multiple functions. It acquires the feature of flexible moving angles and linear behaviour without losing resolution (Star, 2011).

Figure 2-7 Turret milling machine manufactured by Star CNC machine tool Corp (Star, 2011)

2.1.3.7 Bed Milling Machine

The major feature of CNC Bed milling machine is it owns stable structure and has better invulnerability to disturbance (BSI, 2012). It is another type of large size machine which is provided with hardened and ground box ways as well as hardened and ground table surfaces for accurate machining.

2.2 Guiderail Categorisation

The resolution of CNC machine manufacturing will typically reach micrometres. Highly advanced machines can even achieve nanometre levels (BSI, 2014). The accuracy of implementing components is critical to the performance of the CNC machine. The guiderail is a fundamental component and its motion error affects machining accuracy directly (Deng, 2015). The study of guiderail types with different friction mechanisms is fundamental to this research.

2.2.1 Categorisation of the Guiderail by Tribological Mechanism on Friction Surface

2.2.1.1 Sliding Guiderail

A) Elementary sliding contact linear guiderail

This type of linear guiderail is the earliest form, having a simple physical configuration and low cost. It still has wide applications in the modern industry.

All sliding contact guiderails have greater friction coefficient than other types. Because of this, they are commonly deemed to be the secondary options while the designing system for precise positioning applications. However, with lubricant constantly maintained between two relatively moving objects, and thereby, a thin film is formed. Under such condition. The degradation process of guiderail would be mitigated significantly (Waterhouse, 1972).

B) Aerostatic (**Figure 2-8**) or hydrostatic (**Figure 2-9**) linear motion bearings

While extreme accuracy and diminished operation noise must be attained, a guide without mechanical contact between its elements would be frequently adopted. With a pressurised fluid between two relatively moving component, one of them is kept floating by the fluid (Sutar, 2013). Depending upon the fluid in use, it is classified in aerostatic and hydrostatic linear motion bearings. Although the advantage of this type of guides is promising for particular purposes, it brings high cost together with the difficulty in manufacturing and maintenance, and requires expensive auxiliary apparatus. Yet, this type is sometimes used for ultra-precision machines, with air pumps to keep the slide between floating and abrading (Sutar, 2013).

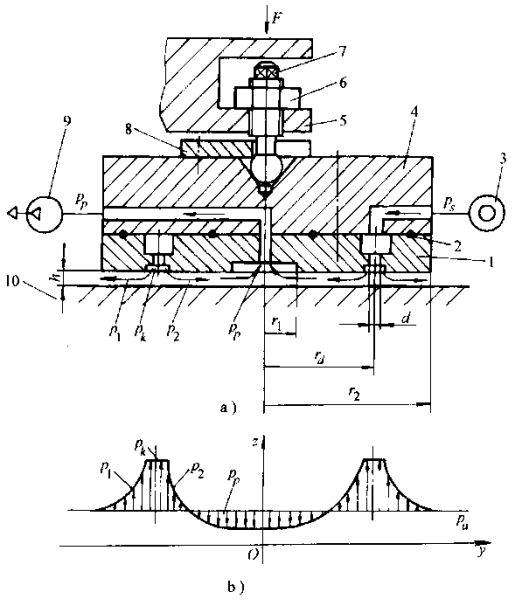

Figure 2-8 Typical structure of the aerostatic guiderails (Sutar, 2013).

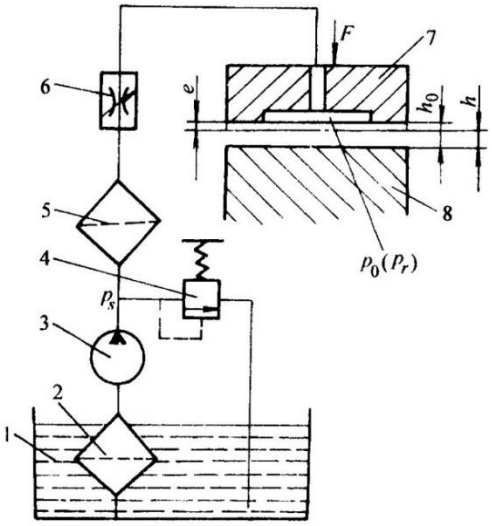

Figure 2-9 Typical structure of the hydrostatic guiderail and oil pump (Sutar, 2013).

2.2.1.2 Rolling Guiderail:

This type decreases friction utilising rolling contact via rolling elements (balls, rollers, etc.) which are placed between two relatively moving objects. There are many manufacturers and each manufacturer provides a wide variety of products (**Figure 2-10**). Because of its superiority over the sliding contact linear motion bearings as described hereunder and because of its availability, this type has won the position as an essential component to the equipment that requires highly accurate positioning operation (Sutar, 2013).

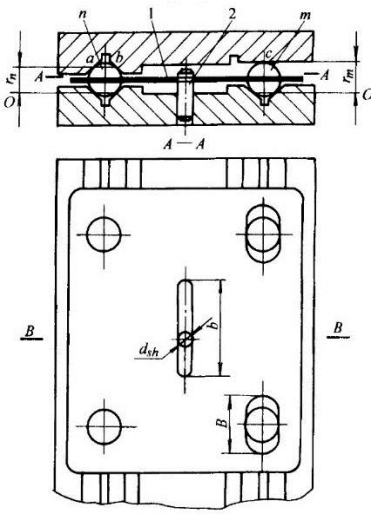

Figure 2-10 Typical structure of the rolling guiderail with rolling balls in between the slide and support to reduce friction (Sutar, 2013).

For the purpose of achieving high-speed and high-precision positioning, the static/dynamic behaviours of transmission systems shall be sufficiently settled in the designing stage of a machine with high level of processing precision. As can be observed from **Table 2-1**, comparing to the rolling guiderail, the sliding guiderail has the property of simpler construction and lower cost. However, the rolling guiderail has a different tribological mechanism between guiderail shaft and ball bearings from that on sliding guide rails. The linear guide system with rolling balls is the more popular and effective transmission system as the lower friction efficient (table), lower wear rate and less friction force induced at ball grooves when compared to the conventional guide with sliding contact interface (Wu, 2009).

Table 2-1 Comparative characteristics of Rolling and Sliding Guideway (Sutar, 2013)

Function	Rolling guide	Sliding guide
Friction	• Friction coefficient: 0.01 and lower • Difference between static and dynamic friction is small. • Change by speed is slight.	• Friction is great • Static and dynamic friction vary greatly.
Positioning accuracy	• Lost motion is slight. • Stick-slip is slight. • Easy to sub-micron positioning	• Lost motion is great. • Stick-slip at low speed is great. • Difficult to achieve sub-micron positioning
Life	• Easy to estimate life	• Difficult to estimate life
Static rigidity	• Generally high • No play because of preload • Easy-to estimate rigidity	• Rigidity is great against load from a single direction. • There is mechanical play. • Difficult to estimate rigidity
Speed	• Wide range of use from low to high speed.	• Unsuitable for extremely low and high speed
Maintenance, reliability	• Long life through simple maintenance	• Precision is lost greatly by deteriorated guide surface.

2.2.2 Categorisation of the Guiderail by Cross-section Shapes

The following are different cross-section shapes of the guiderails:

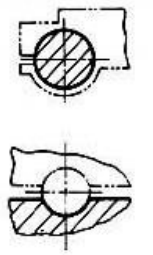

Figure 2-11 Circular Guiderail (Wei, 2010)

1) Circular guiderail (Figure 2-11)

- Steel material
- Easy to manufacture
- Simple structure
- Have small size sample corresponding to CNC machines

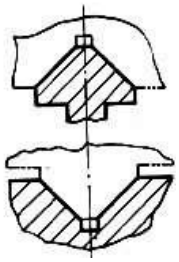

Figure 2-12 Triangle Guiderail (Wei, 2010)

2) Triangle guiderail (Figure 2-12)

- steel material
- Wear concentrated on top surface, not equal distribution
- Complicated to analysis the wear due to complex structure
- Small size product not found

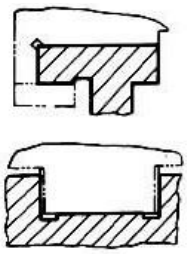

Figure 2-13 Rectangular Guiderail (Wei, 2010)

3) Rectangular guiderail (Figure 2-13)

- Steel material
- wear on flat top and side faces
- Suitable for small size products
- Complex to calculate or simulate

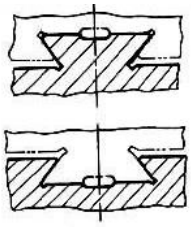

Figure 2-14 Dovetail Guiderail (Wei, 2010)

4) Dovetail guiderail: (Figure 2-14)

- Suitable to equip with oil pump
- Difficult to analyse with complex structure
- More expensive

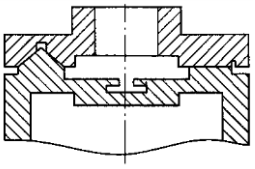

Figure 2-15 Multiplex Guiderail (Wei, 2010)

5) **Multiplex guiderail: (Figure 2-15)**

- difficult to analyse with complex structure
- The most stable but expensive type of guiderails

2.3 Guiderail Accuracy

Although CNC machines offer great precision and versatility in the fabrication of complex parts, machining is an innately slow and expensive process. Straightness errors in the linear stage are basic geometric errors inherent to machine tools and will be directly reflected in the workpiece (Deng, 2015). Attempts to improve the efficiency of machining processes must be tempered by the call for maintaining part accuracy. Therefore, precise allocation operated by machine guiderail to both the work piece and the machine tool is assumed as the prerequisite to high-resolution machining.

Generally, there are four major error sources (Sparham, 2014):

(1) Thermal expansion

In CNC machine manufacturing, the linear positioning accuracy will inevitably suffer due to temperature changes which cause thermal deformation, as there are resources of the heat from surface friction on components, driving motors and tool cutting operation. (Heisel, 2006) Industrial CNC's have evolved in various compensation features, such as feedforward and notch filters, disturbance observation and cancellation schemes (especially indirect drives), as well as torque ripple, geometric and thermal error compensation modules. (Kamalzadeh, 2010)

(2) Machine wear

Surface wear is the principal failure mode of traditional single-material guide rails. The tribological mechanism of the wear is complicated, the resources can be multiple. To prevent abrasion, new types of guide rails have been manufactured in these years with a wear-proof layer bonded onto a traditional

elastic substrate (Wei, 2010). However, as soon as the surfaces of metal have relative friction behaviour, the process of wear starts.

Wear between surfaces may be roughly divided into four categories (Angus, 1957):

a) Lubricated sliding wear: While in the CNC machining, the direction of table movement constantly reverses following the program command. Therefore, maintaining the state of a continuous oil film is more difficult than that of a rotating shaft.
b) At the end of each stroke, the sliding component is momentarily at rest, random occasion may remain so for considerable periods of time (Majda, 2012). This would possibly produce the local failure of the oil film, then change the tribological property and promote metallic contact between the two surfaces. Under such conditions, the possibility of surface tearing off is increased.
c) Dry sliding wear: This type of wear in the case of a machine tool slide (both rolling friction mode and sliding friction mode) may arise from defectiveness, regional lubrication deficiency or uneven sliding/rolling surfaces. (Angus, 1957) In the initial stages, it may merely cause polishing of the surface to take place, but ultimately it tends to result in galling or tearing of the surface part and particularly accelerate the corrosive wear.
d) Abrasive wear: Wear in which a component harder than the worn surface cuts and tears the surface to destruction (Wen & Huang, 2008).Resistance to this form is dependent almost entirely upon the hardness of the material and the thickness ratio of the anti-friction casting surface (Wei, 2010).
e) Fretting corrosion: The extremely localised damage that occurs is caused by the small amplitude of vibration, which does not permit the debris to escape from the initial contact zone (Angus, 1957).

(3) Mechanical deviation (including tool error)

The mechanical deviation caused by geometric errors exerts a significant influence on the machining quality, and it is the major factors affecting the machine tool accuracy. The modelling to such deviation is studied (**Figure 2-16**) and the simulated data of the error such as joint kinematic errors (**Figure2-17**) are analysed. (Majda, 2012) Based on those efforts, methods of developing improved structures of the guide rail to reduce error sources and proposing compensation method for both the straightness and positioning error have been studied (Deng, 2015).

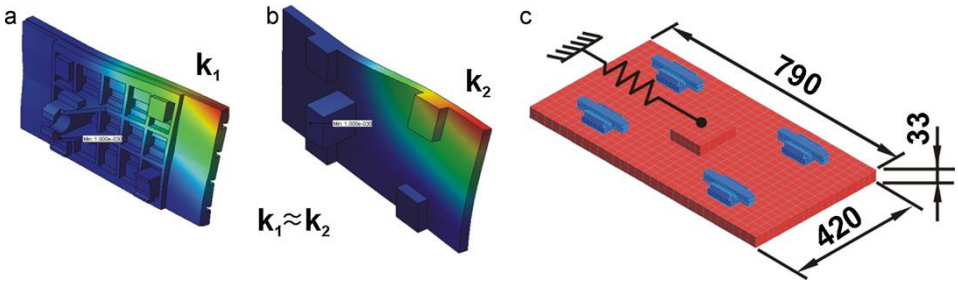

Figure 2-16 Guide way configuration (bottom side); (a) detailed model, (b) simplified model, and (c) model FEM (Majda, 2012)

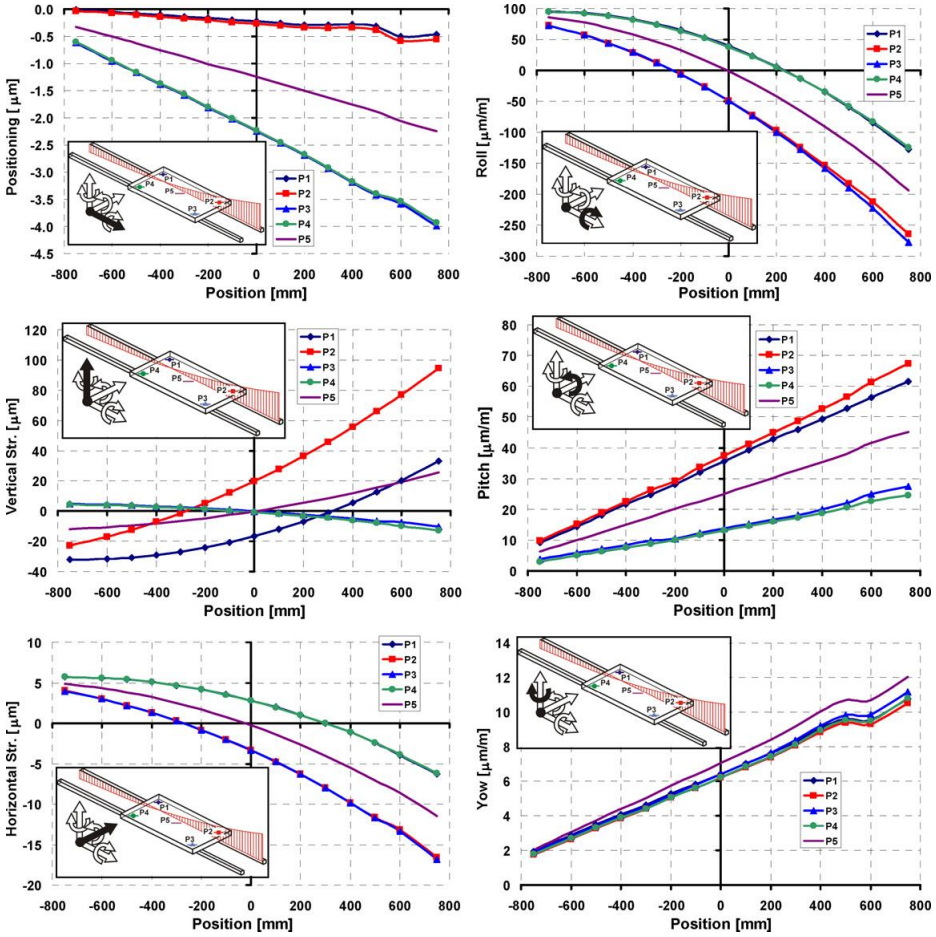

Figure 2-17 Characteristics of joint kinematic errors variant (FEM calculation) (Majda, 2012)

(4) Force acting on the part

Forces acting on the parts as well as tool error and wear collectively constitute the remaining error percentage. (Sparham, 2014) The load of cutting force on the work piece is mainly from three aspects:

a. Contact area between the cutter and the work piece: The greater the contact area present, the more actual cutting of material occurs, therefore more load.(Gorasia, 2009)

b. Feed rate: Speed rate is the terminology refers that the speed of the workpiece moving towards a cutter. The feed rate proportionally increases the forces against the workpiece, especially while tangential to the cutter.

c. The spindle rate: Meanwhile, the cutter spindle rate is positively proportional to the force.

2.4 Wear categorisation

The wear metallic surfaces is almost invariably a cause of injury to the contacting surface- excessive wear causes, in sum, more damage than fracture (Eric, 1972). Wear is the undesirable removal of solids from a sliding or rolling component (Nallasamy et al., 2015). It is the principal failure mode of CNC machine guide rails. Determining the types of wear occur on the particular component is necessary to further analyse wear problem to it.

There are six types of wear occurring on CNC machine guiderails. The wear of guide rails that are tightly protected and running stably in good working conditions is slow and mild and will be dominated by friction fatigue (Wen & Huang, 2008).

(1) Friction fatigue wear:

Mechanism: Friction fatigue is a common mechanism of fatigue wear, which refers to the fatigue failure of surface asperities (**Figure 2-18**) caused by repeated contact and consequent cyclic stress of the asperities under normal pressure and sliding friction (Stachowiak & Batchelor, 2006). Meanwhile, the particle wiped off from the surface would also accelerate the speed of wear.

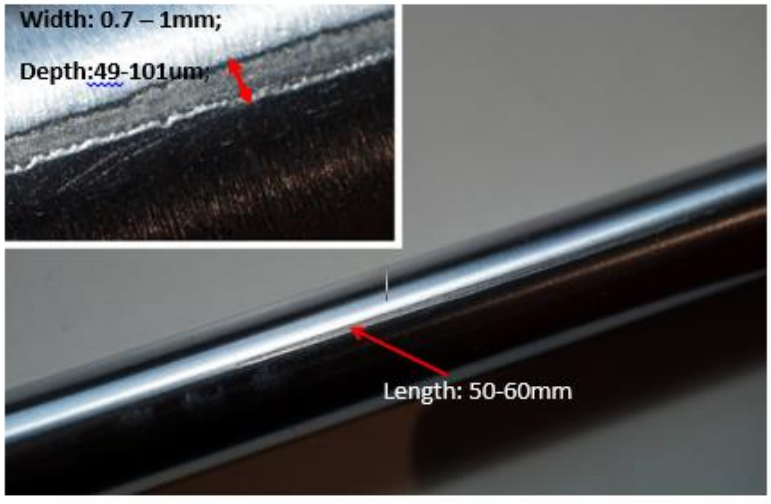

Figure 2-18 Friction fatigue wear on the round guiderail (Bremer, 2014)

Effects: It usually results in a smoother, low-wearing surface on guiderails. (Fitch, 2013)

(2) Grinding abrasion wear:

Mechanism: It is mainly caused by particles between the slide and support of the guiderail when the slide moves under high stress (Fitch, 2013), many very small grooves are produced at relatively low speed across the metal surface (Chandrasekaran, Natarajan, & Kishore, 1991) .

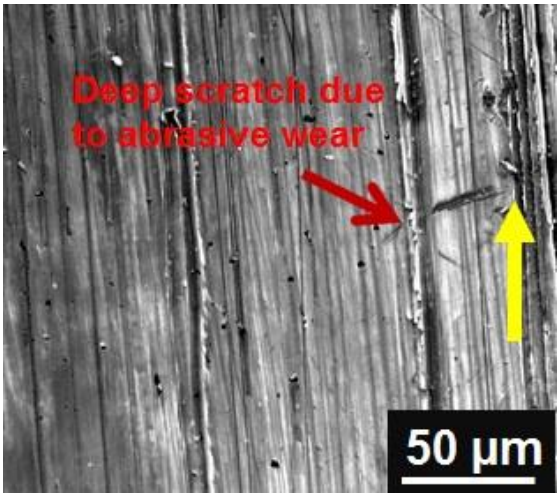

Figure 2-19 View of grinding abrasive wear (Fitch, 2013)

Effects: there will be scratches on the surface of guiderail (**Figure 2-19**), making the slide goes deviant from the straight line in particular positions (Burdekin, Cowley, & Hemingray, 1971).

(3) Corrosive wear:

Mechanism: Corrosive wear phenomena are apparent in machinery. As can be observed from **Figure 2-20**, it is the corrosion that happens on the shaft with the material of AISI 316 and the diameter of the shaft is 40mm. It exists with lubricating systems or working in the severe environment. Most lubricants contain corrosion inhibitors that protect the guiderail from the damage. It is caused by the coolant, lubricant or workshop with corrosive ingredients (Giourntas, Hodgkiess, & Galloway, 2015).

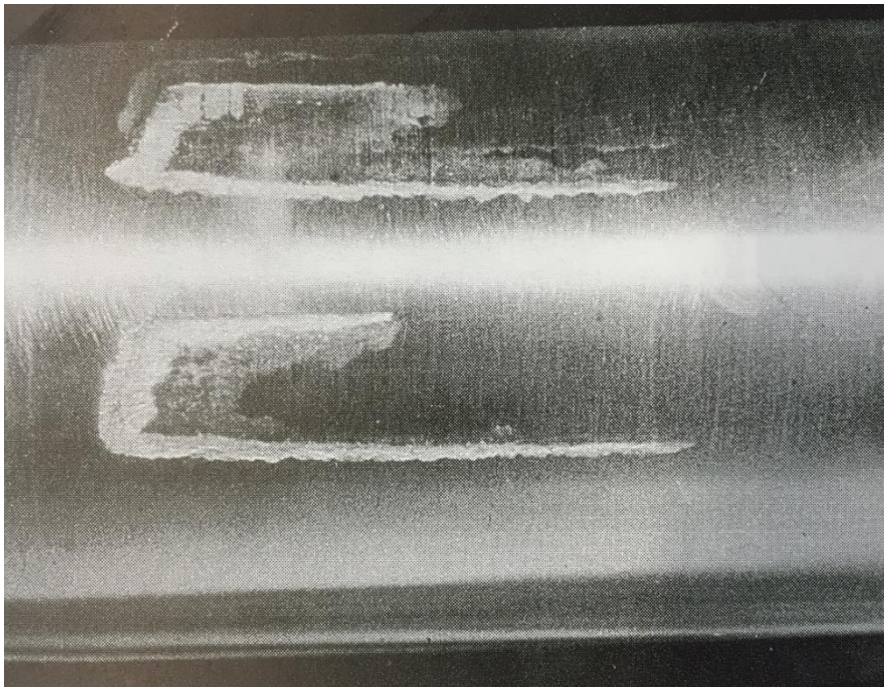

Figure 2-20 Corrosive wear on the shaft surface (Waterhouse, 1972)

Effects: the corrosive wear is often too small to distinguish individually and usually cause unsmooth behaviour or small range vibration to the running slide.

(4) Rusty wear:

Mechanism: The existence of rust wear mainly depends on the humidity of the working area. Due to the oxidative chemical reaction of the metal surface in the presence of moisture (water mainly). The wear involves material removal or loss. It is the dissolution of metal in an electrically conductive liquid by low amperage and may involve hydrogen embrittlement as well. The rusting speed can be increased with increasing temperature rising and other relevant factors.

Effects: the abnormal moving behaviour caused by rusty wear is similar to corrosive wear but more violent. The rusty wear will cause further damage to guiderail if keep on running the machine.

(5) Fretting wear:

Mechanism: Fretting wear (**Figure 2-20**1) is due to reciprocating sliding of extremely low amplitude because of vibration (Brosend, 2012). Mechanically, it can be diminished by reducing or stopping vibration by tighter fit or higher load.

Another solution is improving the lubrication between surfaces by the rougher surface finish. Take lubricant into concern, frequent re-lubricating or choosing the oil with lower viscosity can prevent guiderail from getting severe damage from the wear.

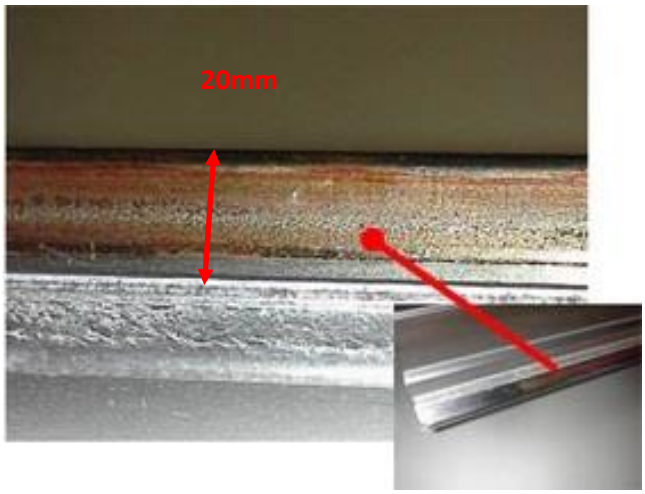

Figure 2-21 The fretting wear on the guide rail surface (Brosend, 2012)

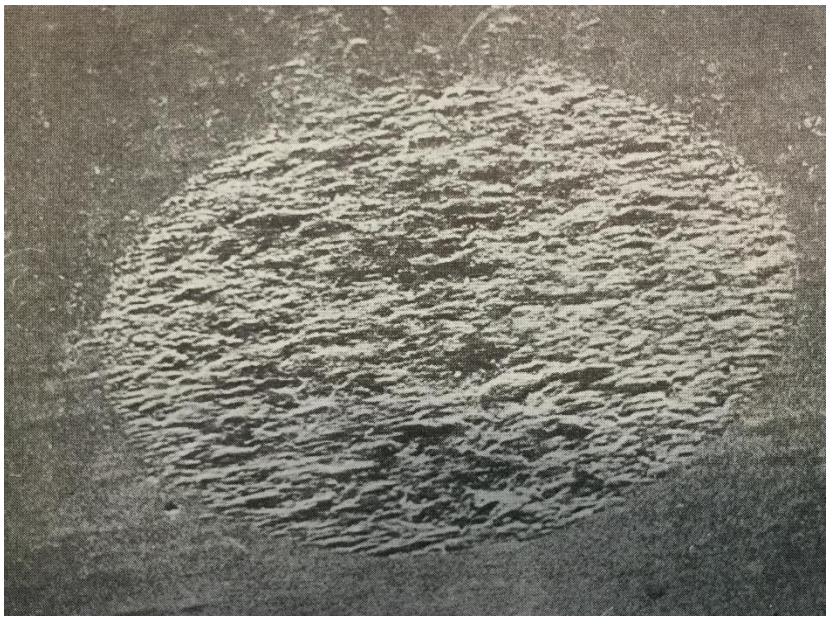

Figure 2-22 Scanning electron micrograph of fretting damage on the aluminium X54 (Brosend, 2012)

Effects: The fretting wear (**Figure 2-22**) causes unsmooth behaviour or small range vibration to the running slide.

Besides the above major wear happening on CNC machine, there are also some other types of wear which participate in the guiderail degradation behaviour in different tribological occasions.

When the slide works at high speed, the temperature will increase. The dominant mechanism of the wear changes (Tan, Zhang, & Hu, 2015). Adhesive wear is one of the further consequences. The adhesive wear is a kind of lancinating damage to the surface of guiderail. Because of high temperature and pressure on the slide surface, the oxidation film or liquid film being squeezed out, then the molecular absorption happens on the naked surfaces between the slide and support. Later moving behaviour of the guiderail causes lancinating damage (Hou, Chen, & Zheng, 1982). Meanwhile, the continuous removal of surface films makes the metal surface has chemical reaction with the additive of lubricant oil, which is called polishing wear.

When the slide works in low speed (rubbing speed), it leads to changes in the wear mechanism and the real contact configuration (Tan, Zhang, & Hu, 2015). It will cause time-dependent but irreversible deformation which is called ‘‘plastic deformation’’ and It also leads to the crawl appearance on the guiderails. The crawl appearance is the typical mechanical self-excitation. It is the phenomenon that happens under sliding friction. The slide changes running speed periodically. Such behaviour speeds up the wear of guiderail (Wei, Li, & Lee, 2010).

2.5 Friction Fatigue Wear

In the thesis, due to the typicality of the friction fatigue wear, such wear is chosen as the object. This section mainly focuses on illustrating the mechanism and effect of the wear.

2.5.1 Tribological Mechanism and Properties

Friction is the "contact force," a force between two surfaces that are in contact that resists the sliding/rolling motion of one surface over the other (Deng, 2015). The friction force exerted by one object sliding/rolling over another object is

always parallel to the contact surface between the two objects and always occurs in a direction opposite that of the motion.

The modern theoretical understanding of friction attributes the friction force to the atomic forces of adhesion between atoms or molecules on the surfaces of the two materials. These forces are similar to the electronic bonding forces that hold the individual atoms together in liquids and solids.

During the friction process, most of the excess energy is transformed into heat by the friction force, though a small part of the excess energy actually abrades, or wears away, the surface of the weaker of the two materials. Friction causes most mechanical objects to wear out as a result of abrasion (the loss of material as the surfaces in contact interact with each other) (Deng, 2015) and because of the heating produced as one surface slides over another.

2.5.2 Static/Kinetic Friction and the Friction Coefficient

There are two types of friction, "static friction" and "kinetic friction."

Static friction occurs between two surfaces that are in contact but are not moving on each other because static friction provides the force that resists the motion of the objects against each other. However, there is a maximum force that the two surfaces in contact can exert. If the drive supplies enough power to overcome this force, the object will begin to move (Yanqing, 2015).

The maximum force of static friction is modelled by as the coefficient of static friction, a quantity that must be measured for each type of material sliding on another type of material, and the "normal force," which is a measure of how hard one surface is pushing on the other.

Kinetic friction occurs when one of the surfaces of objects is moving on the other one. Similar to static friction, kinetic friction models as the coefficient of kinetic friction. For most materials, the coefficient of kinetic friction is less than the coefficient of static friction, so it requires a stronger push to start the object in sliding motion than it does to keep it sliding across the table at a constant speed (Yanqing, 2015 and Wu, 2009).

However, in the field of rolling friction, the tribological property and mechanism are different from which in the field of sliding friction. The rolling friction coefficient “k” is defined as the ratio between rolling friction moment and normal load:

$$k = \frac{FR}{W} = e \tag{2.1}$$

In which F is the pushing force, R is the diameter of the rolling object and W is the load perpendicular to the rolling flat surface (**Figure 2-23**).

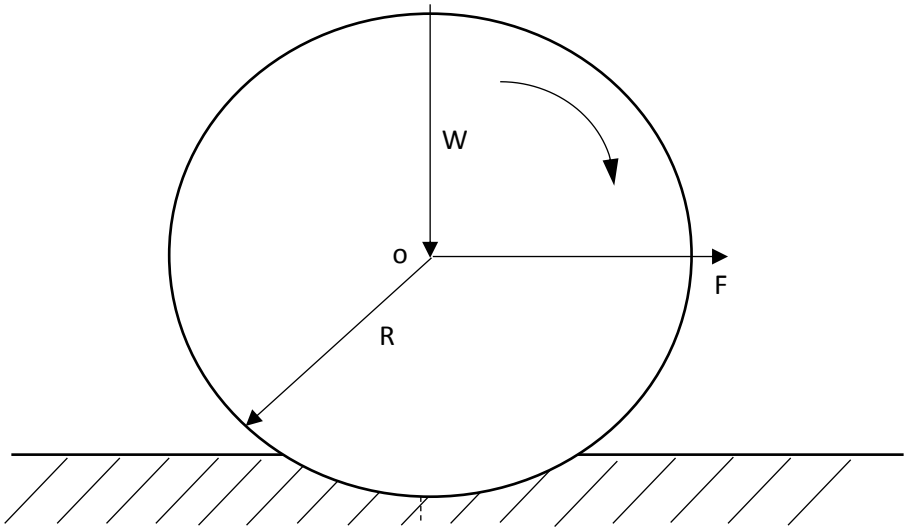

Figure 2-23 Module of rolling friction (Yanqing, 2015).

Therefore, according to the rolling friction principle, there is no distinguish between static friction and kinetic friction. Only on the occasion with the increasing of surface roughness and following the tribological property change, there will be an intermediate state between rolling and sliding friction. Only in such condition, the analysis to static friction such as stick-slip phenomenon makes sense.

2.5.3 Effects of Friction Wear

The analysis of the rolling friction theory and metal wear tribology property are presented (Rabinowicz, 1965). As soon as the metal surfaces touch each other, friction wear process begins. The module of friction fatigue wear asperity in both sliding and rolling condition is also provided (Tan, Zhang, & Hu, 2015).

According to the analysis of Eric. N. Simons (1972), the bearing metal of rolling guide rail must not be so hard as to wear the shaft.

Therefore the effects of guiderail wear by time can be summarised as below:

a. To the guiderail shaft

The most frequent used section on the guiderail would have roughness increase. Then there follows the metal grind out by continuous cycling stress.

b. To the bearing balls

The non-smooth surface and deformation of the balls against round shape will occur as well.

Meanwhile, the particle wiped off from the surface would also accelerate the speed of wear.

2.6 Monitoring Solutions

The monitoring system contains two main functions: measurement and data collection. Monitoring systems utilised in tool wear monitoring have been studied and developed by researchers in recent decades. Girardin et al. (2010) developed a system to analyse instantaneous variations in rotational frequency so as to observe milling operation. Luo (2004) analysed the formation mechanism of tool wear and presented a complete solution to calculate wear using a ball end cutter for high-speed cutting. Ratnam & Shahabi (2008) developed a vision system using high-resolution CCD camera and back-light for the on-line measurement of tool wear. Some of the module or experiment rigs on predicting tool wear and sensing tool change have invented. Guo, Q (2014) developed a system to predict CNC machine tool wear by monitoring cutting force and controlling cutting conditions and complete the prediction by using PPR (Project Pursuit Regression) system.

However, the research and specialised guide rail wear system establishment are relatively rare. The following are instruments which have the possibility to utilise in the guide rail wear in monitoring systems.

2.6.1 Interferometer

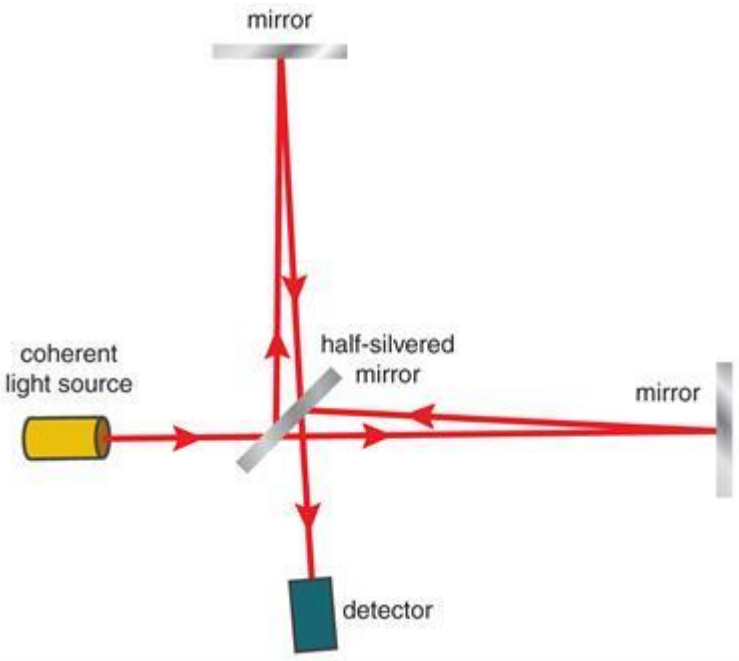

Figure 2-24 Optical mechanism of interferometer (Leach, Flack, Hughes, & Jones, 2009)

Mechanism:

Most interferometers use light or some other form of electromagnetic wave. It is the measurement method product using the phenomenon of interference of waves (usually light, radio or sound waves) and extracting information from the wave (**Figure 2-24**). When two waves with the same frequency overlap, with a phase difference in between, the result shows the meaningful property. Waves that are in phase will undergo constructive interference while waves that are out of phase will undergo destructive interference (Leach, Flack, Hughes, & Jones, 2009).

Also, interferometry extensively uses for displacement measuring, calibration and mechanical stage motion control in precision machining. While monitoring 2-dimensional movement information, the interferometer system has two linear and angular column-referenced interferometers (Leach, Flack, Hughes, & Jones, 2009).

2.6.2 Cylindrical Square and Dial Gauge

Cylindrical square mechanism:

Cylindrical square is the most common instrument used for checking square, flatness of machining parts. It is the tool with a cylinder shape, a hardened material made and the end is lapped to 90° angular accuracy. The 6" cylindrical squares have an accuracy of ±.0001".

Gauge mechanism:

Gauge is the instrument used to accurately measure small distances and angles, amplify the data to make them more obvious to obtain, or use digital cable to transmit the data to computer.

When the CNC machine is under routine maintenance, cylindrical square is equipped on the surface of the slide or drill holder (depend on the checked surface). It measures from the precision surface box with a dial indicator against the cylindrical square, rotate the table 360° and record the value of the measurement.

2.6.3 Dial Gauge with Digital Data Output

The type of digital data output dial gauge has the digital display screen. The data can be transmitted by wire with RS232 port, sorted by the software installed in computer and displayed via excel document. The monitoring range is from 0 to 12.7mm, with resolution of 0.001mm. However, the data sampling is manually but not automatic with sampling frequency.

2.6.4 Laser Tracker

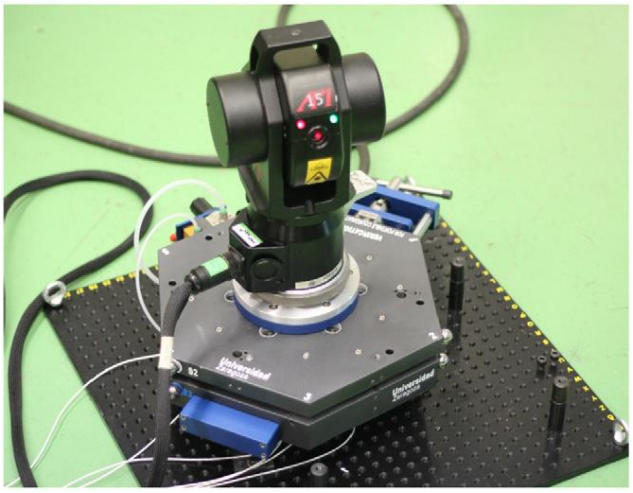

Figure 2-25 Laser tracker with a platform (Kong, 2012)

The laser tracker is the most effective and precise equipment implemented in the machine tool measuring or large object measuring (**Figure 2-25**). The equipment contains two parts, the laser tracker settled on a tripod and ball probe as a reflector. When taking the measurement, the laser tracker firstly set up a on a tripod and the connection between those two parts are established. Then the operator removes the ball probe from the base of the laser tracker and carries it smoothly to the object being measured, the tracker automatically follows the movement of the ball probe during the measuring process.

2.6.5 Gradienter

Gradienter is the micro meter, attached to transit's telescope which allows the angle of incline to be measured in terms of the angle's tangent instead of in degrees and minutes **(Mross, 2015)**.

2.6.6 Optical Autocollimator

Figure 2-26 Typical Optical autocollimator (the reflection part) (Mross, 2015)

An autocollimator (**Figure 2-26**) is an optical instrument for non-contact measurement of angles. There are typically two types of autocollimators implemented in the industries, the visual autocollimator and Electronic one. They both work by projecting a laser beam onto an aligning target mirror, while measuring the flatness, deflection of the returned image against a scale which using an electronic detector produces the deviation from originally settled straightness. A visual autocollimator can measure angles as small as 0.5 arc second, while an electronic autocollimator can be up to 100 times more accurate (Mross, 2015). Electronic l autocollimators are used as angle measurement standards, for monitoring angular movement over long periods of time and for checking angular position repeatability in mechanical systems (Morel, 2015).

2.6.7 Capacitance Probe

Non-contact capacitive sensors work by measuring changes in an electrical property called capacitance. Capacitance describes how two conductive objects with a space between them respond to a voltage difference applied to them. (Lion, 2015) When a voltage applies to the conductors, an electric field is created between them causing positive and negative charges to collect on each object (**Figure 2-27**). If the polarity of the voltage is reversed, the charges will also reverse.

Capacitive sensors use an alternating voltage which causes the charges to reverse their positions continually. The moving of the charges creates an alternating electric current which is detected by the sensor.

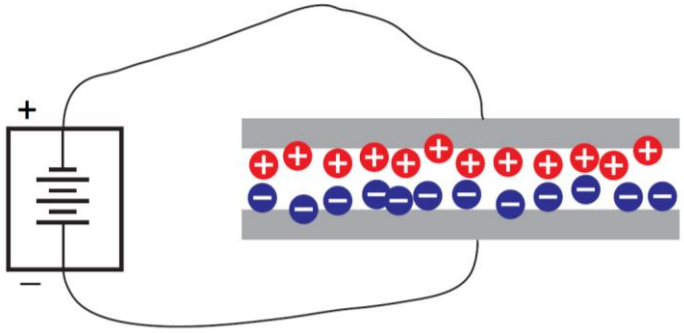

Figure 2-27 Applying a voltage to conductive objects (Lion, 2015)

Applying a voltage to conductive objects causes positive and negative charges to collect on each object. It creates an electric field in the space between the objects. (Lion, 2015)

The product of the capacitive sensor can acquire resolution of 0.05nm, measurement range from 50um to 2mm. The diameter of the smallest sensing area may reach to 0.5mm. (Lion, 2015)

2.7 In-process Monitoring Solution

2.7.1 Definition of In-process Monitoring

Doing the monitoring during the working period of CNC machine (Vacharanukul, 2008), pre-after drilling/milling on workpiece but not during the working period.

The in-process monitoring solution is with advantages of (Bosetti & Bruschi, 2010):

a. No need to deliberately exclude the outer disturbance;

b. No need to dismantle the components of CNC machine;

2.7.2 State-of-art of the In-process Monitoring Technology

The major research of the guiderail wear measuring approaches is mainly based on the mode of static measuring or “pre-after” calibration solution. Deng

et al. (2015) developed a linear stage with improved structures for reducing the error sources and proposed a macro–micro compensation method for the straightness motion error to support the further compensation to straightness error. Bosetti and Bruschi, (2010), discussed the concept of in-line monitoring to machine cut surface, however, still solving different situation to guiderail wear monitoring system. Hongxiang, et, al. (2015) have studied on the shaft roundness in-situ inspection using a V-block displacement probe (**Figure 2-28**). Although from the Abbe error control prospect, the solution successfully avoid such problem, but the contact of two surfaces would still bring extra wear and affect the quality of the system (**Figure 2-29**). Therefore, according to the literature, there is no effective solution particularly to the case of in-process monitoring on guiderail wear.

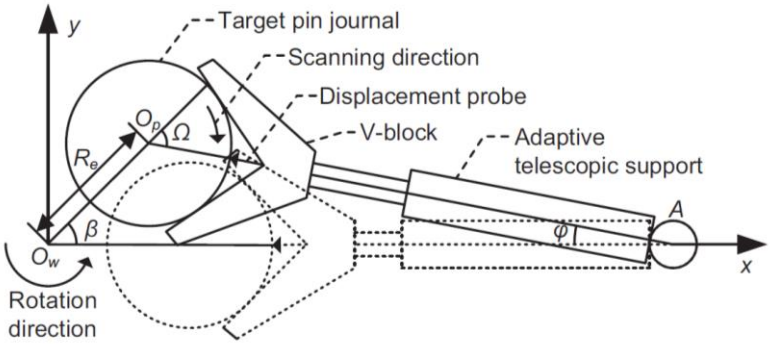

Figure 2-28 Geometrical principle of the in-situ measuring mechanism (Bosetti and Bruschi, 2010)

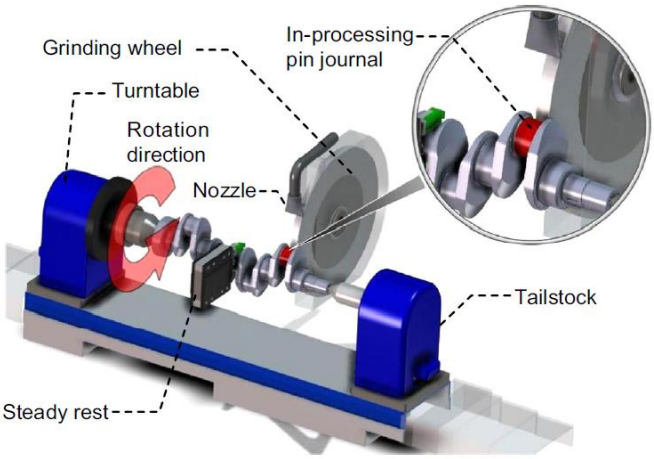

Figure 2-29 Demonstration of pin chasing grinding in an oscillating grinding machine (Bosetti and Bruschi, 2010)

2.7.3 Guiderail Wear In-process Applicable Solutions Study

Monitoring the guiderail wear in-process monitoring design should face towards two main obstacles:

(1) The outer disturbance during the tooling of the CNC machine
(2) The uncertainty of measurement result which is from geometric error, assembly tolerance, resolution limitation and measurement error (Lou, 1997).

Referring to such assumption, an idea from electronic signal process field has brought into consideration. In the field RF characterisation, Brocard et al. 2014 have applied the technology of noise coupling to solving the 3D digital signal transmission. Generally, the solution is splitting the original MOS into dopes and sorting the signal by coupling circuit and completing the offset to the noise. Bronckers, et al. (2010) utilised a referencing signal to do the offset to independently adopted signal to filter the unnecessary noise. Helmy & Ahmed A, (2008), also mentioned the technology of coupling the noise to both RFIC analogue signal and the DC power signal cross talk.

2.8 Geometrical error budget

Definition to error budget

The error budget is a necessary parameter for the designing of the rig and analysing to the experiment result. It calculates each type of possible error from various resources and the distribution of each one. After this, it accumulates each one error together and carries out the result of possible tolerance of the whole system. It provides estimation to potential errors with a machine axis that leads to deviations from the desired motion (Kong, 2012).

In the field of geometric error analysis, the error resources can classify as the following:

a) Moving behaviour straightness error: In guiderail behaviour case, it can be roughly categorised as rolling, yawing and pitching (**Figure 2-30**):

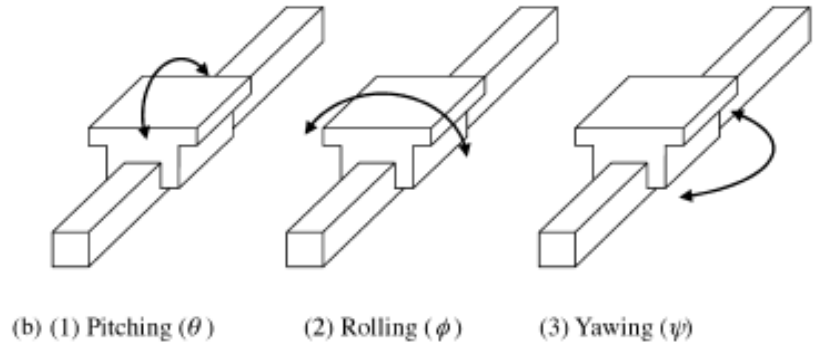

Figure 2-30 The deviant motions of a guiderail (**Kong, 2012**)

b) Rolling element bearing error: the motion of linear bearing balls is not perfectly aligned.
c) Thermal growth: the thermal expansion of the object being measured and the deformation of the instrument used to measure it.
d) Measuring approach repeatability and reproducibility:
e) Repeatability: It is evaluated by the difference of repeated measuring result while the entire objective situation is stable and the measuring solution is the same.
f) Reproducibility: It is the standard to evaluate if the measuring solution can be reproduced by other operators while the object condition is the same.
g) Alignment error: It represents the error brought by the deviation of measuring tool while in the measuring.
h) Parallax error: It results from viewing a marker, which is separated by some distance from the scale or object being measured, at an incorrect angle.
i) Abbe error: The Abbe error is the principle that illustrates error results from alignment of machine axes if the measurement scale is not co-axial with the axis of measurement.
j) Resolution error: Due to the limitation to the resolution of measuring instrument, it can be treated as rounding error, which the value would not over than half of the resolution value.

k) Calibration error: The error of the measuring instrument inherited from calibration process.

2.9 Summary

2.9.1 Study Object Selection

2.9.1.1 CNC machine

Figure 2-31 CNC machine categorisation

Therefore, according to the categorisation in **Figure 2-31**, due to the extensive use, simple and flexible configuration of the CNC machine, turret mill and knee mill are chosen to be the study project.

2.9.1.2 Rolling circular guide rail

1) The selection to the circular guide rail with rolling ball bearings to the table is correspondent to the selected CNC machine type.
2) Rolling guiderail is the most widely utilised type of guiderail in the target CNC machine type;
3) Rolling guiderail is with a relatively low coefficient of friction, represents the trend in the future.
4) Round cross section guiderails are the space-saving type, allows compact design.

The meet to the requirement of such type of guide rail will be discussed in section 3.7 of the literature summary.

2.9.1.3 Friction fatigue wear and symptoms

The following chart (**Figure 2-32**) is the categorisation of CNC machine guiderail wear:

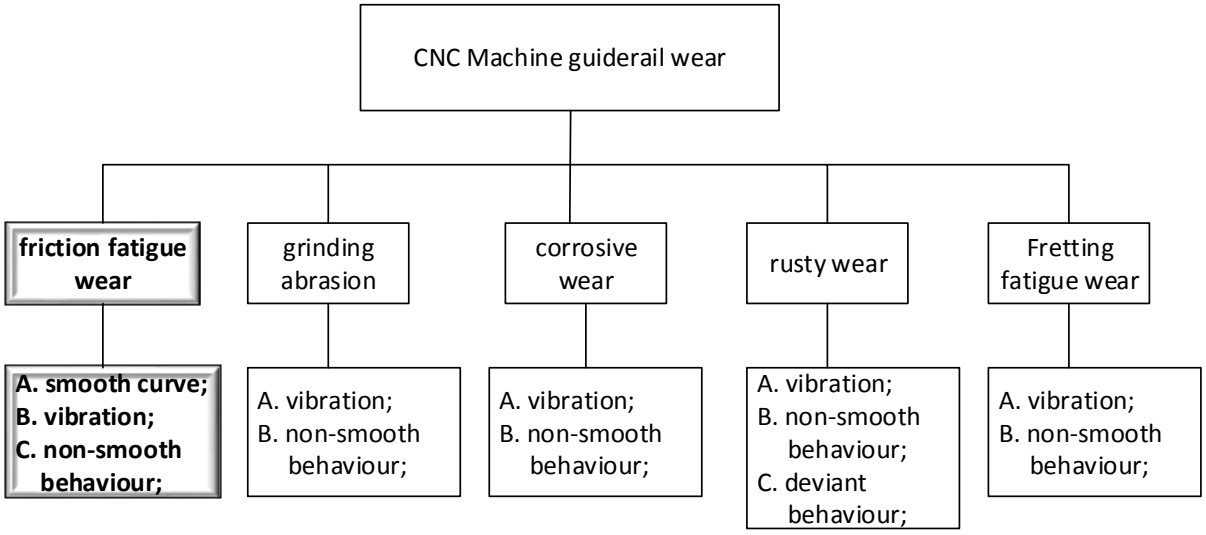

Figure 2-32 CNC machine guiderail categorisation

The reason for choosing friction wear is because referring to the conclusion from the literature review, researchers in the industry highly agree with the major issue of the friction wear to guide rail. Therefore, friction fatigue wear is the major one that is worth studying.

The effects and symptoms of friction wear can be summarised as follow (**Table 2-2**):

Table 2-2 Effect of Wear to each Component

Component	Effects
Guiderail	1. coating surface& part grind out on particular length; 2. roughness value on guiderail increases;
Bearing balls	non- smooth surface & deformation against round shape;

The symptoms of the friction wear can be concluded as below:

a. smooth curve on particular length;

b. small range vibration happens on random positions;

c. non-smooth behaviour.

2.9.2 Research Approach Discussion

2.9.2.1 Monitoring solution to experiment

According to the literature study in monitoring approaches, capacitance probe can be the preferable choice for the following reason:

1) the instrument is with high resolution to meet the discussed level of modern CNC machine resolution;
2) the instrument is with the function of automatic signal sample and output and high signal sample frequency;
3) the instrument is the type of contactless measuring machine which will not lead to extra noise by touching reference surface.

2.9.2.2 Error budget

Since the resolution of the CNC machine can reach the micrometre level, the building of a physical experiment rig would unavoidably bring in an extra geometric budget. Under this circumstance, the analysis to error budget is necessary to the experiment design. The related factors are:

a. Moving behaviour straightness error
b. Rolling element bearing error
c. Thermal growth
d. Measuring approach repeatability and reproducibility
e. Alignment error
f. Parallax error
g. Abbe error
h. Resolution error
i. Calibration error

2.9.2.3 Research gap: in-process monitoring

1) Nowadays monitoring solutions are mainly regular checking (1 year/ 6months regular check). Part recalling happened due to lack of in-process wear monitoring.

2) Present monitoring method is still way too complicated and inconvenient. It needs three prerequisites:

a. no outer disturbance while checking

b. taking a long period for wear monitoring

c. components need dismantling in advance, it causes further re-assembly and calibration work.

With the realisation to in-process monitoring, the above problem all can be solved.

2.9.3 Requirement

The following **Table 2-3** presents the detailed requirement:

Table 2-3 Requirement of the Project

TITLE	DATA	SOURCE
Wear Measurement Resolution	1μ m	BS ISO 230-2:2014
Linear Position Measurement Resolution	1mm	Linear sensor manual
Accuracy	1μ m/m	BS ISO 230-2:2014
Measurement Range	+20μ m	BS ISO 10791-1:1998
Experiment Rig Length	300-500mm	CNC Machine Brochures
Rig Components Scales	Save space& easy to equip Stiffness; Material should be the same or with ;	Literature: (Deng, Jin, & Zhang, 2015)
Data Collection	Easy to collect (raw data transform to digital data)	product documents
	0.001 second sampling precision	Vs/r (Vs: speed of slide movement; R: resolution settled)

TITLE	DATA	SOURCE
Motor Speed (linear)	Capable of drive the ball screw with 50mm/s ~ 1m/s; Enough smoothness while in lowest speed;	Literatures& Calculation: (Deng, Jin, & Zhang, 2015)
Error Budget	Geometric error budget to the physical rig should be analysed and taken into account while analysing the data.	(Kong,2012)
In-process Monitoring	Option a: System be capable of resist to the outer disturbance. Option b: with system function of coupling or offset to the noise.	(Bosetti & Bruschi, 2010):
Take Costs into Account	Low costs ; Easy to get the product	Constraint to experimental validation

3 AIM AND OBJECTIVES

3.1 Aim

The aim of the research is to establish a system to realise the in-process monitoring of the wear of guiderails on CNC machine, analyse and visualise the wear efficiently.

3.2 Objectives

The objectives of this research are listed as follows:

a. Identify and categorise types of the wear on CNC machine guiderail, then select the major type of wear as the study object in the research.
b. Study the mechanism, effect and conclude the symptoms of the wear; define the requirement of an industrial monitoring system for further study according to the symptoms of the wear.
c. According to symptoms and requirements, design proper approaches to monitor each particular type of symptoms.
d. Design the in-process part referring to the characteristics of the disturbance that different from static monitoring solution.
e. Integrate and assess the system through systematic experiments.
f. Complete the validation to the proposed solutions through expert judgement.

4 METHODOLOGY

For the purpose of implementing the research, the methodology is proposed as follow. As can be seen in the **Figure 4-1**, the methodology is divided into four phases with actions and deliverable.

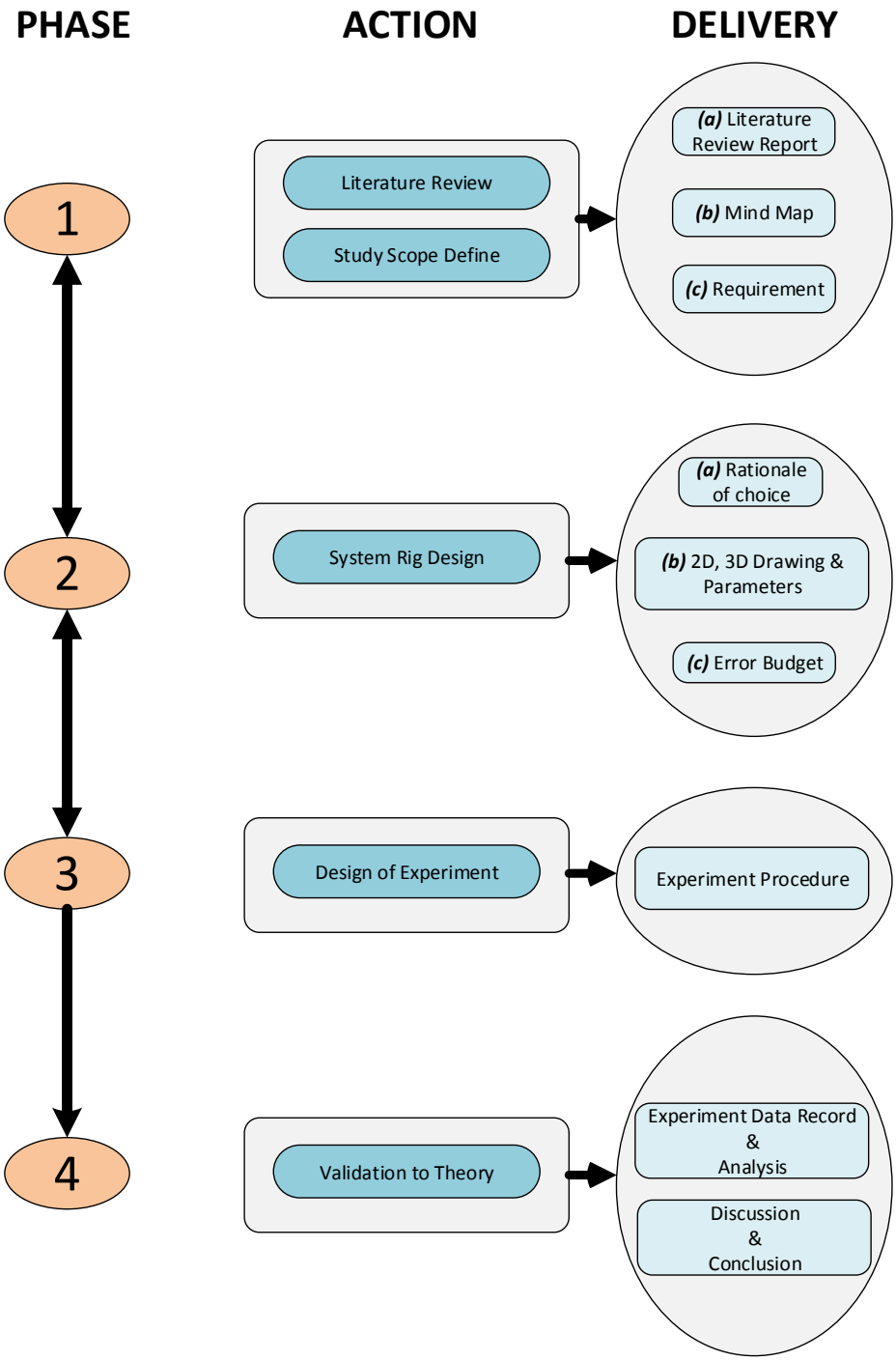

Figure 4-1 Research methodology

In the first phase, according to settled Aim & Objective, the literature review referring to different areas has been carried out. Referring to such review, state-of-art to the research area has been defined. It is the solid support to the contribution to new knowledge in this research. Concerning the designing of the system, the thesis has made study and discussion on multiple options to each component of the future design in the review part.

The literature review report is carried out in this phase, representing as the exploration and definition to the study scope. Meanwhile, the summary in the report would theoretically support the following system rig design part.

The mind map in **Figure 4-2** is another deliverable in the first phase. It contains structured outline of the whole literature review and clearly illustrated the main content of the research. The concept of the research idea can be approached step by step through the details of mind map. In the mind map, the relationship among each study object and the selection to the study scope is clearly represented. As can be seen from the mind map, those parts with red texts are the ones included in the study scope, those with black texts are mentioned and have given a briefing in the literature reading as well. Those contents with rectangular lines are the key points which the research focuses.

According to the conclusion of the literature review and defined Aim and Objectives, the requirement to the design is settled. It contains the resolution, accuracy and other crucial standards. It is regarded as the fundamental principle to rig components, monitoring solutions selecting and also what the whole system design eventually meets.

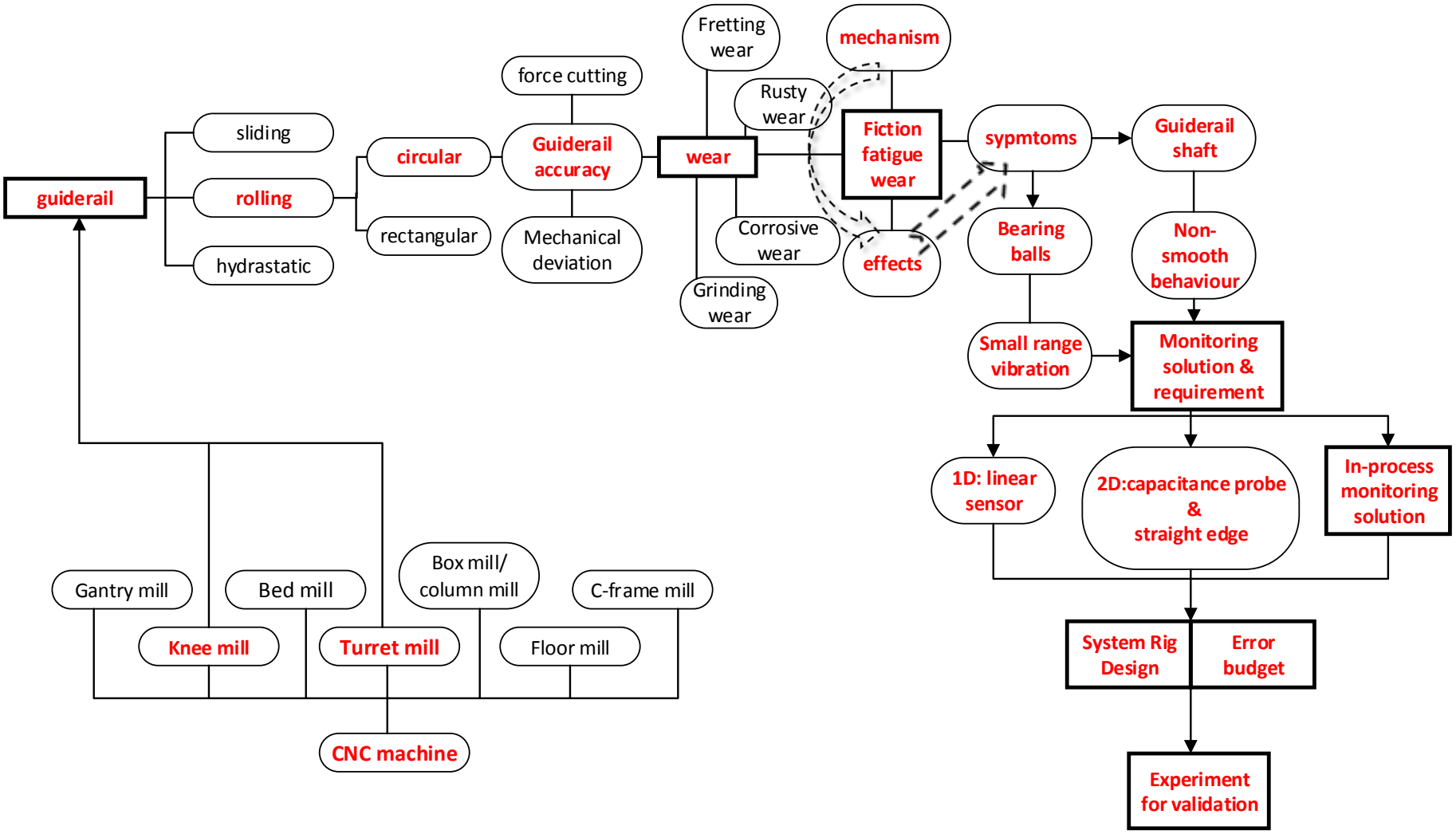

Figure 4-2 Mind map of the Project

In the second phase, referring to the settled requirement, it clearly discussed the rationale of choices to components belonging to each part. Comparison among all the applicable choices and reasons to each decision are provided as well. By such conclusion, the system experiment rig is built up, 2D and 3D drawings are represented with detailed parameters. Above all, the rig design part illustrated the error budget to the established real rig with the calculation result of expanded uncertainty.

In the third phase, the detailed experiment content and steps are carried out. It divided the whole plan into each independent experiment and arranged them in sequence. Each step has declared experiment title, object and content. The first step to achieve is the establishment of the rig which strictly follow the design, following with calibration based on the study of error budget. The second step is the monitoring system building up and function test to make sure the proper working of the system. The third phase is wear simulation which makes wear in different levels of degradation on the guiderail samples, then follows the monitoring system implementation part to acquire the data and make a contrast to the wear tested by high resolution equipment to verify the result from the experiment. Above all, during the wear test, in-process monitoring solution is adopted and tested by deliberately making external disturbance.

In the fourth phase, the theory validation part presents the result of analysis to the experiment data and conclusion to the discussion.

5 DESIGN OF THE EXPERIMENT

5.1 Introduction

According to the conclusion of literature review, the wear on CNC machine guiderail is to the micrometre level, the resolution of the monitoring system and the control to the accuracy is important. On the other hand, in the experimental validation part (**Figure 5-1**), uncertainty resources and the in-process monitoring solution need to be concerned. Therefore, how to discriminate between the wear signal and deviation caused by other aspects and proper designing to the experiment is of importance.

In this part, the monitoring objects and specific measuring strategies are discussed and settled. Then the designing of each part of the rig with proper analysis and calculation is illustrated. In each part of the rig, the uncertainty resources are discussed and the uncertainty value (combined standard uncertainty and expanded uncertainty) is calculated. The thesis represents the novel design of the in-process monitoring strategy based on both the state-of–the-art of the mechanical monitoring solution and the idea of electronic signal coupling approach, and then follows the experiment plan and results of the validation of the hypothesis of the design.

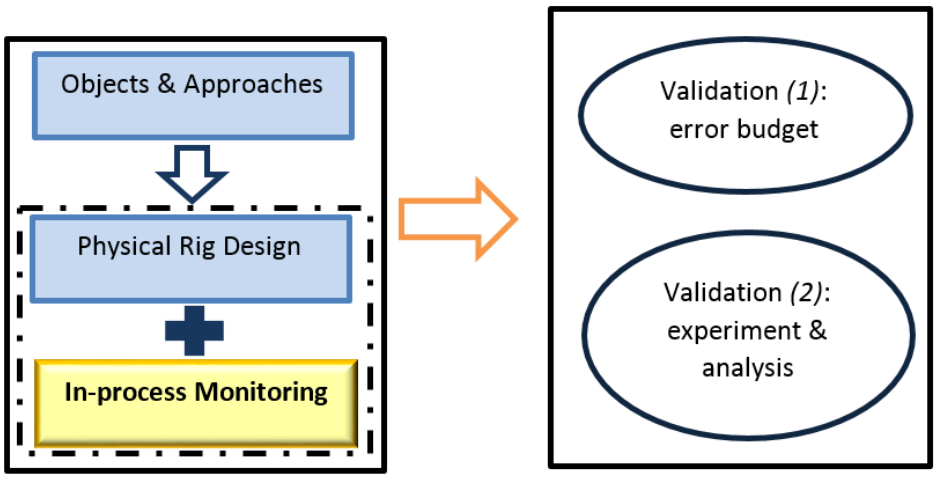

Figure 5-1 The structure of the experiment design and validation

5.2 Monitoring Objects and Approaches Settling

The study objects and corresponding appropriate measuring solution shall be defined in advance of the designing and implementation. This part of the thesis illustrated the three symptoms of the wear and clarified the particular approaches to be the guidance of the following rig design.

5.2.1 Friction Wear Symptoms

According to the conclusion of the literature reading, the effects and symptoms of friction wear can be summarised as the following **Table 5-1**:

Table 5-1 Effects and Symptoms

Component	Effects
Guiderail	1. roughness value on guiderail shaft surface increases, because of the repeating abrading between ball bearing and shaft surface; 2. further coating surface& part grind out and the curving concave along the trail of moving balls exists as time goes by;
Bearing balls	1. non- smooth surface on each ball appears caused by the abrading between metal; 2. material wiped off over time and leads to deformation against round shape;

The symptoms of the friction wear can conclude as below (**Figure 5-2**):

Frist stage:

a. non-smooth behaviour;

b. small range vibration happens on random positions, which with the frequency of 1kHz~2kHz (Wu, 2009);

Second stage:

a. smooth curving deviance against straightness of the movement of particular length, from 10um to 50um (BS ISO 230-2:2014).

b. the vibration gets severe, with higher amplitude but same level of vibration frequency.

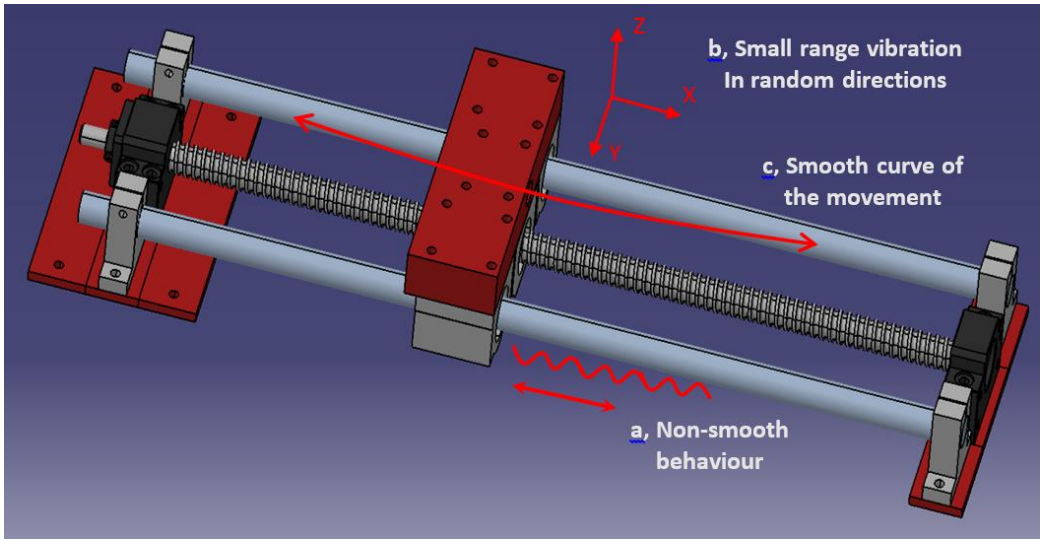

Figure 5-2 The symptoms caused by friction wear

5.2.2 Corresponding monitoring solution

(1) To the non-smooth behaviour of the rolling table, the change to the current of the stepper motor or the vibration of the movement can be monitored to analysis the roughness increasing.

(2) To the small range vibration, the optical equipment or other high-resolution distance measuring equipment mounting on the rolling table can be utilised.

(3) To the deviation of the movement on particular length, the optical equipment or other high-resolution distance measuring equipment mounting on the rolling table can be utilised as well.

5.3 Physical Experiment Rig Design and Build up

According to the above summary, the designing process to the complete monitoring system is represented, each part is analysed to anticipate the uncertainty for further calculating of the error budget.

5.3.1 Guiderail, Ball Bearing and Ball Screw

5.3.1.1 Design Consideration

1. The length, the diameter of the cross section, especially the shape of the guiderail shall be correspondent to the type of CNC machine chosen to study.
2. The tribology mode of the moving table should be chosen by taking the mainstream of the component selection in the CNC machining industry into account.
3. It is necessary to consider the solution of fixation to both the guiderail and the ball screw, to minimise the stress caused by the equipping.
4. The thermal deformation of each component should consider.
5. The deformation caused by the joining of the ball screw through moving table should consider as well.

5.3.1.2 Instrument Selection and System Component Parameters

1) According to the technical document of the CNC machine (Danford, Matthew, 2007 and Gorasia, 2009), the guiderail utilised on the keen mill is circular ones in major, some use triangular ones or rectangular ones. The length is from 340mm to 800mm, which with the diameter of the circular ones is from 16mm to 25mm. Therefore the parameter of the selected guiderail, ball bearing and ball screw is shown on the below **table 5-2**:

Table 5-2 Parameters of the components

	Length	Diameter	Number	Tolerance
Shaft	500mm	16mm	2	0 ~ 11μm
Ball Screw	510mm	20mm (outside) 16mm (inside)	1	±20μm
Ball Bearing	44mm	3.175mm	2 bearings 50 balls in 5 rows	0 ~ -9μm

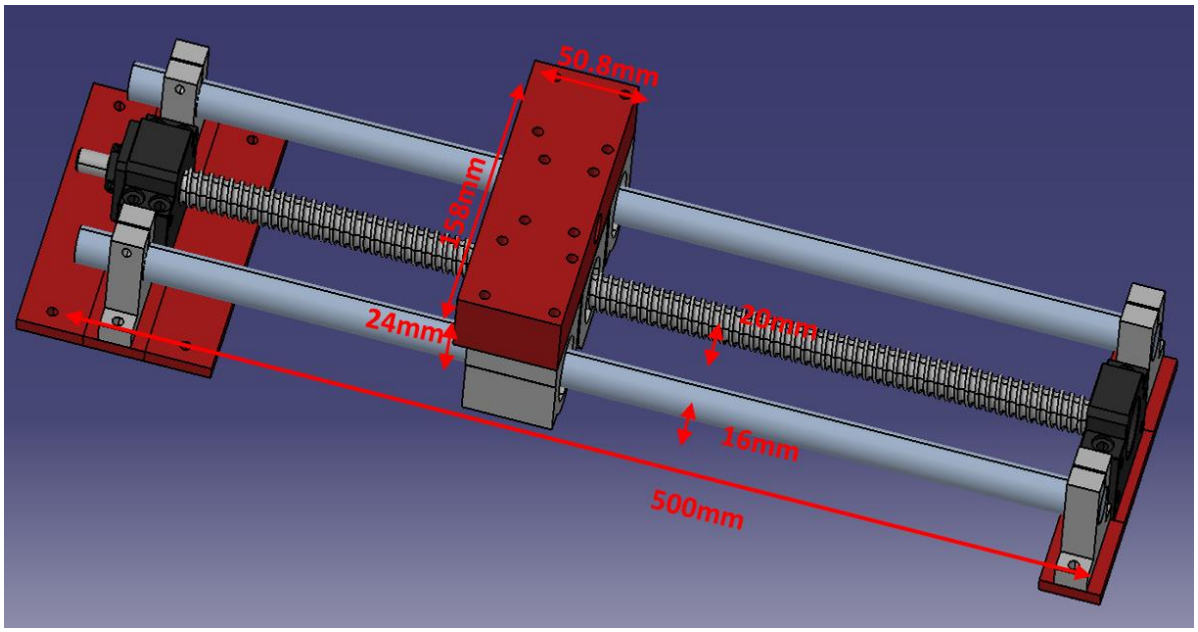

Figure 5-3 Configuration of the guiderail and ball screw

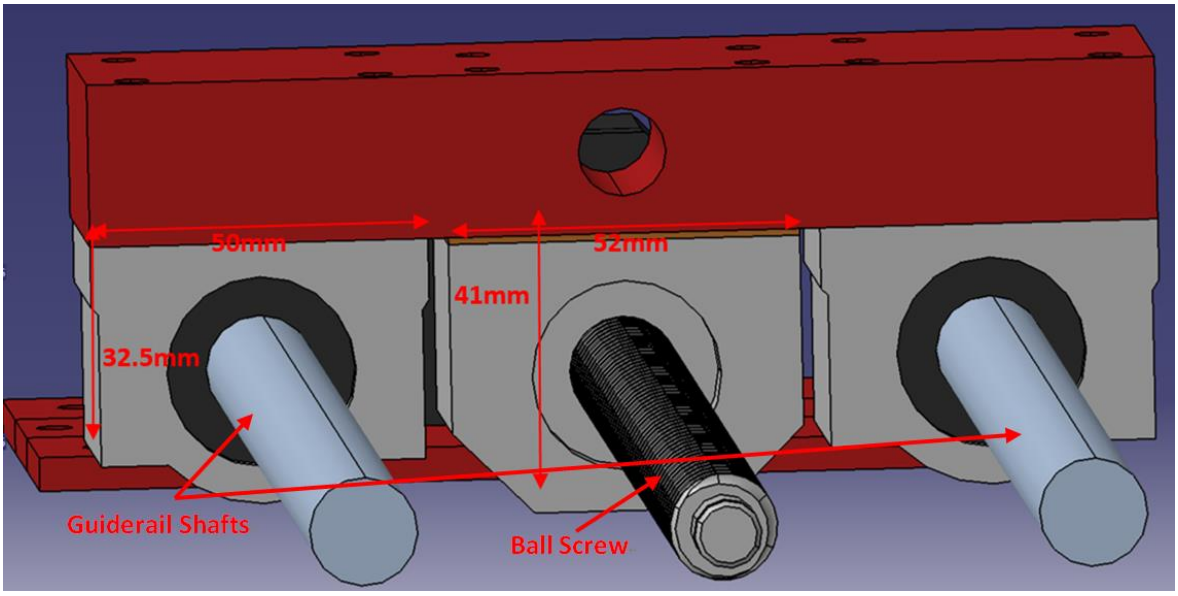

Figure 5-4 Configuration of the ball bearings

2) While equipping the guiderail rig, the base shall settle on a flat marble base to make sure the equipping against deviation. The guiderail shaft and the ball screw are fixed with supports on each side. All the components are fixed with bolts on the panel (**Figure 5-4**).

The instability caused by vibration from the motor and the rolling table may bring deviation to the parallelism of the shafts and ball screw (**Figure 5-5**).

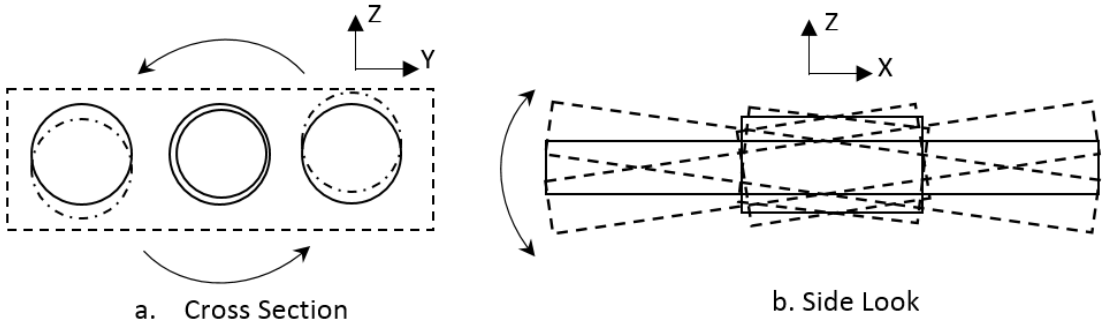

Figure 5-5 The deviation to the parallelism of the guiderail shafts and the ball screw

Therefore, building up a frame to the whole system is necessary. The rectangular frame shows in **Figure 5-6**. The bars of the frame is aluminium and with the inner structure shows in **Figure 5-7**.

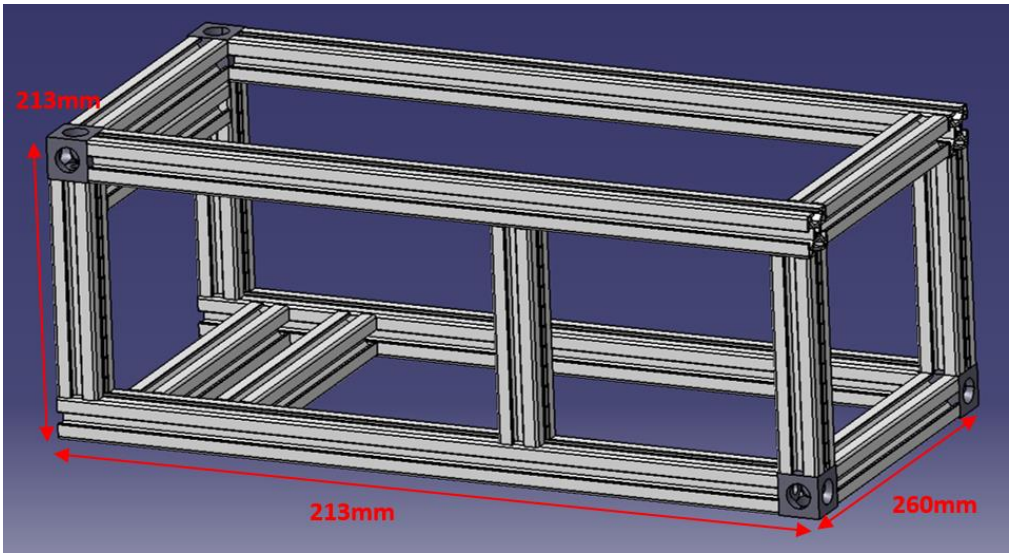

Figure 5-6 The frame built up for the rolling system

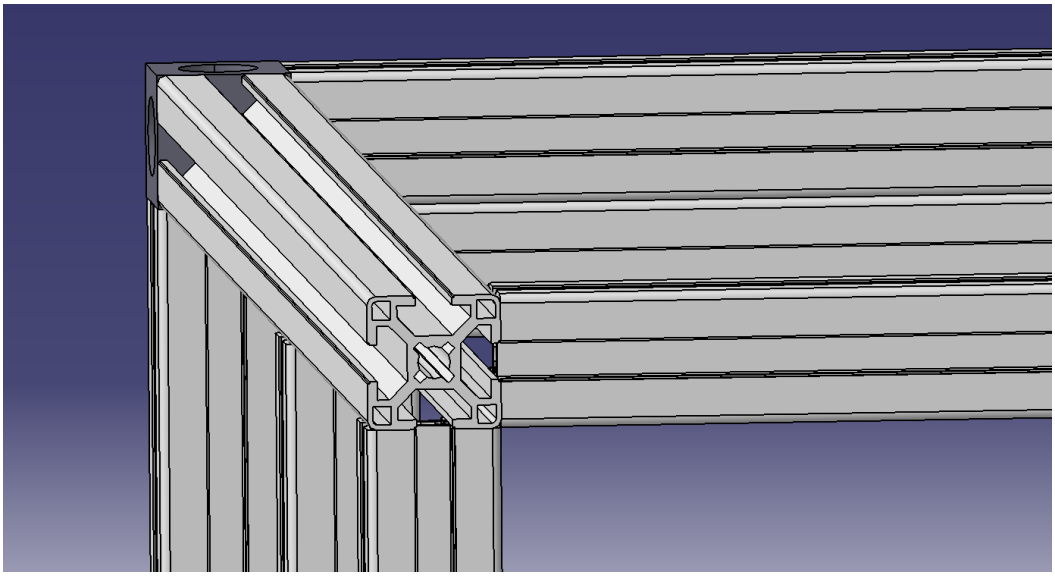

Figure 5-7 The cross section of the frame material (aluminium)

The rig frame (including the aluminium frame and the foundation of driving system) is based on an experiment rig of PHD program and revised in this project. The structure parameter is shown in the following figures from **Figure 5-8** to **Figure 5-9**.

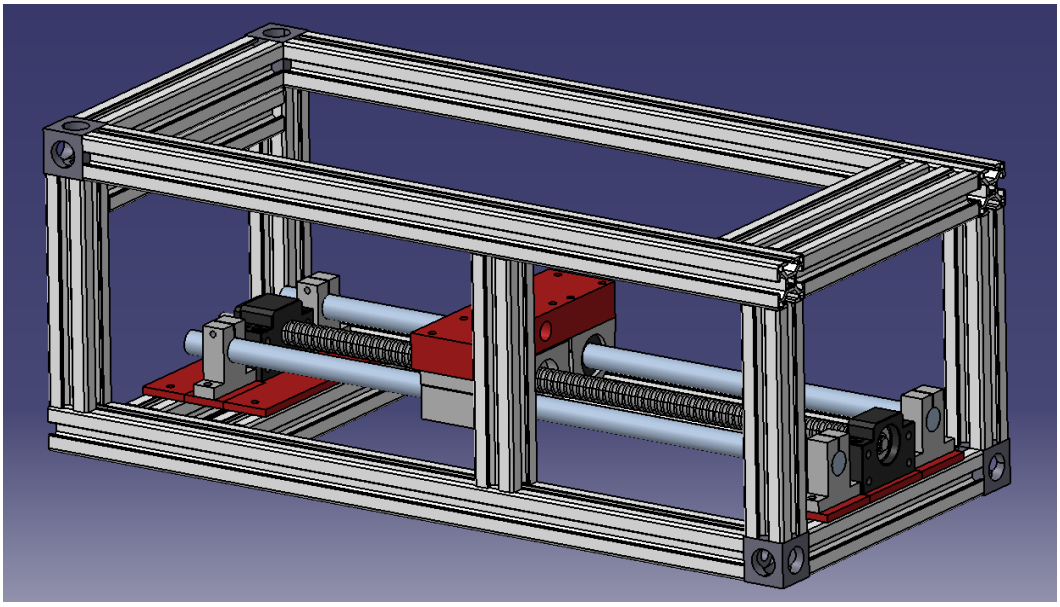

Figure 5-8 The frame and the rolling system equipped part 1

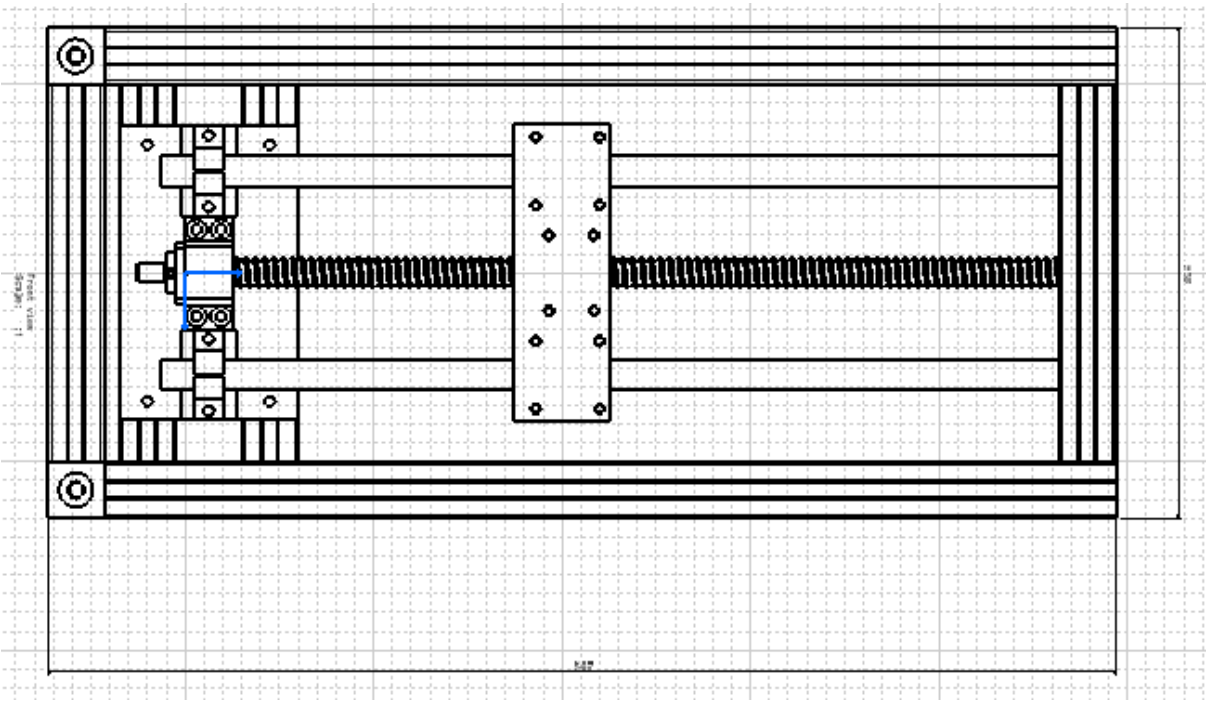

Figure 5-9 The frame and the rolling system equipped part 2

5.3.1.3 Uncertainty Analysis

The error resources and the value of uncertainty are as following:

- Frame straightness error:

  In this section, the tolerance is defined as t, length of the structure is l.

Since the tolerance of the chosen aluminium structural frame is 0.3mm maximum for 2000mm long, the width of the frame is 158mm, therefore the value of the error is:

$$u_f = t \times \frac{l}{2000} = 0.3 \times \frac{158}{2000} = 0.023mm \quad (5.1)$$

- Guiderail support base panel flatness & assembly error:

  Since the flatness tolerance of the chosen aluminium panel is 0.1mm maximum for 1000mm long, therefore the value of the error is:

$$u_{pf} = t \times \frac{l}{1000} = 0.1 \times \frac{100}{1000} = 0.01mm \quad (5.2)$$

  Since the deflection permissible of the aluminium panel with 4mm thickness is$\pm 1\%$, therefore the value of the assembly error is:

$$u_{pa} = t \times \frac{l}{1000} = 0.01 \times 4 \times \frac{100}{1000} = 0.004mm \quad (5.3)$$

- Support error& assembly error:

  According to the data sheet of the linear shaft support, the tolerance of the support is 0~0.02mm. Since there are two shaft supports, the value of support error in the system is 0.04mm. The value of the assembly error is:

$$u_{sa} = t \times \frac{l}{1000} = {}^{0.01}/_{2} \times 8 \times \frac{48}{1000} = 0.00192mm \quad (5.4)$$

- Shaft error:

  According to the data sheet of the linear shaft, the tolerance of the shaft is 0~0.011mm. Since there are two shaft supports, the value of supportu_s error is 0.022mm.

- Ball bearing shell error:

  According to the data sheet of the ball bearing, the tolerance is 0~ -0.013mm. Since there are 2 shaft supports, the value of the support $u_b$error is 0.026mm.

- Table error and assembly error:

  Since the flatness tolerance of the chosen aluminium panel is 0.1mm maximum for 1000mm long, therefore the value of the error is:

$$u_{pf} = t \times \frac{l}{1000} = 0.1 \times \frac{158}{1000} = 0.016mm \quad (5.5)$$

  Since the deflection permissible of the aluminium panel with 4mm thickness is$\pm 1\%$, therefore the value of the assembly error is:

$$u_{pa} = t \times \frac{l}{1000} = {}^{0.01}/_{6} \times 24 \times \frac{158}{1000} = 0.006mm \quad (5.6)$$

- Table moving deviation error:

  The Deviation of the moving table can be separated into 3 directions following X, Y and Z directions, according to the manual of ball bearings, the tolerance of the ball bearing is 9μm. Therefore the deviation can be:

  X-direction error: u_{bx} is $0.009mm$;

  Y-direction error: u_{bx} is $0.009mm$;

  Z-direction error: u_{bx} is $0.009mm$;

5.3.2 Drive System

The driving system is connected to the ball screw to drive the table move to align with X axis repeatedly, to simulate the movement in actual CNC machining process.

The foundation of driving system is also based on the experiment rig of PHD program owned by Dr Cristobal.

5.3.2.1 Design Consideration

a. The movement of the motor should be smooth enough on the settled speed.
b. The propulsion of the motor should be just above the necessary kinetic driving force but should not higher than one order of magnitude because the over high propulsion may overcome the phenomenon of unsmooth behaviour caused by wear.
c. The motor shall be controlled by a driver. The driver is capable of settling the moving speed in advance. It is to change the moving speed according to the experiment plan.

5.3.2.2 Instrument Selection

1) Comparison between stepper motor and servo motor

Stepper Motor: Stepper motor is the type of open-loop control motor, the rotation of the motor is controlled by the driver and the control unit, usually with

ARDUINO program. The controller transfers the electric pulse signal to angular displacement. It rotates by steps according to the pulse period.

The features of the stepper motor are:

a. Well sustainability: Since the stepper motor would be under relatively firm retentive force supplied by the magnetising current. Therefore the sustaining to stasis would achieve by stepper motor without having a mechanic brake.
b. Easy to achieve angular control and speed control, the angular is positive to the pulse.
c. With high torque and well responsiveness.
d. The error of each step will not accumulate any further.
e. Cost effective.

Servo Motor: It is the system with motor, encoder, disc driver and close-loop control system to guarantee the resolution. It outputs constant torque with settled angular speed.

The features of the servo motor:

1) With high reliability and so as to the const.
2) Parameters of the controlling system need to set according to the structure rigidity and load condition. The utilising of the component is relatively complicated.
3) Better performance in high speed working condition.
4) When the terminal load has a wide range of change, the servo motor has better stability.

   The comparison is on the **Table 5-3** in below:

Table 5-3 Comparison Result

	Stepper Motor	Servo Motor
Low speed reliability	√	X
Location precision control	√	√
Control and program operability	√	X
Cost efficiency	√	X

Therefore, the conclusion of the comparison is:

Stepper motor: applicable to stable terminal load, simple movement, low speed;

Servo motor: applicable to terminal load, complex movement, high speed.

To the system in this thesis, stepper motor is more suitable.

2) Stepper motor selection:

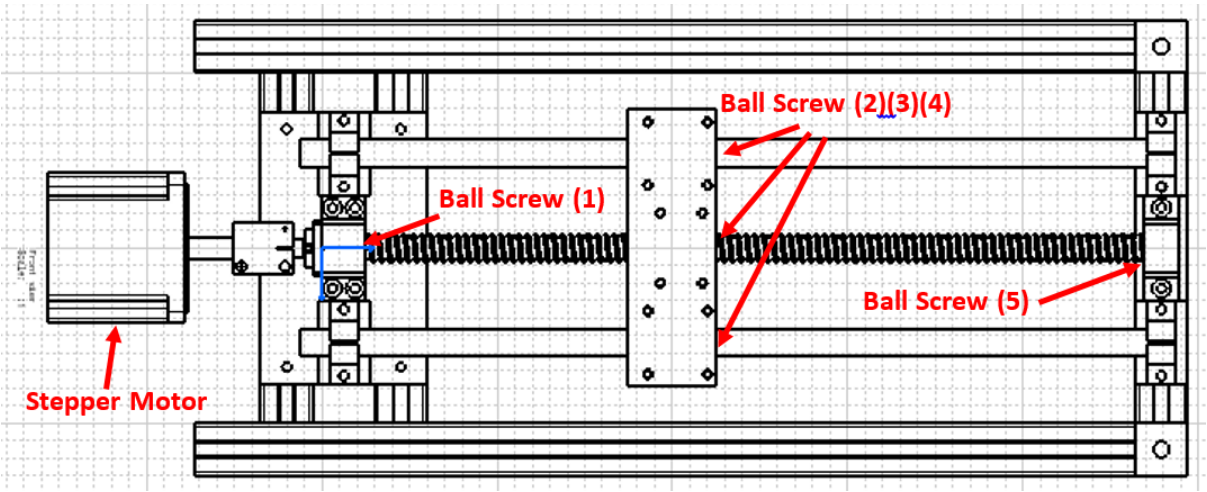

Figure 5-10 Top View of the Rig with Stepper Motor

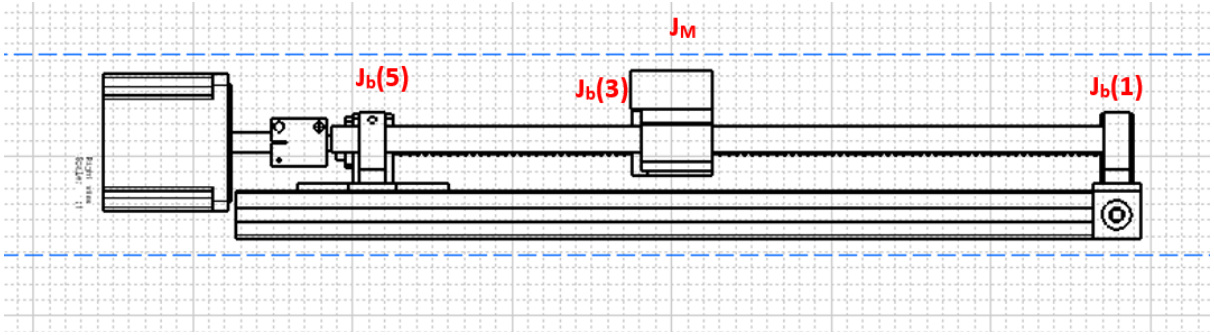

Figure 5-11 Side View of the Rig with Stepper Motor

The rotational inertial of the system is the combination of 3 ball bearings on the ball screw (**Figure 5-10** and **Figure 5-11**) and also the weight of the working table (diameter of the bearing balls r_b is 3mm, the number of balls in the ball bearing 1 and 5 n_B is 15 each, weight of each ball m_b is 0.89g, weight of the shaft m_{shaft} is 0.63kg, radius of the shaft r_{shaft} is 8mm and the length h_{shaft} is 500mm, the weight of the ball bearing m_B is 189g and the table panel m_{panel} is 1.4915kg):

$$J_L = J_{B1} + J_{B3} + J_{B5} + J_{shaft} + J_w$$

$$= n_{B1} \times r_b^2 \times m_b + n_{B3} \times r_b^2 \times m_b + n_{B5} \times r_b^2 \times m_b$$

$$+ \frac{m_{shaft}}{12}\left(3{r_{shaft}}^2 + {h_{shaft}}^2\right) + \left(3 \times m_B + m_{panel}\right) \times (P \,/\, 2\pi)^2$$

$$= 15 \times 1.515^2 \times 0.89 \times 10^{-3} + 15 \times 4 \times 1.515^2 \times 0.89$$

$$\times 10^{-3} + 15 \times 1.515^2 \times 0.89 \times 10^{-3} + \frac{0.63}{12}(3 \times 0.8^2 + 5^2)$$

$$+(3 \times 189 \times 10^{-3} + 1.4915) \times \left({}^{0.5}/_{2\pi}\right)^2$$

$$= 180.225 \times 10^{-5} + 1.41 + 0.1014$$

$$\approx 1.52\ (kg \cdot cm^2) \qquad (5.7)$$

The frequency of the excitation signal and maximum driving signal are:

$$f_0 = (N_0/60) \times (360/\theta_S)$$

$$= (500/60) \times (360/1.8)$$

$$= 1660Hz \tag{5.8}$$

$$f_1 = (N_1/60) \times (360/\theta_S)$$

$$= (800/60) \times (360/1.8)$$

$$= 2560Hz \tag{5.9}$$

The moment of force to the load is:

$$T_L = [\mu(m_{shaft} + 3 \times m_B + m_{panel}) \times g \times {}^{P}/_{2\pi}] \times 10^{-2}$$

$$= [0.04(0.63 + 3 \times 189 \times 10^{-3} + 1.4915) \times 10 \times {}^{0.5}/_{(2 \times 3.14)}] \times 10^{-2}$$

$$\approx 8.56 \times 10^{-3}(N \cdot m) \tag{5.10}$$

Taking the acceleration period t is 2 seconds, therefore the moment of acceleration force Ta is:

$$T_a = J_L \left(\frac{\pi}{180}\right) \theta_s \left[\frac{f_1 - f_0}{t}\right] \times 10^{-2}$$

$$= 1.52 \times (\tfrac{3.14}{180}) \times 1.8[\tfrac{2560-1660}{2}] \times 10^{-2}$$

$$\approx 0.214(N \cdot m) \tag{5.11}$$

Thus the moment of moment of driving force T is:

$$T = T_a + T_L$$

$$= 0.214 + 8.56 \times 10^{-3}$$

$$\approx 0.22(N \cdot m) \tag{5.12}$$

It is to say that while driving the system to run by stepper motor, the holding torque of the stepper motor should be more than $0.22N \cdot m$. Then, the stepper motor with model number Nema 17, which with the holding torque of $0.44\ N \cdot m$, is selected.

5.3.2.3 Data Acquisition and Analysis

The stepper motor is driven by the stepper motor driver and also controlled by the Arduino, the following (**Figure 5-12**) is the wiring graph:

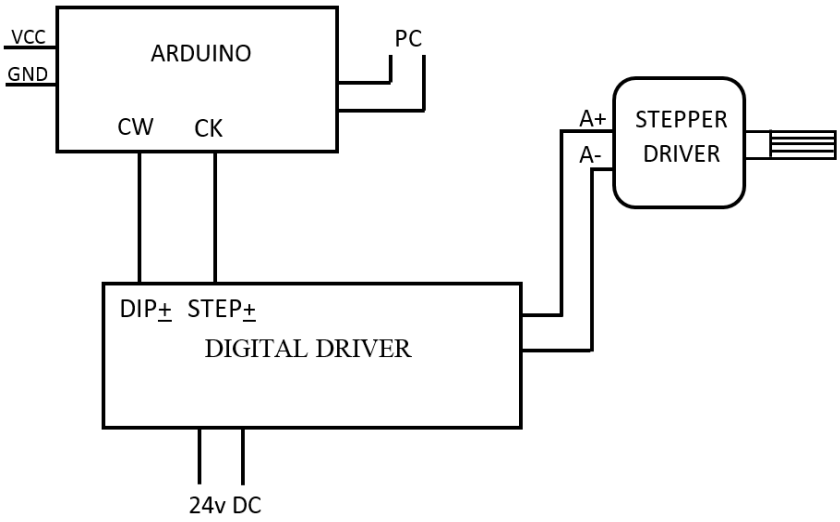

Figure 5-12 Wiring Graph of the Motor Controller

5.3.2.4 Uncertainty Analysis

According to the data sheet, the step motor has the tolerance of +/- 5% non-accumulative error regarding the location of any given step. Therefore, the selected stepper motor with 1.8 degree steps will be within a 0.18-degree error range. Since there is no movement on Z axis lead by stepper motor, the Z axis error contributed by stepper motor can be considered as zero. The resulting in linear error on X axis Um is (the angle speed shall be transferred in to linear speed:$^{\omega_{error}}/_{2\pi}$):

$$u_m = P \times (^{\omega_{error}}/_{2\pi})$$

$$= 5 \times (\frac{0.18}{2\pi})$$

$$= 0.0025mm \quad (5.13)$$

5.3.3 Linear Position Monitoring System

In the experiment design, relative position of the moving table is considered as the reference (X axis value of the final data figure) for the further comparison and calculation to each particular value rather than the time. Therefore, in the system, monitoring to the position while moving on the guide rail is another crucial case in the whole design.

5.3.3.1 Design Consideration

d. The resolution of the linear sensor should be accordant to the wear size level.
e. The linear position sensing equipment shall not interfere the Y axis moving, vibration caused by the roughness increasing and the deviation on multiple directions.

5.3.3.2 Instrument Selection

1) Linear encoder

The mechanism of the linear encoder is detecting and measuring changes in position by on/off sequence in contactless approach. It provides a defined number of digital pulses (5-V DC typically) per revolution or per unit. The resolution of the linear encoder may reach to 1nm at a maximum rotating speed of 100m/s.

However, the linear encoder needs to be mounted on the side of the moving table and causes unnecessary weight and gravity centre deviation.

2) Inductive sensor

An inductive sensor (**Figure 5-13**) is a non-contact device that monitors ratio changes in impedance (effective resistance) of a coil to get the positioning information. The produced voltage changes with the inductance of the coil and proportional to the position. The product can reach to the resolution on micrometre level.

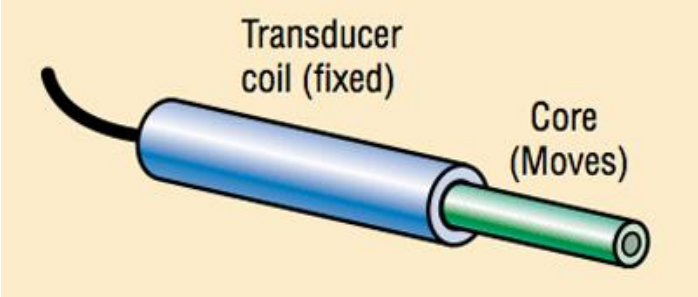

Figure 5-13 Mechanism of the Inductive sensor (Hydraulics & Pneumatics, 2012)

3) LVDTs (linear variable-differential transformer) and MVDTs (magnetostrictive linear displacement transducer)

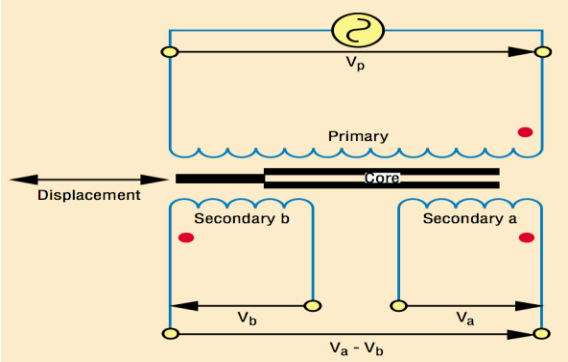

Figure 5-14 Mechanism of LVDTs (Hydraulics & Pneumatics, 2012)

LVDTs (**Figure 5-14**) is a non-contact transducer that converts linear displacement into an identical electrical output signal. The output voltage contains two properties: the amplitude which proportional to the position and the phase which indicates the direction of moving behaviour.

MLDTs (magnetostrictive linear displacement transducer):

A magnetostrictive position transducer is also a non-contact device that detects the position of a magnet. The magnet moves along the length of the sensing element and is attached to the object whose position is to be determined.

4) Resistive sensor:

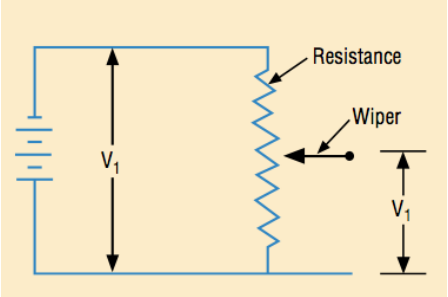

Figure 5-15 Mechanism of Resistive sensor (Hydraulics & Pneumatics, 2012)

The resistive sensor is also commonly known potentiometer. An electrical circuit with constant voltage is produced across the conductive strip. A wiper moves along the strip, from which it picks up voltage (Figure 5-15). Voltage increases as the wiper moves closer to the positive end of the strip and it is proportional to the positioning.

Table 5-4 Selection to the 1D positioning sensor with requirement

REQUIREMENTS	LINEAR ENCODER	INDUCTIVE SENSOR	LVDTs	MAGNETOSTRICTIVE	INTERFEROMETER
Measurement Resolution: 1μ m	√	√	√	√	X
Accuracy: 1μ m/m	√	√	√	√	X
measurement Range (linear):±20μ m	N/A	N/A	N/A	N/A	N/A
Experiment Rig Length: 300-400mm	√	√	X	√	√
Rig Components Scales: 1) Save space& easy to equip 2) Stiffness; 3) Resist of "crawling"; 4) Resistant to rust;	N/A	N/A	N/A	N/A	N/A
Thermo Affect Response: Option A: Thermal deformation negligible or easy to measure; Option B: Best performance on resistance to thermal;	X	√	√	√	X
Data collection: a. Easy to collect (raw data transform to digital data) b. 0.001 second sampling precision	X	√	√	√	X
Low costs &Easy to get the product	√	√	X	√	√

Therefore, as a product, the proper choice of the linear sensing part is the inductive sensor (As can be observed from **Table 5-4**, rationale of choice is provided). However, concerning about the design to the following experiment in this project is aiming to validation to the principle, so the finally chosen sensor is the potentiometer with a resolution of millimetres.

5.3.3.3 Data Acquisition and Analysis

Resistive sensors are not generally provided with any form of signal conditioning electronics. The user is responsible for ensuring that appropriate electrical parameters are evaluated. These parameters include - but are not limited to - excitation voltage, power dissipation, and wiper current, as it relates to the input impedance of the controller. The signal can be adopted and transferred to digital data by DAQ equipment and analysed by computer via LABVIEW.

5.3.3.4 System Component Parameters

In the system, the adopted potentiometer is the 115L08E502 produced by VISHAY. The main specifications are illustrated in the following **Table 5-5**:

Table 5-5 Parameters of the potentiometer

Travel Range	25mm ~ 1000mm
Accuracy	≤ ± 0.05% for ≥ 100mm ≤ ± 0.025% for ≥ 200mm
Resolution	1mm
Temperature	-55˚C ~ +125 ˚C
Working Power Supply	+9V

5.3.3.5 Uncertainty Analysis

According to the data sheet, the potentiometer has the tolerance of +/- 0.05% while the measuring size is over than 100mm. Meanwhile, since there is no movement on the Z axis driven by the stepper motor, the Z axis error

contributed by the stepper motor can be considered as zero. Therefore, the resulting linear error from the selected sensor in the wear area (200~300mm) is:

$$u_l = L \times \pm 0.05\% \tag{5.14}$$

Range of the linear error is from 0.1mm to 0.15mm.

5.3.4 Wear Monitoring System

The wear monitoring system shall be the major part of the whole design for which monitoring the symptoms of the wear: non-smoothness and the table deviation.

5.3.4.1 Design Consideration

a. The resolution of the wear monitoring sensors should be in accordance with the wear size level which is on micrometer level.
b. The mounting location of the sensor shall take the following factors into account:
    1. the distance between the wear source and sensor shall be shorten to guarantee that the wear signal can be owned by sensors;
    2. be assured not to diminish the wear signal while transmitting to the sensor from the guiderail and ball bearings;
c. Sampling speed and the working period need to meet the requirement settled;
d. The equipment size needs to be small and components contained in the system should be easy to equip and as less as possible;
e. The capability of avoiding wear-unrelated inference must consider.

5.3.4.2 Instrument Selection

1) Vibration monitoring sensor selection

According to the literature review, the non-smooth behaviour while moving on the guiderail is mainly coming from two resources: guiderail shaft surface asperity and the worn ball bearings.

The first applicable detecting method is mounting the Hall Effect sensor on the stepper motor current wire. The mechanism is that the stepper driver has the function that while the motor is rotating, if the rotational drag from the load increases, then the driver will automatically change the current to increase the impulsion.

Another solution is utilising the accelerometer to monitor the vibration caused by the roughness of the shaft surface. The accelerometer has the function that receives the vibrating signal on the particular direction. Therefore, while using the sensor, it needs to be mounted on the machine in stableness and as close to the vibration resource as possible.

Comparing with the first option, the second one is more suitable to the design because of the following reasons:

1) Monitoring the vibration altitude value is more direct than testing the current change;
2) The implementation of the accelerometer is less complicated comparing with assembling the Hall Effect sensor. Data from the accelerometer is easier to be analysed as well.

Therefore, in the design of this project, the accelerometer is adopted as the non-smooth travelling behaviour monitor and mounted on the top of the table where above the vibration resource – guiderail shaft surface.

2) Rolling table deviation monitoring sensor selection

The deviation of the table (**Figure 5-16**) while rolling on the guiderail can be the motion in vertical direction is termed the vertical vibration mode, the rocking motion θ about y-axis is termed the pitching vibration mode, the rocking motion ψ about z-axis is termed the yawing vibration mode and the rocking motion φ about x-axis are termed the rolling vibration mode.

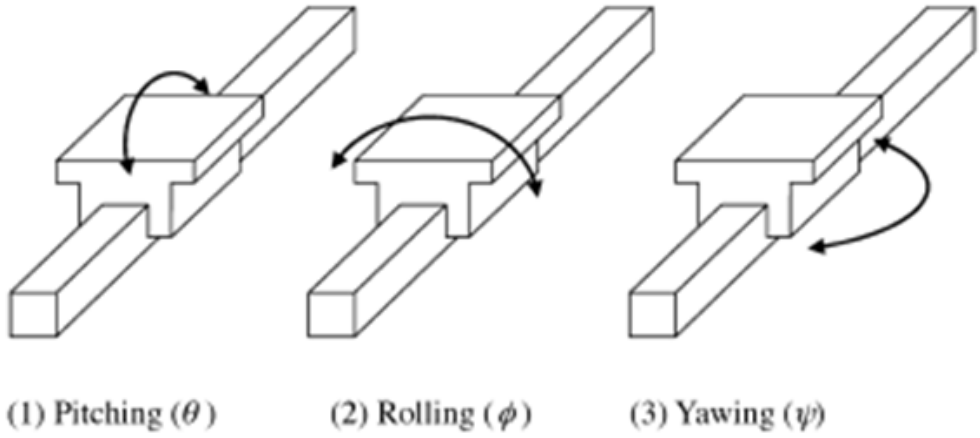

Figure 5-16 Three behaviour modes of the rolling table (Kong, 2012)

According to the literature review, the capacitance probe is chosen as the deviation monitoring sensor. Meanwhile, when deciding the relative position of the sensor shall consider about the fundamental principle of designing precision machining monitoring system, which is:

- The working system shall be separated from the monitor system in case of the crosstalk phenomenon, that the noise from CNC machine would run into the system and make it lose the function as referencing.
- The physical structure of the monitoring system should be based on the "close loop" shape, on the purpose of decreasing the resonance of the system.

Above all, the magnetic stand is placed at the edge of the table to make arms of the stands extend out from the rig as much as possible.

In the system, the rolling behaviour can be monitored by the capacitance probes as the following module (**Figure 5-17**):

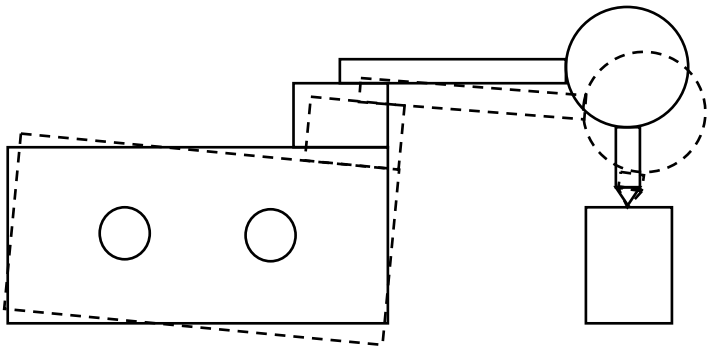

Figure 5-17 Rolling behavior of the Capacitance and Stand Arm

The extreme situation is that the left side of the guiderail has wear on the top surface and the right side of the wear has wear on the bottom surface, as shown in the **Figure 5-18**. In such case, the rolling table reaches the biggest angle of inclination, it can be simplified as the following two triangles:

$$h_0 = m_l + m_r = 0.05 + 0.05 = 0.1mm \tag{5.15}$$

$$sin\emptyset = \frac{h_0}{w_t} = \frac{0.1}{158} = 1/1580 \tag{5.16}$$

In the above formulas, the m_l and m_r are distance of the vertical deviation on each long and short side, w_t is the width of the rig panel.

Situation 1: the base of the stand is located at point A, end of the table:

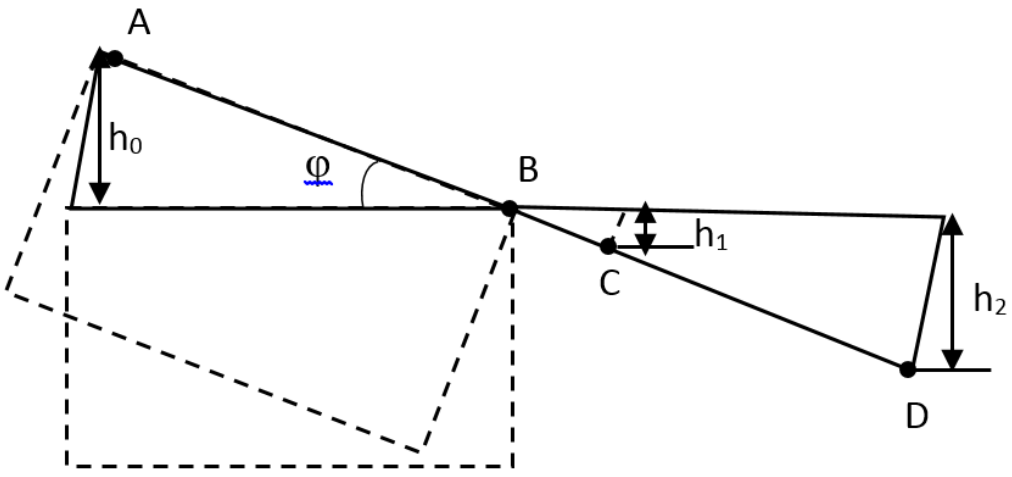

Figure 5-18 Angle and Height of the Deviation

Then the capacitance probe is assembled on point C:

$$h_1 = (l_a - w_t)sin\emptyset = \frac{165-160}{160} = 3 \times 10^{-3}\text{mm} \quad (5.17)$$

Situation 2: the base of the stand is located at point A, another end of the table:

Then the capacitance probe is assembled on point D:

$$h_1 = l_a \times sin\emptyset = \frac{165}{1600} = 0.103\text{mm} \quad (5.18)$$

Conclusion:

Comparing the two different situations, it is evident that placing the base of the stand at point B has more reflection value to the deviation of the table. Then it is easy to measure the changing value via capacitance probes in the experiment.

5.3.4.3 Data Acquisition and Analysis

All the sensors adopted in the design are linked to a DAQ produced by National Instrument. The DAQ is used for receiving the output of those sensors and transferring the signal to digital data. The next stage of the system is using the LABVIEW program to realise the sampling and digital data collection. Collected data from the LABVIEW program is saved in excel files for further analysis and calculate via Matlab. The data collection process is shown in the **Figure 5-19**:

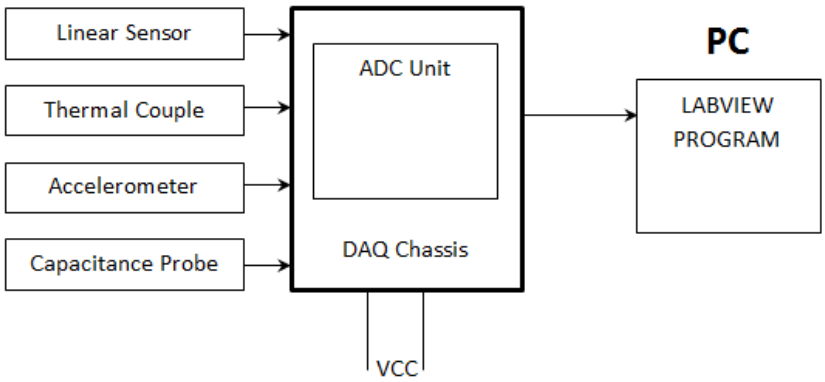

Figure 5-19 Data transferring sequence

The data acquisition sequence of the LABVIEW program shows in the bellowing **Figure 5-20**:

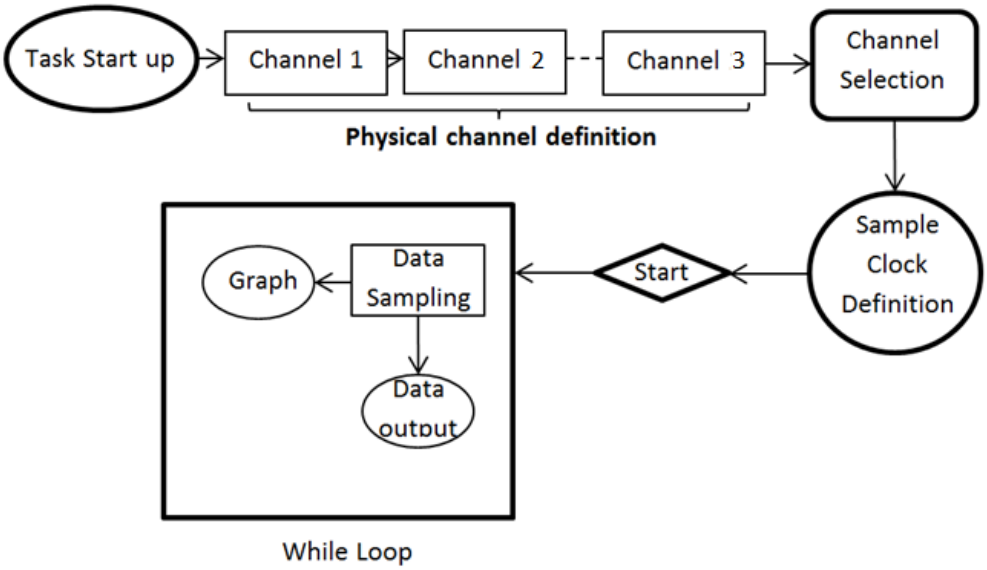

Figure 5-20 LABVIEW Data Acquisition Sequence

5.3.4.4 System Component Parameters

1) Accelerometer: The chosen accelerometer is the one produced by DYTRAN with module number: 3055B2. Parameters are shown on the bellowing **Table 5-6**:

Table 5-6 Accelerometer Parameters

Module number	DYTRAN 3055B2
Sensor direction	Z axis
Sensitivity	100mV/g
Range for output	±50g's
Frequency range	1 ~ 10kHz
Equivalent electronical noise	0.0004g
Linearity	±1%

2) Capacitance probe:

The chosen capacitance probe is PX405HC manufactured by Lion Precision, parameters of the tool provides on the bellowing **Table 5-7**:

Table 5-7 Capacitance Probe Parameters

Module number	Lion Precision CPL190
Sensitivity	1.000Volts/mil
Resolution	0.2μm/mil
Range	±5.000mils
Frequency	flat to 10000Hz; band width (-3dB): 17000Hz;
Linear Error	0.004% of range
weight	60g

5.3.4.5 Design of the stand arm

In the design, the stand arm to the capacitance probe has three options which are with typical vibration resistant structure. They are the “T” shape, “L” shape and the “π” shape. Referring to the settling point of capacitance probe, the length of the stand arm is 200mm and the height is 50.8mm. After FEM simulation, the results of three different shapes (**Figure 5-21**, **Figure 5-22**, and **Figure 5-23**) are as shown in the following (parameters of the simulation are: sin wave vibration with 100N amplitude, 2kHz frequency on one fixed side. The material of the component is aluminium, 5mm thickness):

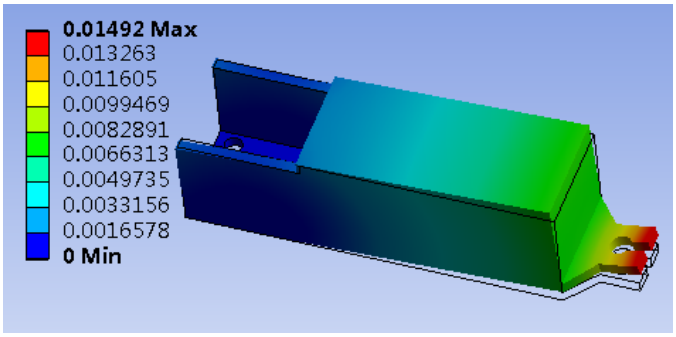

Figure 5-21 “π” shape stand arm FEM simulation result

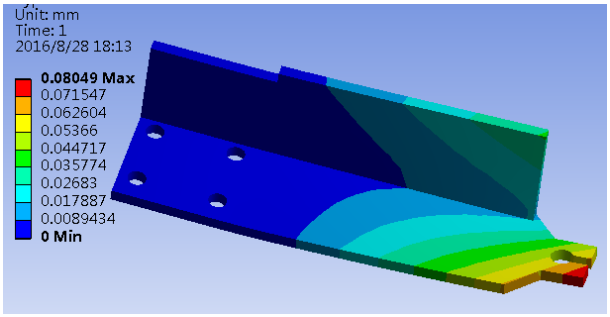

Figure 5-22 “L” shape stand arm FEM simulation result

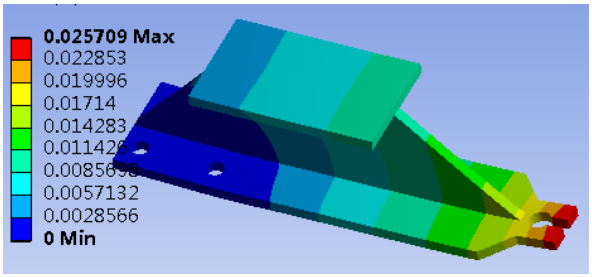

Figure 5-23 “T” shape stand arm FEM simulation result

As can be seen from the result, the “π” shape has the least vibration amplitude in the same condition. Therefore, considering the efficiency of space utilising, the stand arm in the project is designed in a “T” shape which resists the bending utmost, which within 1% of the measuring range. Therefore, since the measuring range is from 10um to 50um, the bending shall be controlled within $\beta=4\times10^{-7}$m.

In the experiment, for the purpose of validation to the principle, the “T” shape stand arm is replaced by anepoxy resin (PTFE) panel made by 3D printing with the length L=158mm and width b=20mm. The thickness of the panel “h” is calculated as below:

According to the formula of the bending, the bending ω_B:

$$\omega_B = -\frac{FL^3}{3EI} \tag{5.19}$$

F is the force, L is the length of the stand arm, E is the elasticity modulus of the material, I is the inertia moment, h is the thickness of the stand arm, b is the width of the stand arm.

$$I = \frac{bh^3}{12} = \frac{(20\times10^{-3})\times h^3}{12} \tag{5.20}$$

$$\omega_B = -\frac{FL^3}{3EI} < \beta \tag{5.21}$$

$$\text{Therefore: } h > (\frac{4F}{b\beta E})^{1/3} \times L \tag{5.22}$$

Considering the weight of the capacitance probe and the signal wire is 100g, the force on the end of the stand arm is:

$$F = 1N \times 2 = 2N \tag{5.23}$$

Therefore, taking E=71×10^9 Pa, the thickness of the panel should be:

$$h > 20mm \tag{5.24}$$

5.3.4.6 Uncertainty Analysis

1. Abbe error 1: Capacitance probe stand arm error:

   The aluminium stand arm has the resolution error of 0.2mm by manufacturing.

2. Abbe error 2: Stand arm assembly error:

   The deflection permissible of the aluminium panel with $l_d = 20mm$thickness is $t = \pm1.8\%$, therefore the value of the assembly error is:

   $$u_{pa} = t \times l_d \times \frac{l}{L} = 0.018 \times 20 \times \frac{158}{1000} = 0.0057mm \tag{5.25}$$

3. Abbe error 3: Stand arm vibration error:

   As calculated, the vibration error brought by the stand arm on Z axis is 0.004mm.

4. Abbe error 4: Probe assembly error:

   The stand arm assembly hole has the drilling tolerance of 0.2mm, which means the assembled probe might have deviation against vertical axis caused by the looseness (**Figure 5-24** and **Figure 5-25**).

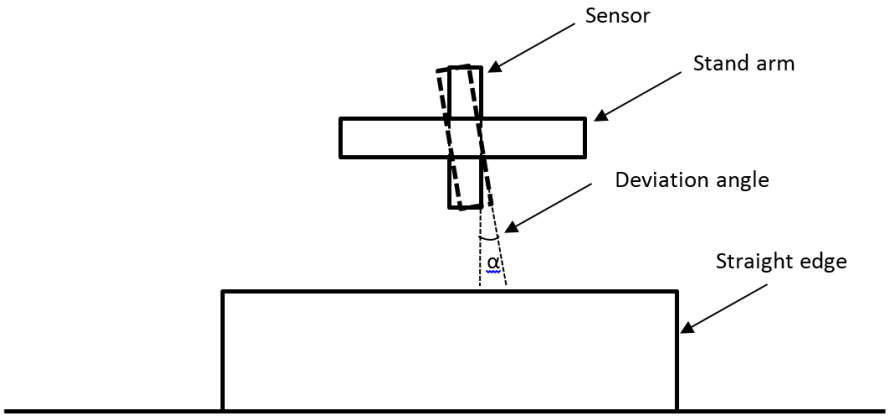

Figure 5-24 Side look of the capacitance probe and the straight edge (1)

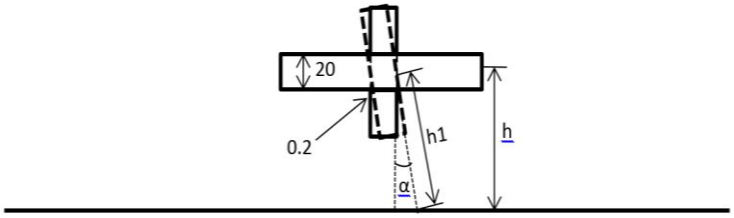

Figure 5-25 Side look of the capacitance probe and the straight edge (1)

In the above figure, the looseness between the stand arm and the sensor is 0.2mm, and α is the deviation angle of the sensor.

$$\cos\alpha = \frac{20}{\sqrt{20^2+(0.2)^2}} = \frac{h}{h_1} \tag{5.26}$$

$$h = \frac{20}{2} + 5 = 15mm \tag{5.27}$$

$$\text{Therefore } h_1 \approx 15.00075mm \tag{5.28}$$

$$u_p = h_1 - h = 0.00075mm \tag{5.29}$$

5. Straight edge flatness error:

   The selected straight edge has the flatness of 0.5μm, which manufactures by the precise machining centre of Cranfield University.

6. Calibration error:

   The capacitance probe has the resolution of 0.0002mm which is on nanometre level.

5.4 In-process Monitoring realisation

As mentioned in the literature review, the ultramodern approach of the CNC machine guiderail monitoring has no resistance to the outer disturbance and the isolated condition for the monitoring process is of necessity. Therefore, the in-process monitoring solution considers as the novelty of the project. In the design, an idea brought from the electronic field is applied and making the offset to the noise and other disturbing vibration via the bi-channel system and leave the signal brought by guiderail wear solely.

The definition of “in-process” is that taking advantage of the idle time slot during CNC machine runs, distinguished from shutting down or processing period.

5.4.1 Design Consideration

a. The resolution of the wear monitoring sensors should be accordant to the wear size level which is on micrometre level.
b. The mounting location of the sensor shall take the following factors into account:
   1) Be mounted vertically above the wear resource;
   2) be assured not to diminish the wear signal while transmitting to the sensor from the guiderail and ball bearings;
c. Sampling speed and the working period need to meet the requirement settled;
d. The equipment size needs to be small and components contained in the system should be easy to equip and as less many as possible;
e. The invulnerability to external disturbance, which means the capability of avoiding wear-unrelated inference must be considered.

5.4.2 Data Acquisition and Analysis

Taking the pair of accelerometers as an example, in the following drawing, sensor No.1 and sensor No.2 are mounted parallel along the guiderail. Therefore the data processing sequence is shown in the **Figure 5-26**. The system adopts data of the accelerometer signal by the same sampling frequency. Then complete the coupling of the data to realise offset to the

disturbance, as is shown in **Figure 5-27**. In the theory, since the physical condition and the sensor selected to the system is the same, the final data represented shall be the signal of the wear solely. The same solution to acquire in-process wear data can be applied to capacitance probes as well.

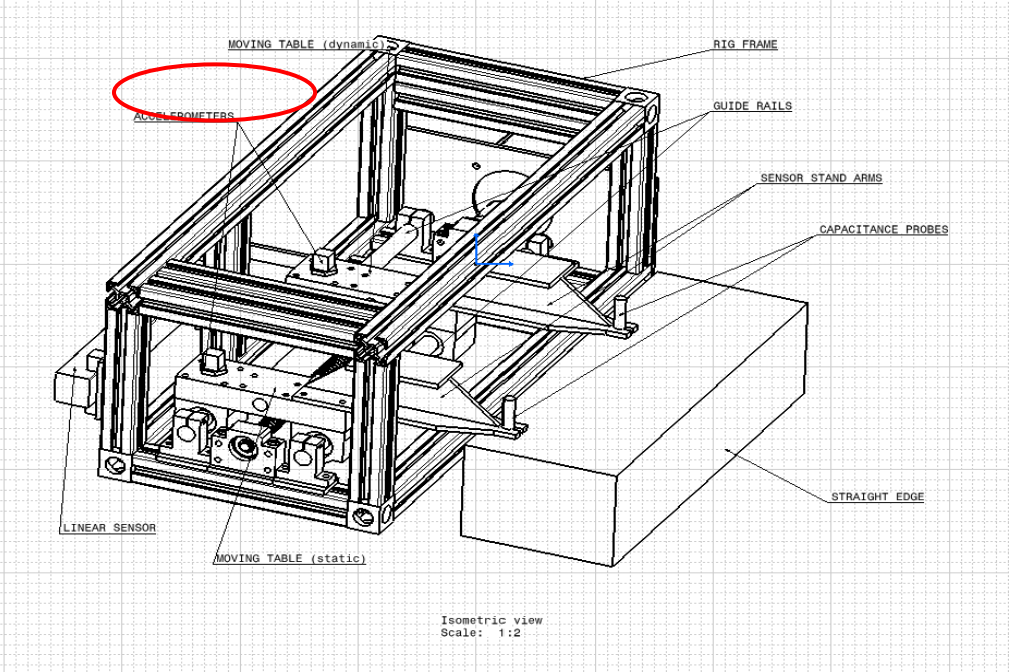

Figure 5-26 The 2D drawing of the experiment rig

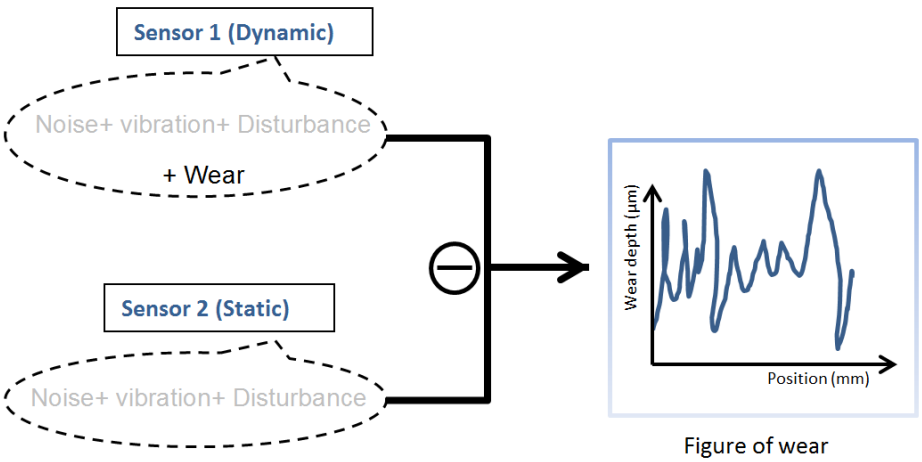

Figure 5-27 In-process data processing sequence

5.4.3 System Component Parameters

The sensitivity of the accelerometer is 100mV/g, which means that each 1V voltage refers to the 10g accelerometer. Meanwhile, the selected capacitance probe in the system has the sensitivity of 1.000Volts/mil. All the sensors' output is analogue signal and needs to be adopted and transfer to digital signals. According to these, the data acquired from the sensors are in voltage, then transfers into acceleration and distance change.

5.5 Experiment & Validation

After the design of the experiment rig, component selection and parameter calculation, the uncertainty analysis shall be calculated first, to anticipate the error brought into the final result. Then based on this, the rig can be constructed under proper control. Then the validation to the theory of in-process monitoring can be completed.

5.5.1 Error Budget

The uncertainty

The calculated error budgets which affect the Z-axis accuracy are on the following **Table 5-8**:

Table 5-8 Error Budget

Source of uncertainty	Value	Units	Probability Distribution	Divisor	Sensitivity Coefficient	Standard Uncertainty
frame straightness	0.023	mm	normal (k=2)	2	1	0.0115
panel flatness	0.01	mm	normal (k=2)	2	1	0.005
Panel assembly	0.004	mm	normal (k=2)	2	1	0.002

Source of uncertainty	Value	Units	Probability Distribution	Divisor	Sensitivity Coefficient	Standard Uncertainty
Support flatness (left)	0.02	mm	normal (k=2)	2	1	0.01
Support flatness (right)	0.02	mm	normal (k=2)	2	0.05	0.005
Support assembly (left)	0.00192	mm	normal (k=2)	2	1	0.00096
Support assembly (right)	0.00192	mm	normal (k=2)	2	0.05	0.000048
Shaft straightness (left)	0.011	mm	normal (k=2)	2	1	0.011
Shaft straightness (right)	0.011	mm	normal (k=2)	2	0.05	0.00055
ball bearing shell (left)	0.013	mm	normal (k=2)	2	1	0.0065
ball bearing shell (right)	0.013	mm	normal (k=2)	2	0.05	0.000325

Source of uncertainty	Value	Units	Probability Distribution	Divisor	Sensitivity Coefficient	Standard Uncertainty
table	0.016	mm	normal (k=2)	2	1	0.008
Table assembly	0.006	mm	normal (k=2)	2	1	0.003
Table deviation	0.009	mm	Rectangular	$\sqrt{3}$	0.33	0.0017
Stand-arm resolution	0.2	mm	Triangular	$\sqrt{6}$	0.05	0.0041
Stand-arm assembly	0.0057	mm	normal (k=2)	2	1	0.00285
Stand-arm vibration	0.0004	mm	normal (k=2)	2	1	0.0002
Straight-edge flatness	0.0005	mm	normal (k=2)	2	1	0.00025
Probe deviation	0.00075	mm	normal (k=2)	2	1	0.00075
Calibration error	0.0002	mm	normal (k=2)	2	1	0.0001

Since the experiment data analysing part is for the calculation of the difference between original value and the value after wear, the stable error which does not change during the monitoring shall not include in the error budget. Therefore, uncertainties affect the measurement accuracy are:

1. Table deviation: $u_{td} = 0.0017mm$
2. Stand arm vibration: $u_{sv} = 0.0002mm$
3. Probe deviation: $u_{pd} = 0.00075mm$

4. Calibration error: $u_{ce} = 0.0001mm$

The combined standard uncertainty of the system u_c is:

$$u_c = \sqrt{(u_{td})^2 + (u_{sv})^2 + \left(u_{pd}\right)^2 + (u_{ce})^2} \quad (5.30)$$

$$= \sqrt{(0.0017)^2 + (0.0002)^2 + (0.00075)^2 + (0.0001)^2}$$

$$= 0.00189m$$

$$= 1.89mm$$

The expanded uncertainty (while K=2.95% confidence) is:

$$U = 1.89 \times 2 = 3.78mm \quad (5.31)$$

Since the measuring range is 10~ 50μm, the percentage of uncertainty p is:

$$p = \left(\frac{3.78}{50-10}\right) \times 100\% = 9.45\% \quad (5.32)$$

5.5.2 Experiment Plan

The whole experiment is based on a marble base in the thermal static laboratory in Precision Machine Centre of Cranfield University. Which means that the disturbance from outside the system is diminished to ignorable level and the temperature during the whole experiment process is stable in 23 degrees, the influence of the temperature is eliminated. The following flow chart in **Figure 5-28** is the general experiment structure:

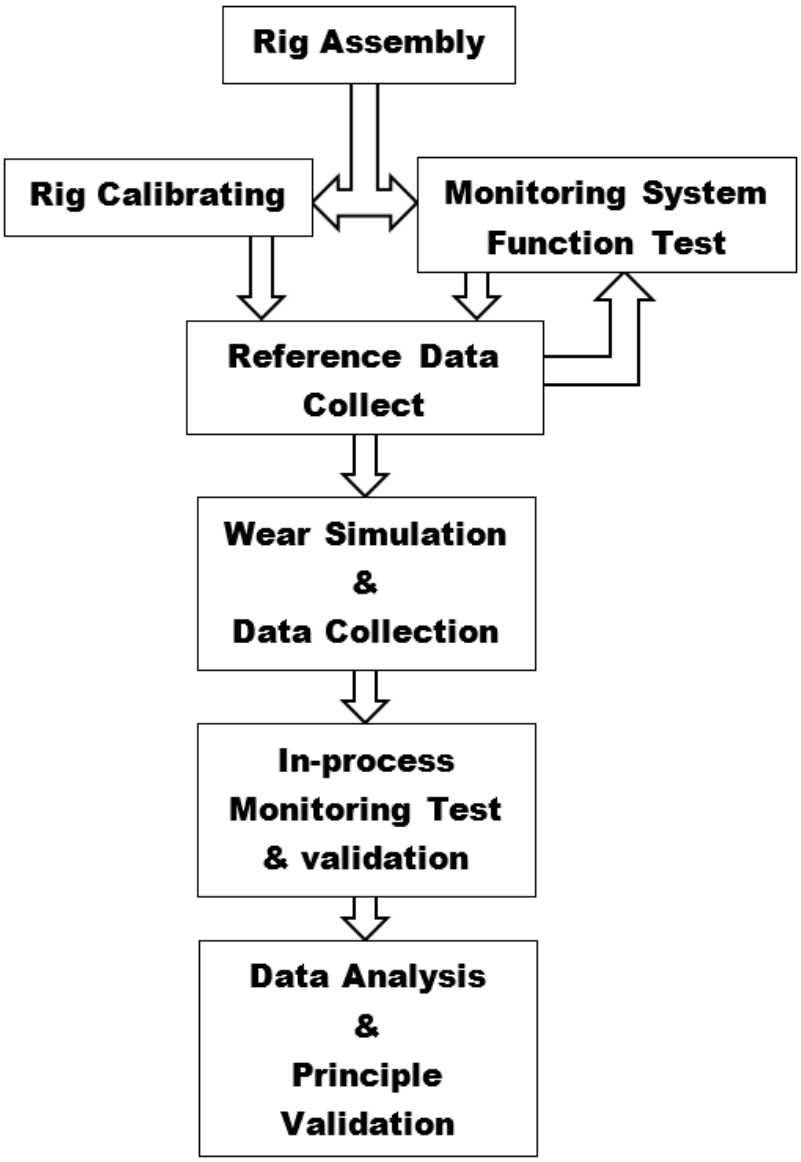

Figure 5-28 Experiment Structure

5.5.2.1 Experiment A:

Experiment Title: Rig Assembly

Experiment Objective: construct the rig according to the 3D drawing for the following experiments

Experiment Content:

1) Complete the rig base establishing (**Figure 5-29**) and test the flatness of the rig base on the marble table.

It is necessary to test if the four edge of the rig base is stable enough.

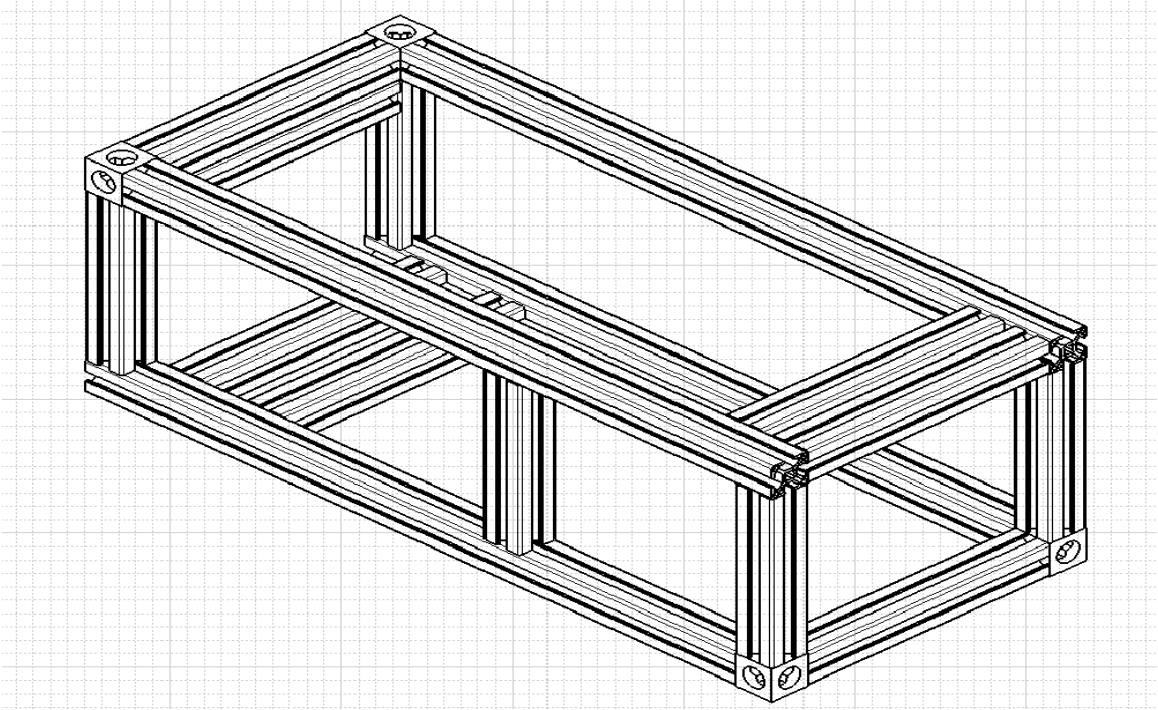

Figure 5-29 The Rig Base

2) Complete the assembly of guiderail components and ball screw components. The guide rail part contains the following components on **Table 5-9,** the completed rig part are shown in figures from **Figure 5-30** to **Figure 5-33**:

Table 5-9 List of Components

Component Name	Number of Pieces
Guiderail shaft	2
Rolling support (including ball bearing)	4
Rolling table	2
Rail shaft support	4
Ball screw	1
Ball nut	1
Ball screw floating bearing	1
Ball screw fixed bearing	1

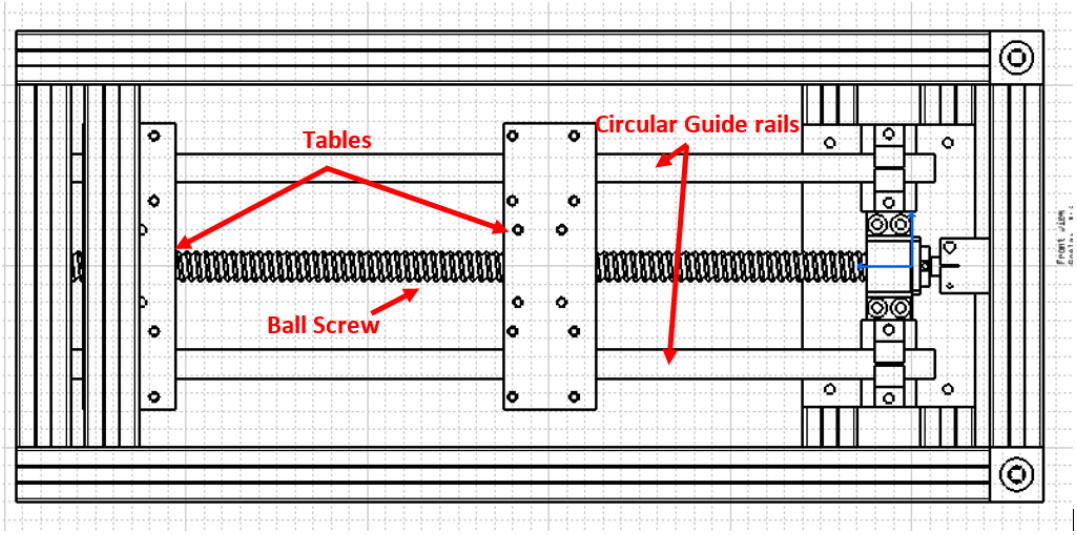

Figure 5-30 Top view of the rig

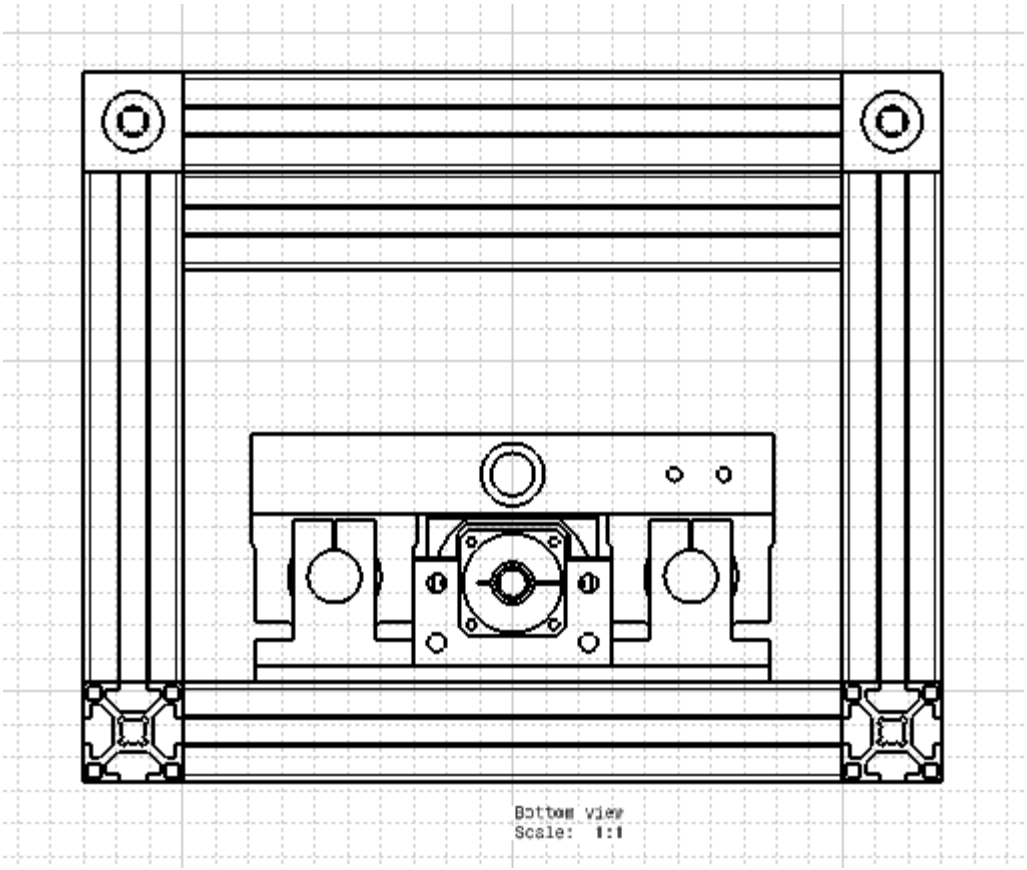

Figure 5-31 Side view on X direction

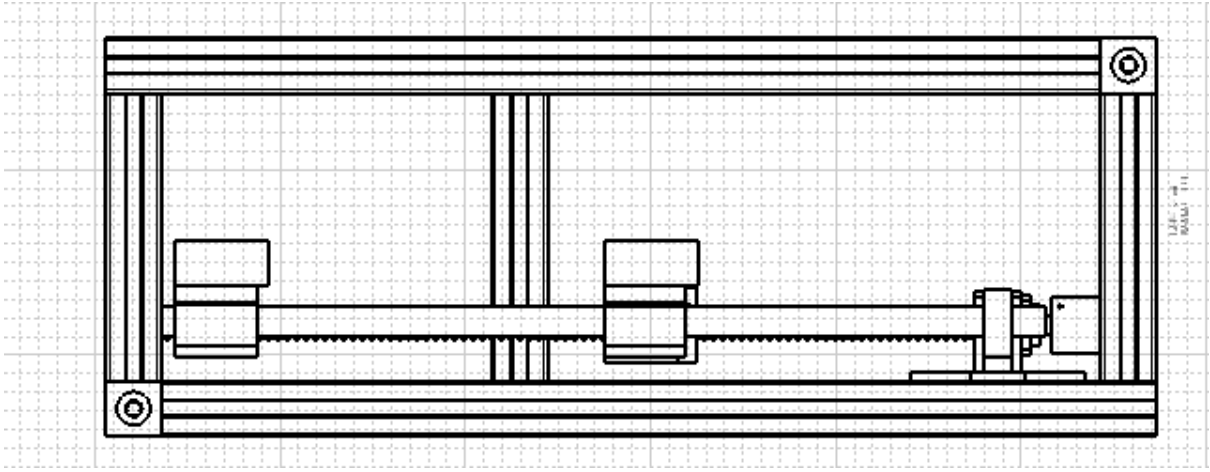

Figure 5-32 Side view on Y direction

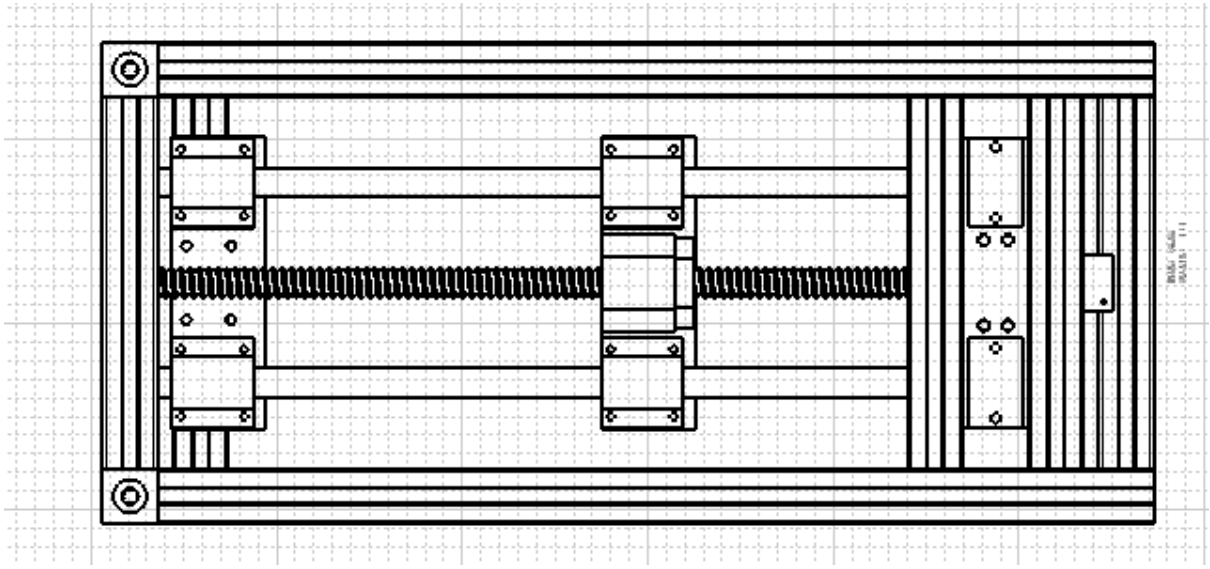

Figure 5-33 Upward view of the rig

3) Retest to confirm if the four edge of the rig base is stable enough after assembling the guiderail components.
4) Using capacitance probes or flatness aligner to test and calibrate the flatness of the table.
5) Complete the assembly of the stepper motor as shown in the **Figure 5-34**:
   A. Complete Fixture of the motor to the machine.
   B. Connect the ball screw with the motor on the coupling.
   C. Complete testing the motor operation by utilising Arduino controller.

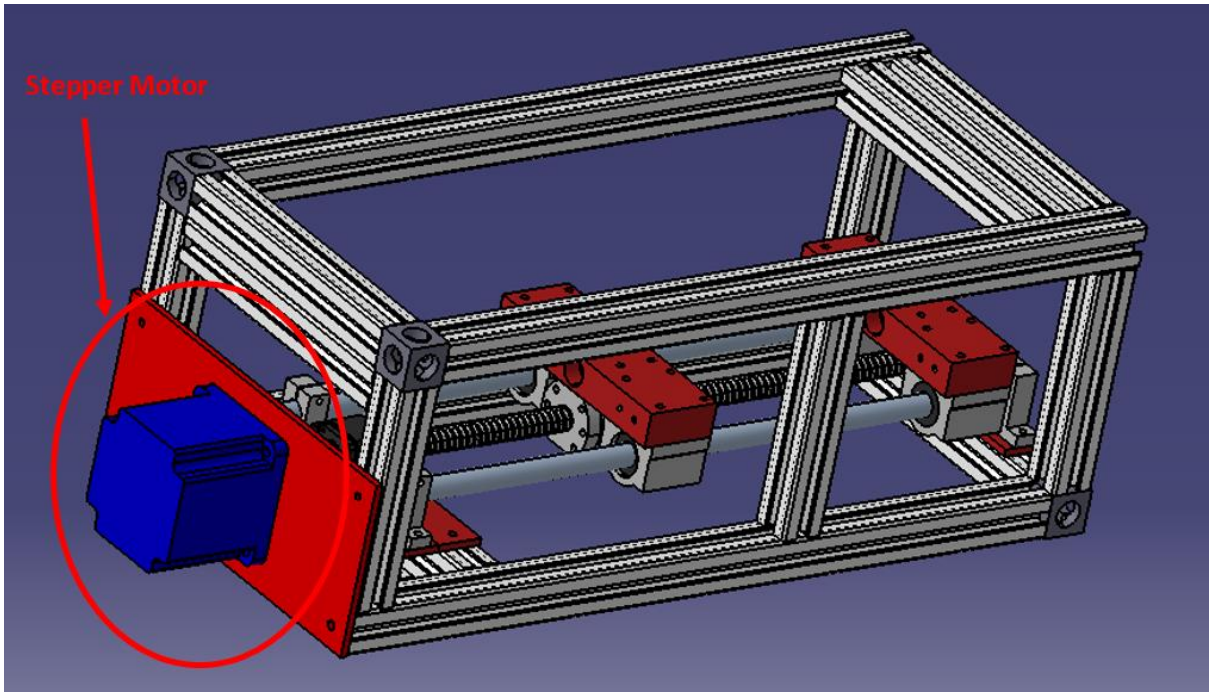

Figure 5-34 Assembly of Stepper Motor

6) Complete the assemble and calibration to the linear sensor as shown in **Figure 5-35**;

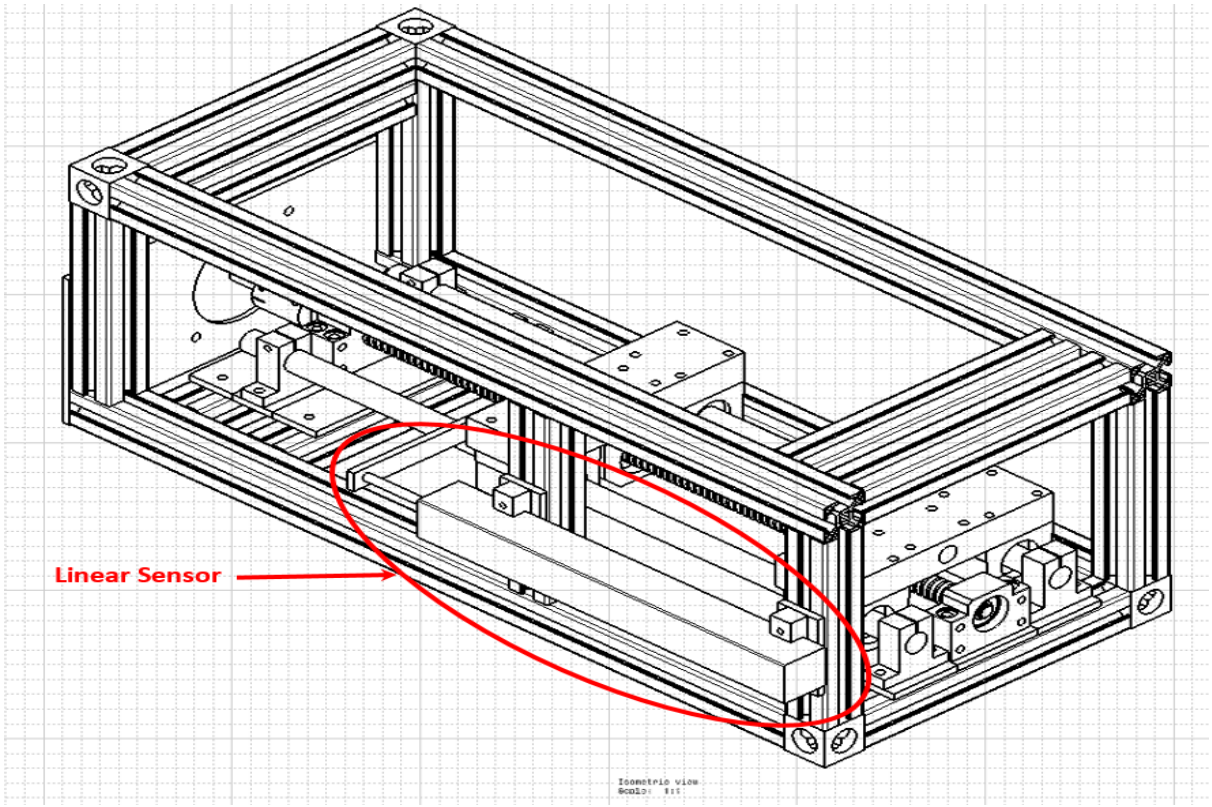

Figure 5-35 Assembly of Linear Sensor

7) Complete allocation to the metal straight edge on the marble base as shown in **Figure 5-36**.

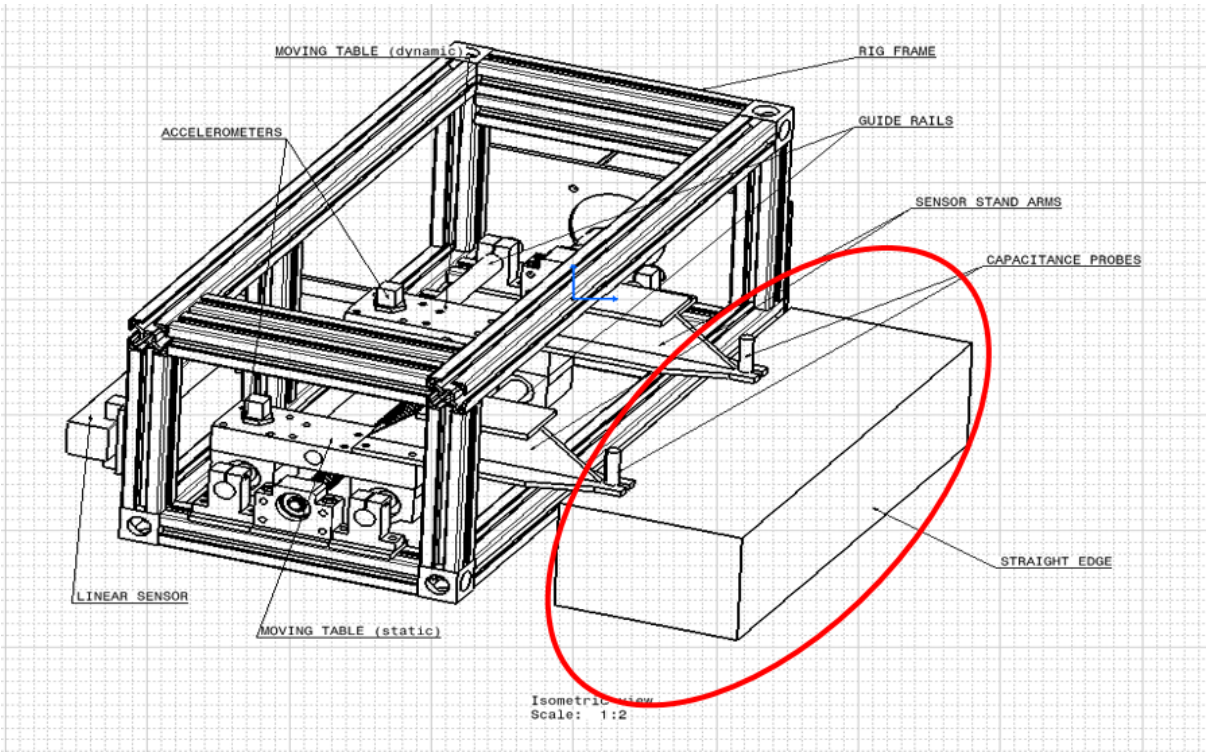

Figure 5-36 Assembly of Straight Edge

8) Use capacitance probe or flatness aligner to test the surface flatness of the straight edge to make sure it meets the requirement (**Figure 5-37**). Meanwhile, make sure the metal straight edge and the rig frame is separated, with relative parallel position, for the purpose of separating the monitoring system and the CNC machine running system.

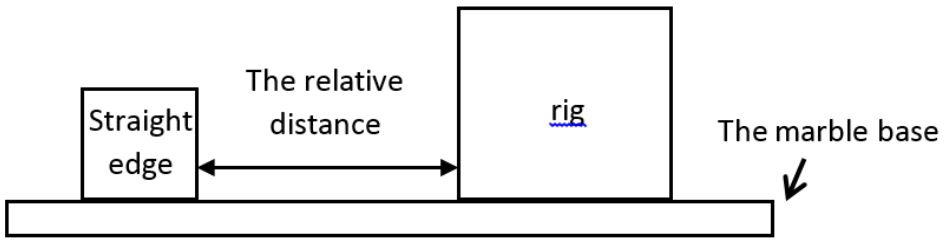

Figure 5-37 Relative Position of Straight and the Rig

9) Complete the assembly of capacitance probe and the sensor stands, calibrate the relative position of the stand in between the straight edge and the rolling/static tables (**Figure 5-38**).

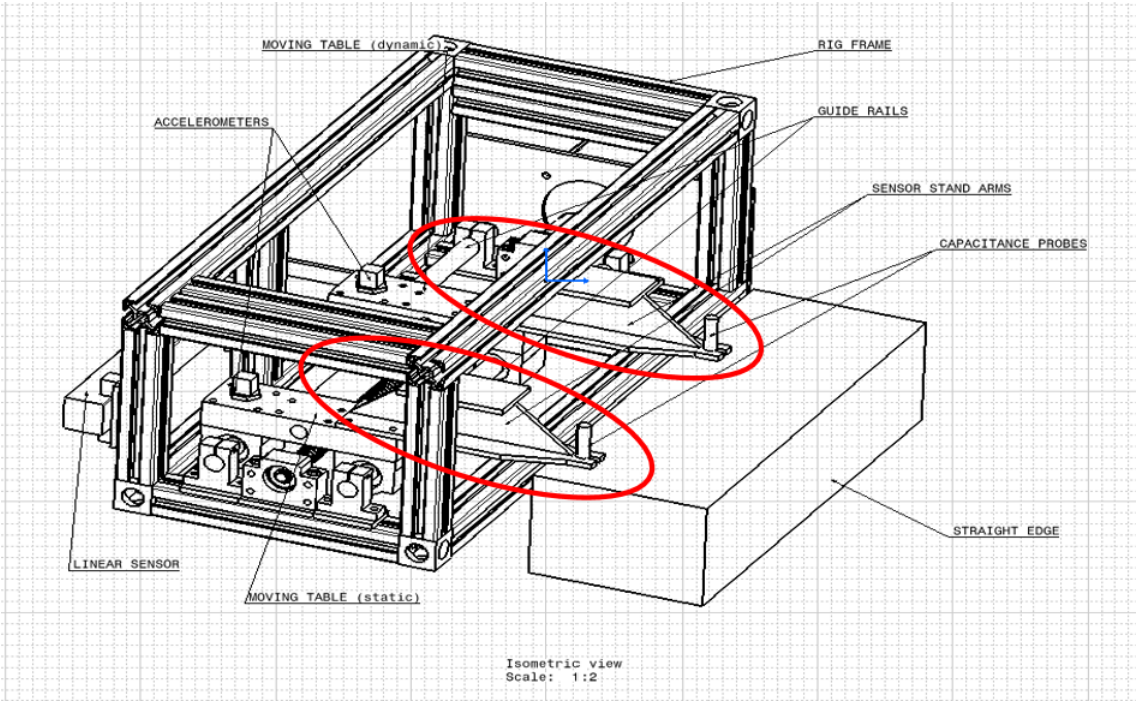

Figure 5-38 Assembly of Capacitance Probes and Stand Arms

10) Complete the assembly to the accelerometer mounting on the top of the rolling table with wax **(Figure 5-39)**.

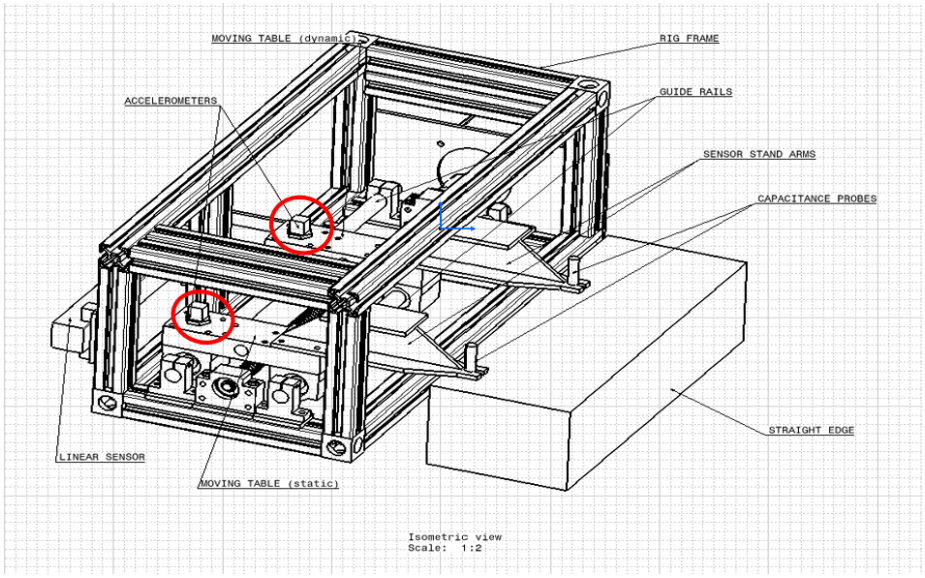

Figure 5-39 Assembly of Accelerometer

5.5.2.2 Experiment B:

Experiment Title: rig calibration

Experiment Objective: calibrate the components to minimise the error of assembly

Experiment Content:

1) Calibrate the position of capacitance probes and sensor stands.

Sensor stands:

The 2 stands should be located at the same relative position to the tables and with the same gesture.

To calibrate the relative position of sensor stands to the table by screwing bolts, the following requirement should be reached:

(1) The relative position of the sensor stands installed on the tables shall be the same in Z axis, as is shown in **Figure 5-40**;
(2) The Y and Z axis edge of the sensor stands must be parallel to the Y and Z axis edge of the table, as is shown in **Figure 5-40**, in order to reduce the Abbe error.

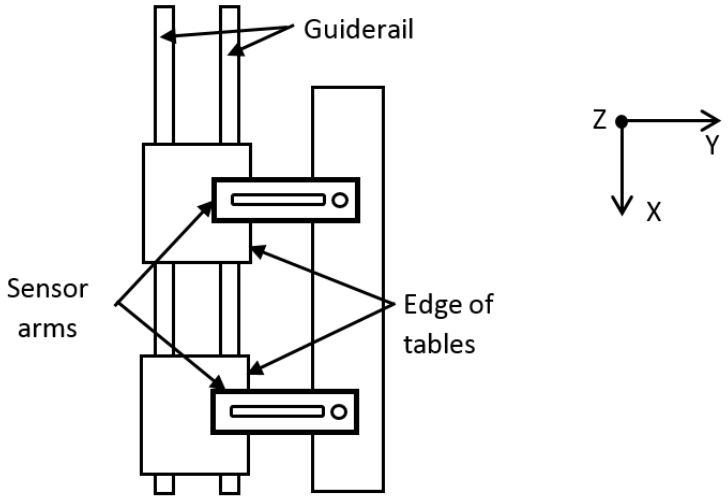

Figure 5-40 Relative Positions of sensors and the Rig

Capacitance probe:

Step 1: Assemble the capacitance probes to the sensor arms and guarantee the axis of the probes is perpendicular to the surface of the straight edge on Z direction (**Figure 5-41** and **Figure 5-42**).

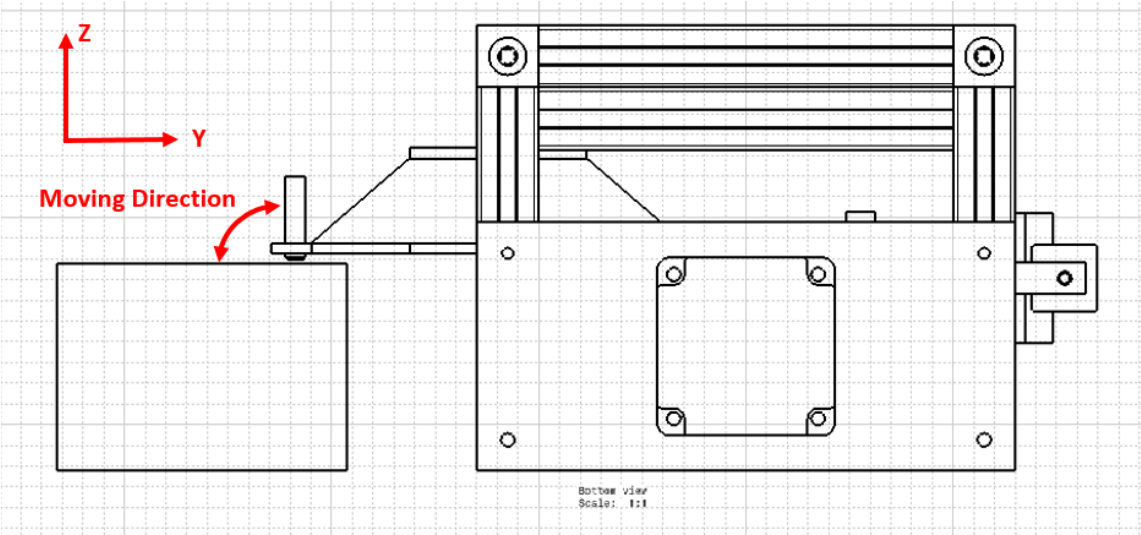

Figure 5-41 Angle of the arm on YZ plane

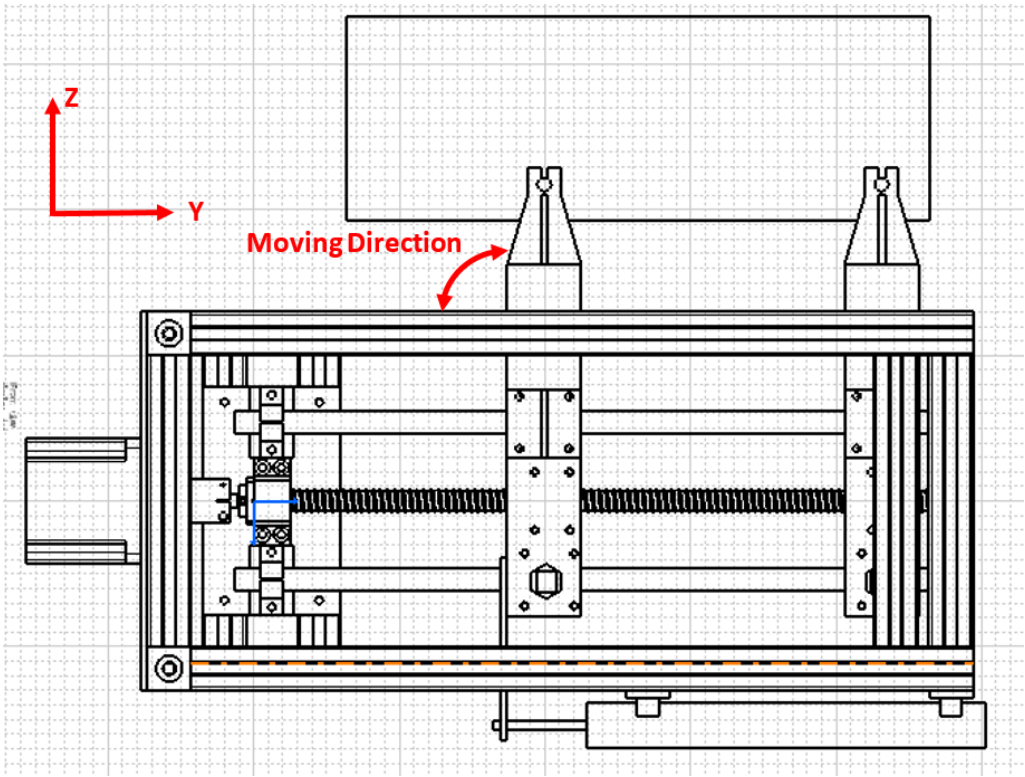

Figure 5-42 Angle of the arm on XY plane

Step 2: Turn on the driver of the capacitance probe and calibrate the distance between the sensing surface of the capacitance probe and the reflecting surface of the straight edge, confirm the distance is within the measuring area of the capacitance probe, which is 254um.

Step 3: Calibrate the initial reading value of the capacitance probes by moving the position to the clamp, guarantee the values are correspondent (**Figure 5-43**).

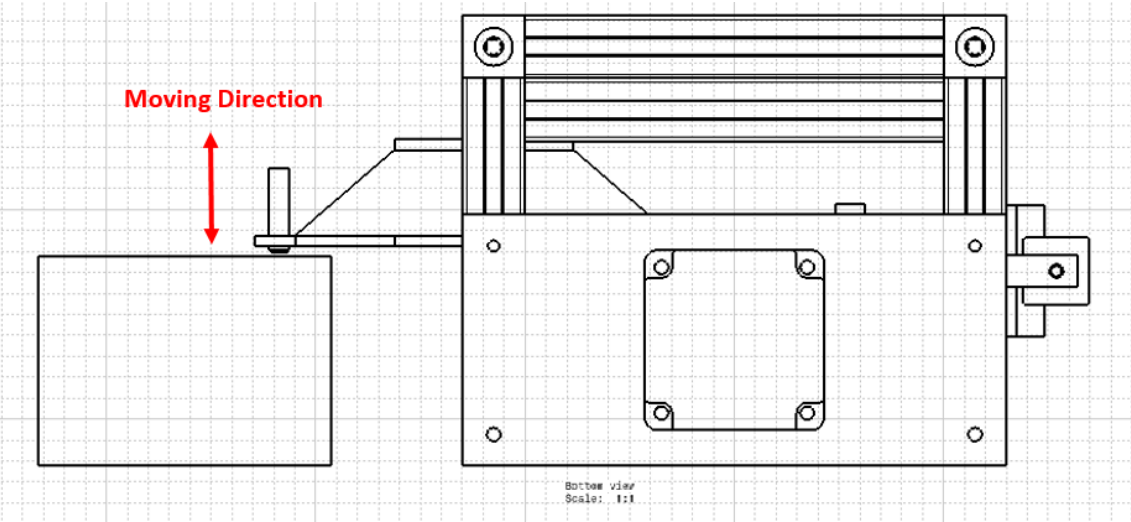

Figure 5-43 Relative Moving Direction of the Straight Edge and Sensor

Step 4: To check the alignment of the two probes along X axis, using the solution of flipping over the ruler on X axis to check if the changing value of the two sensors at the same (**Figure 5-44**).

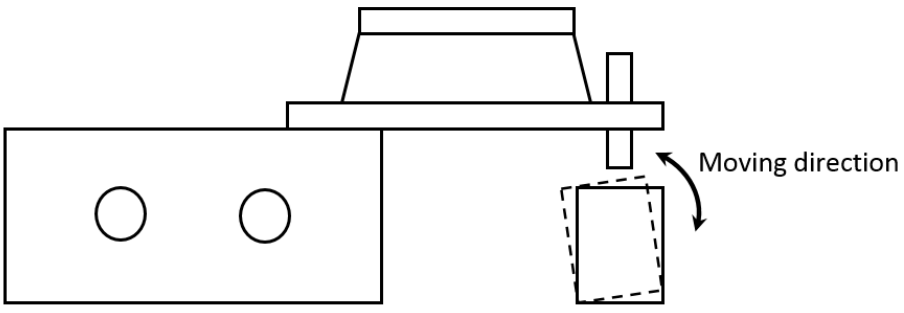

Figure 5-44 Relative Deviation of the Straight Edge

5.5.2.3 Experiment C:

Experiment Title: Monitoring system equipping and function testing

Experiment Objective: Complete settling and calibrating to the linear positioning system, vibration system and the deviation monitoring system. Then, use the calibrated monitoring systems to collect referencing data for further wear monitoring and comparison.

Experiment Content:

Step 1: Settle the moving speed:

According to the stepper motor data sheet, below than 100RPM (1.67round/s) of the rotating speed is suitable;

Then the constant moving speed of the table after acceleration is:

$$V=w \times Vr=5 \times 1.67=8.35mm/s \tag{5.33}$$

According to the manual of the CNC machine, the speed is no beyond the working speed of the CNC machine guiderail. Meanwhile, according to the Nyquist Sampling Theorem, the sampling frequency shall be two times of the signal, and 10 times in the engineering design. Since the accelerometer measuring range is from 1Hz to 10kHz, also according to the literature review, (Giourntas, 2015, Yanqing,v2015 and Vi´afara, 2005), the size of the particle is from 1 um to 25um. Therefore, the linear speed of the motor is: (In the formula, $\mathrm{V_m}$is the speed of stepper motor, $\mathrm{f_{sample}}$ is the sampling speed of DAQ, s is the smallest moving distance per sampling duration)

$$V_m = \left(\frac{f_{sample}}{10}\right) \times S \tag{5.34}$$

$$= \left(\frac{10 \times 10^3}{10}\right) \times 1 \times 10^{-3}$$

$$= 1mm/s$$

Therefore in the experiment, according to the calculation of the roughness frequency and also the measuring range of the accelerometer, 1mm/s (0.2 round/s) is selected as the moving speed of the rig.

Transfer to the motor, which the micro step is set as 200 steps per round (which is 1.8 degree per step), the delay of the threshold is 5 to the speed of 1mm/s.

Step 2: Set up the linear positioning equipment:

1) Complete the assembly to the potentiometer on the frame and connect the measuring shaft to the moving table (**Figure 5-45**).
In case of the connection between the potentiometer and the moving table would infect to the deviation of the table while moving on guiderail with wear on it, the two connect joint on the Fig should not use lock nuts but bearings to guarantee the stiffness on X axis but flexibility on the YZ surface.

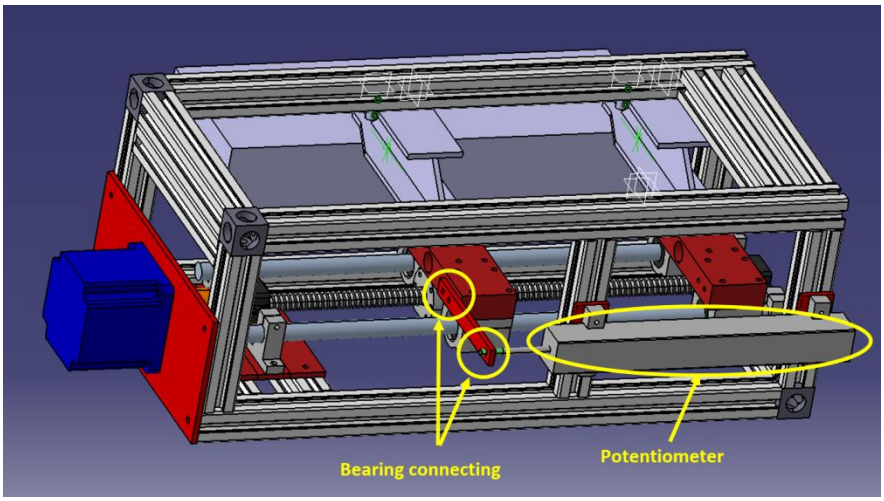

Figure 5-45 Assembly Points of the Linear Position Sensor

2) Connect the three pins to the DAQ and use LABVIEW to realise the position data acquisition.

Step 3: Set up the accelerometers on each of the tables, guaranteeing the following two conditions:

a. The two accelerometers should be allocated on the exactly same relative position to the tables and as near to the wear resource as possible, in order to make sure receiving the same vibration signal;
b. With the precondition that the base of the sensor does not interfere with the bolts, two accelerometers should be mounted as close to the source of the vibration (the guiderail shafts) as possible (Wu, 2009), for the purpose of receiving highest altitude of the vibration signal (**Figure 5-46**).

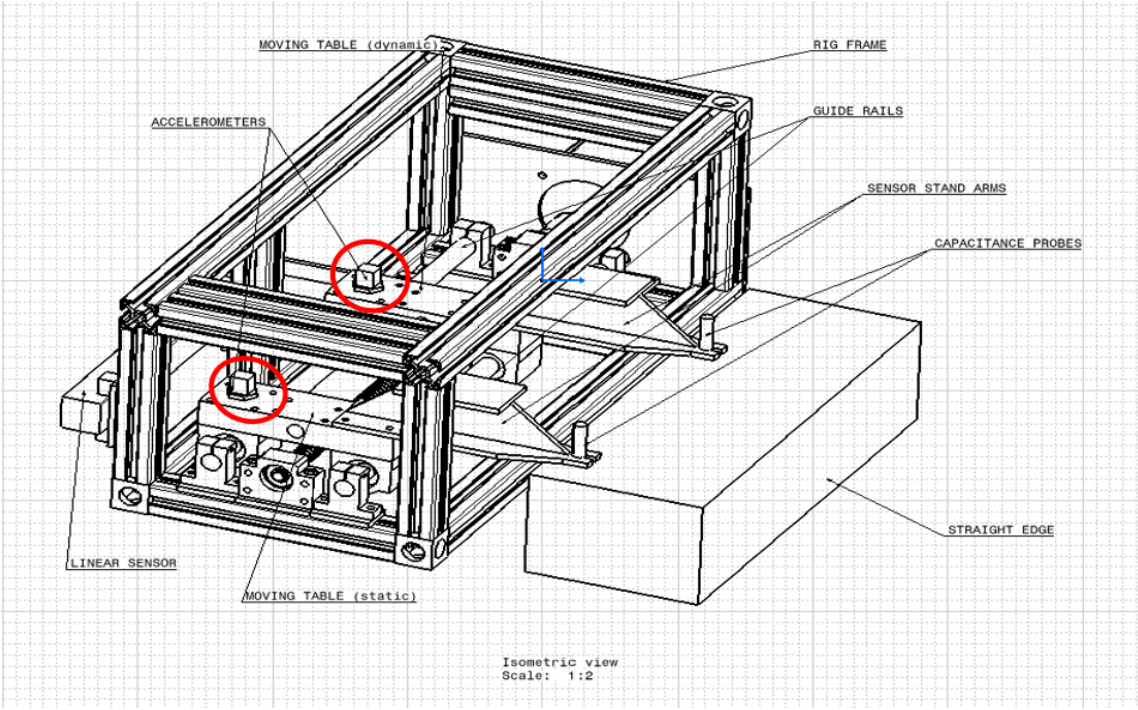

Figure 5-46 Assembly of Accelerometers

Step 4: Repeat the connection process of sensor to the DAQ, and use LABVIEW to realise the vibration signal receiving.

Step 5: Repeat the steps in Experiment B to recalibrate the capacitance probe, then realise the digital signal acquisition via LABVIEW.

Step 6: Collect and record the referencing data for the rest of the test:

1) Settle the stepper motor via ARDUINO to drive the moving table along the guiderail for 5 turns with settled constant speed.

2) Turn all the sensors on and record the data of relative position, the data of vibration during the process that the stepper motor working on

constant speed, and the data that the relative position changes between the capacitance probe and the straight edge.

3) Use Matlab to sort the data, transfer each of the original data from time domain to frequency domain.

4) Calculate the average of the vibration altitude, the average of distance. Visualise the data to graph, representing the result as the state of the system while assuming there is no wear on it.

5) Record the data as reference to the following wear monitored data, the guiderail used in this experiment is marked as pair (1).

The following **figure 5-47** is the rig after completing the assembly.

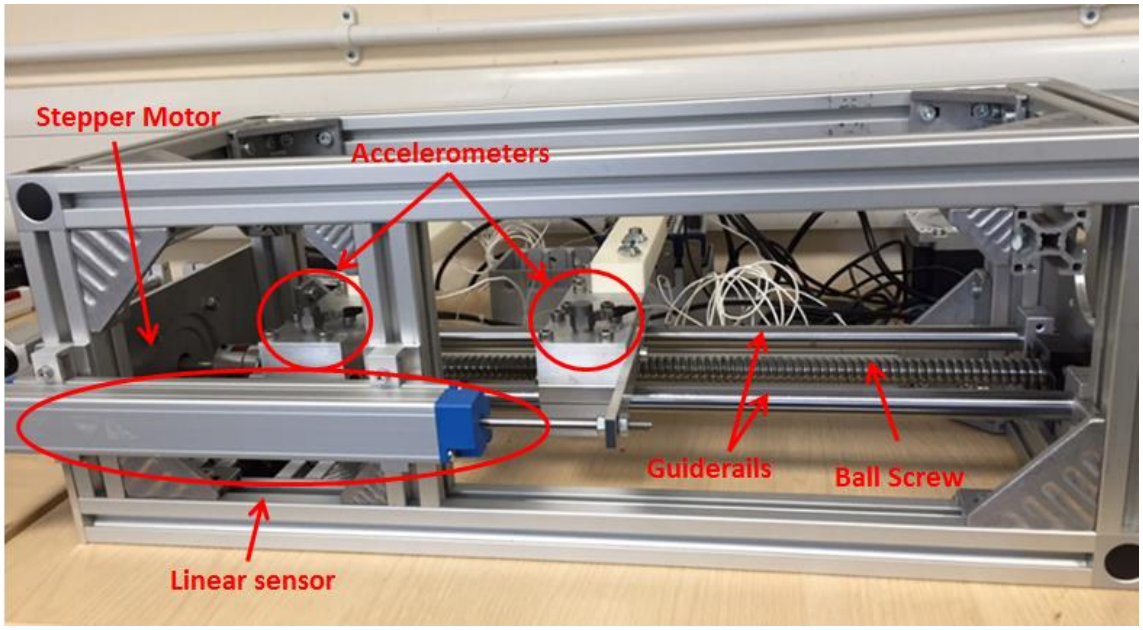

Figure 5-47 Complete Experimental Rig

The following **Figure 5-48** is the assembly of the accelerometers:

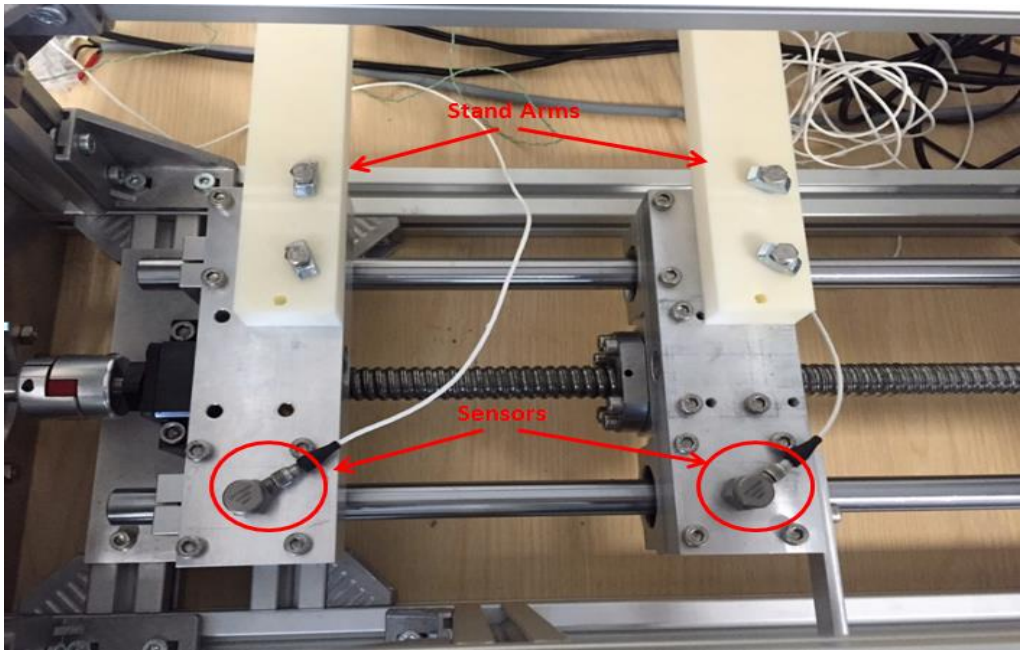

Figure 5-48 Complete Experimental Rig 2

The following **Figure 5-49** is the assembly of the capacitance probes and the straight edge:

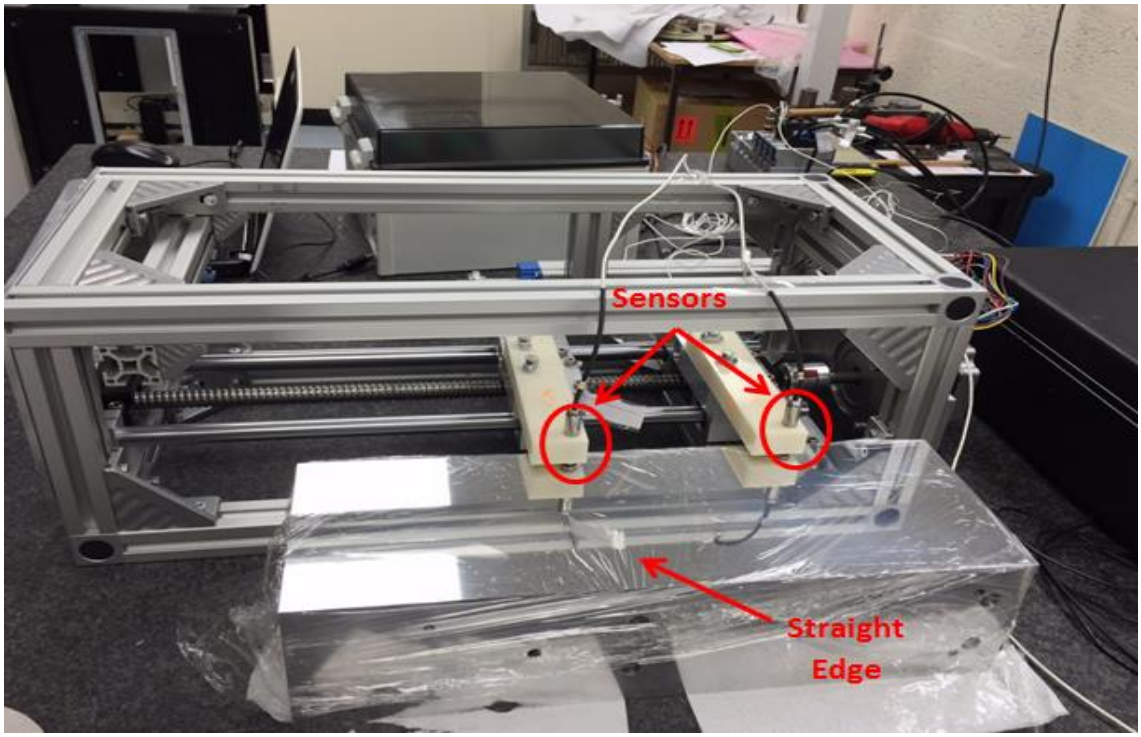

Figure 5-49 Complete Experimental Rig (with Sensors and the Straight Edge)

5.5.2.4 Experiment D:

Experiment Title: monitoring system function test 1: repeatability test.

Experiment Objective:

To test the repeatability of the monitoring system;

Experiment Content:

Part A: repeatability test:

Step 1: Mark the four pairs of guiderails. Since the first pair of guiderails used in the Experiment C is already marked as pair No.1, the rest are marked as pair No.2, No.3 and No.4.Define the data of each pair of the guide rail as a group. Therefore, there should be four groups of data after complete experiment.

Step 2: Repeat the work of initial data collection in Experiment C to the rest of the three groups of guiderail.

Step 3: While moving the table over the oil paint and scotch tape surface, record the data from the capacitance probes with LABVIEW to make contrast to original data and calculate the depth change while moving over the oil painting and scotch tape area. Then compare with the measured paint/tape change to see if the sensor measured result is accordant with it.

Step 4: Use Matlab to compare five controls in each group of the data and calculate the difference value among them, then calculate the ratio to amplitude of the average. Taking a_1 as output of capacitance probe Static,$a_2$as output of capacitance probe dynamic, the difference is:

$$d = |a_1(n) - a_2(n)| \tag{5.35}$$

Then, define d_1 as the result of the first test. Therefore, define d_2 as the result of the second test, d_3 as the result of the third test, d_4 as the result of the fourth test, d_5 as the result of the fifth test.

The average of the five groups' difference is:

$$a_v(n) = \frac{\sum_{i=1}^{5} d_i(n)}{5} \tag{5.36}$$

Step5：calculate the difference of capacitance probes between each result and the average:

Taking shaft No.1 as example, the difference between $d_1$and a_v:

$$a_{d1}(n) = \sqrt{\frac{1}{5}\sum_{i=1}^{5}(d_i(n) - a_v(n))^2} \quad (5.37)$$

5.5.2.5 Experiment E:

Experiment Title: monitoring system function test 2: In-process monitoring system

Experiment Objective:

To validate the novelty of the thesis, testing the outer disturbance offset ability of the in-process monitoring principle and solution.

Experiment Content:

In order to make the experiment simpler and easy to analyse, the whole Experiment E is under the situation that there is no wear on the guiderail. The test is solely on the purpose of verifying the signal coupling function.

Step 1: When the two capacitance probes on each of the table are settled, deliberately make outer disturbance by using a wooden hammer to knock the marble base. The purpose is to simulate the disturbance outside from the CNC machine (**Figure 5-50**).

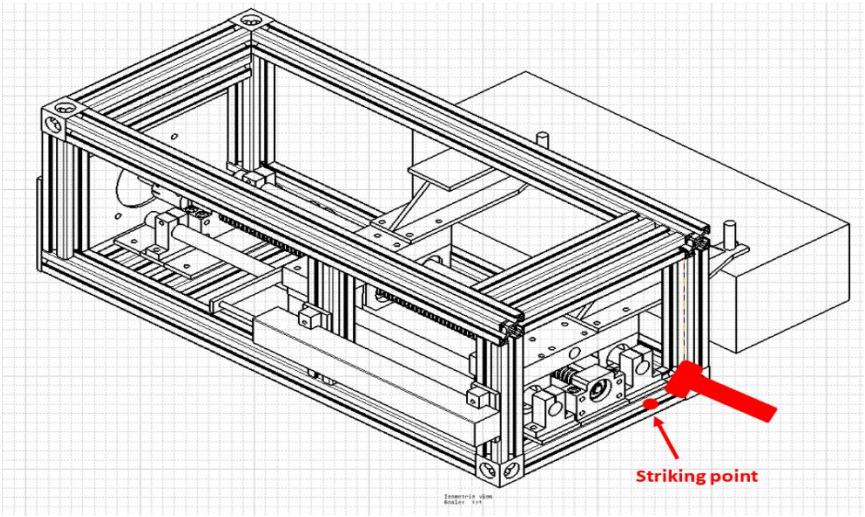

Figure 5-50 Striking Point to the Rig

Step 2: Collect the data from these two capacitance probes with the same sampling frequency and make the contrast to inspect if the 2 sensors at different positions reflect the same data from outer strike. The contrast involves 2 aspects:

1) The time difference by receiving the striking signal;
2) The difference to amplitude of the striking signal;

Step 3: utilising Matlab to make coupling, then contrast to the original data to check if the data averages are accordant;

Step 4: Repeat Step 1, but deliberately make outer disturbance by knocking the rig frame. This solution is to simulate the disturbance from the CNC machine itself (Figure 5-51).

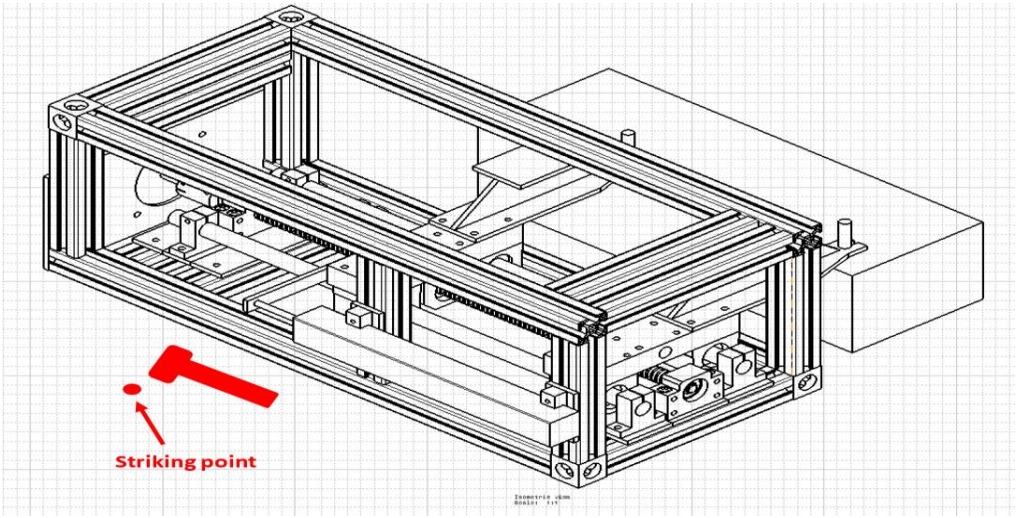

Figure 5-51 Striking Point to the Rig 2

Step 5: repeat the content in step 2 and step 3, to inspect the outer disturbance effect and the capability of in-process monitoring solution.

5.5.2.6 Experiment F:

Experiment Title: friction fatigue wear simulation& data acquisition

Experiment Objective:

According to the effect of friction fatigue wear described in literature reading part, simulate the wear on the guiderail and ball bearings for further testing. To

make wear in the third region (the wear region) of the guiderail and ball bearing via capacitance probe and micrometre to monitor the depth and width of the groove until the deepest point reaches to 100um.

Experiment Content:

- **Guide way part:**

  a. The rough surface simulation:

Use emery paper to wipe on the surface of the guiderail shaft in pre-settled wear length. According to the literature review, (Giourntas, 2015, Yanqing, 2015 and Vi´afara, 2005), the size of the particle is from 1 um to 25um, therefore the type of emery paper can be chosen from the following sheet:

Table 5-10 Emery Paper Parameters

Particle grit	Diameter (um)
500	20 - 14
600	14 -10
800	10 – 7
1000	7 – 5
1200	5 – 3.5
1400	3.5 – 3
1600	3 – 2.5
1800	2.5 – 2
2000	2 – 1.5
2500	1.5 – 1
3000	1 – 0.5

The selected types of paper are: 500 grit, 1000grit, 1600 grit, 2000 grit, 2500 grit and 3000 grit.

b. Smooth curve simulation:

1) Calculate the length, width and depth of the abraded area shown on **Figure 5-52** and **Figure 5-53**: e.g. (from sample of supplier):

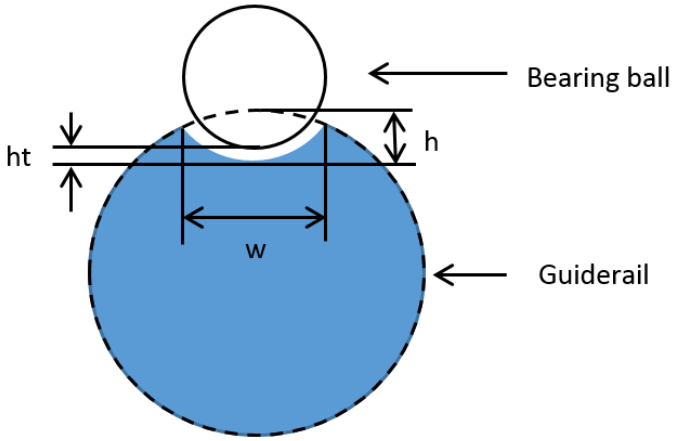

Figure 5-52 Relative Position of Components (with wear on)

Bearing ball diameter (f)=3.175mm, W=0.7~ 1mm; ht= t1 (tolerance of bearing ball)+t2 (tolerance of shaft)=6+9=15um=0.015mm;

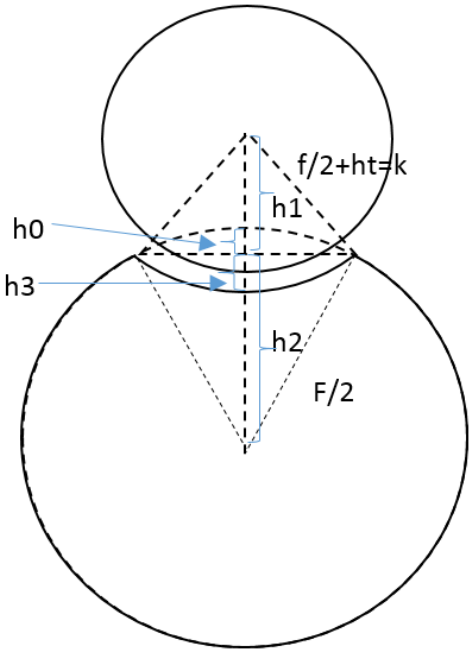

Figure 5-53 Relative Position of Components (with wear on) 2

Therefore:

$$h = h_0 + h_3 \tag{5.38}$$

$$h_0 = \frac{F}{2} - h_2 \tag{5.39}$$

$$\text{Assuming } k = \frac{f}{2} + h_t \tag{5.40}$$

$$h_1 = \sqrt{k^2 - \frac{w^2}{2}} \tag{5.41}$$

$$h_2 = \sqrt{(F/2)^2 - (w/2)^2} \tag{5.42}$$

$$h_3 = k - h_1 \tag{5.43}$$

So: $$h = h_0 + h_3 \tag{5.44}$$

$$= \left(\frac{F}{2} - h_2\right) + (k - h_1)$$

$$= \frac{F}{2} - \sqrt{\left(\frac{F}{2}\right)^2 - \left(\frac{w}{2}\right)^2} + k - \sqrt{k^2 - (w/2)^2}$$

Therefore:

a. w=0.7mm:
   h=0.049mm;
b. w=1mm:
   h=0.101mm;

After calculation, if the width of the wear is 0.7~ 1mm, the depth of the groove can reach to 49– 101um.

c. Implementation:

Step 1: allocate the two shafts horizontal on the table;

Step 2: As shown on **Figure 5-54**, using ink pen to draw a line on the shaft which is parallel to the axis;

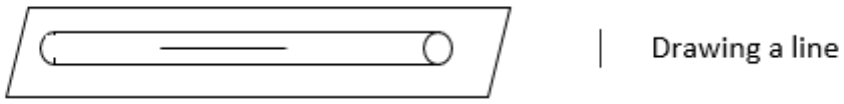

Figure 5-54 Marking the Wear Position

Step 3: using file to wipe on the shaft along the line;

Step 4: As shown on **Figure 5-55**, using dial gauge and micro meter to monitor the depth and width of the groove until the deepest point reaches to 101um;

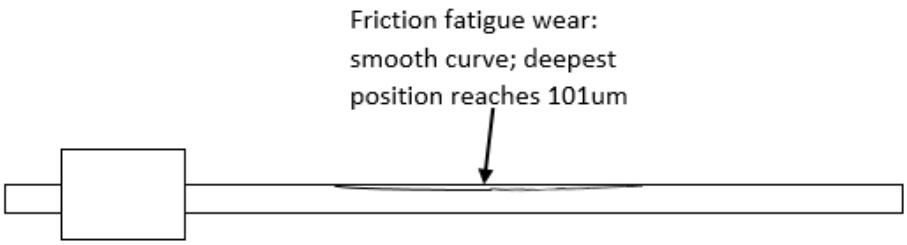

Figure 5-55 Side View of the Smooth Curve Wear

Step 5: As shown on **Figure 5-56**, re-assembly the guiderail to make the groove of shaft No.1& No.2 meet the trail of bearing balls on the top.

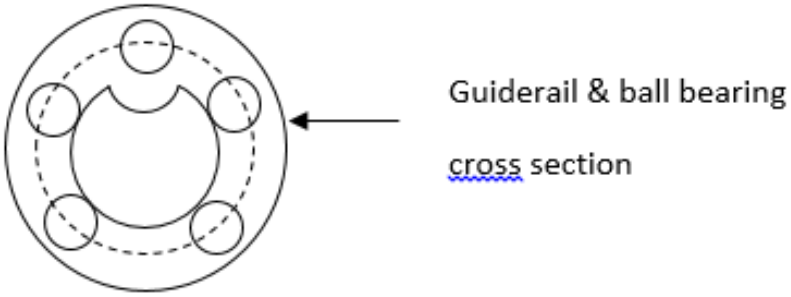

Figure 5-56 Guide rail and Ball Bearing Cross-section Figure

- **simulate the wear of rolling balls:**

Step 1: Dismantle the bearing;

Step 2: As shown on **Figure 5-57**, using abrasive paper to do the sanding to balls via 3 directions: pitching, rolling and yawing.

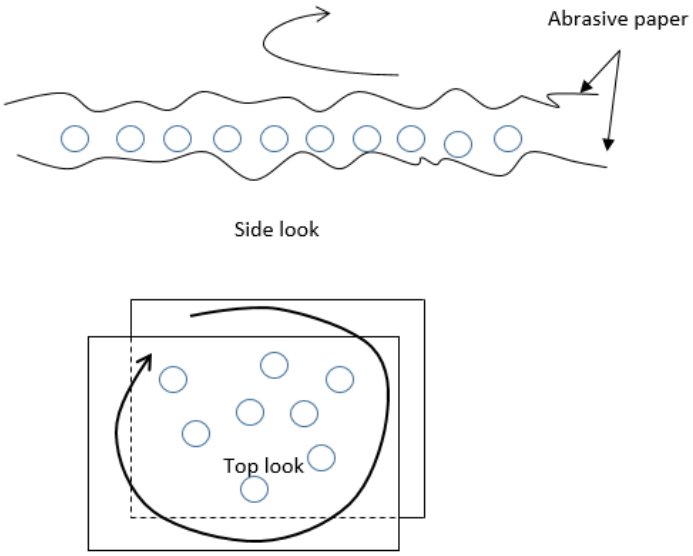

Figure 5-57 Approach to the Wear of Balls

Step 3: Using micrometre to measure the average wear amount that correspondent to the wear amount on the guiderail;

Step 4: complete re-assembly of the ball bearing;

a. Re-assembly the components and turn on the stepper motor for 10 minutes, and test the temperature of the parts to check if the temperature is stable enough, in order to eliminate the thermal disturbance.
b. Repeat the approaches of B part to collect the data and analyse the data via Matlab;
c. Add in the outer disturbance via solution mentioned in C part to validate the in-process theory.

5.5.2.7 Experiment G:

Experiment Title: measure the symptoms of the wear

Experiment Objective:

Complete the measurement of the wear produced on experiment F to validate the function of the wear monitoring system.

Experiment Content:

Part a. Smooth curve on particular length:

Solution: capacitance probes assembled on the table against the face of metal straight edge, moves with the table on guiderail.

Phenomenon expected: the capacitance probe shows unidirectional constant value changes:

a. bigger value changes than vibration;
b. happens on particular positions;
c. unidirectional changing;

Part b. random vibration:

Solution: the same to the smooth curve detection;

Phenomenon expected:

(1) The value of capacitance probe changes in a small range;

(2) Two directions changing;

(3) Happens in random places, even in the place that guiderail has never been used before and no wear.

The solution and sequence of collecting guiderail wear data shall strictly follow the experiment D, to guarantee the repeatability and reproducibility.

5.5.2.8 Experiment H:

Experiment Title: In-process monitoring system with capacitance probes

Experiment Objective:

Complete the validation to the function of in-process deviation monitoring system and count the wear in.

Experiment Content:

As shown on **Figure 5-58**, capacitance probe No.2 allocates on static table. It is in the same relative position as capacitance probe No.1 on the rolling table.

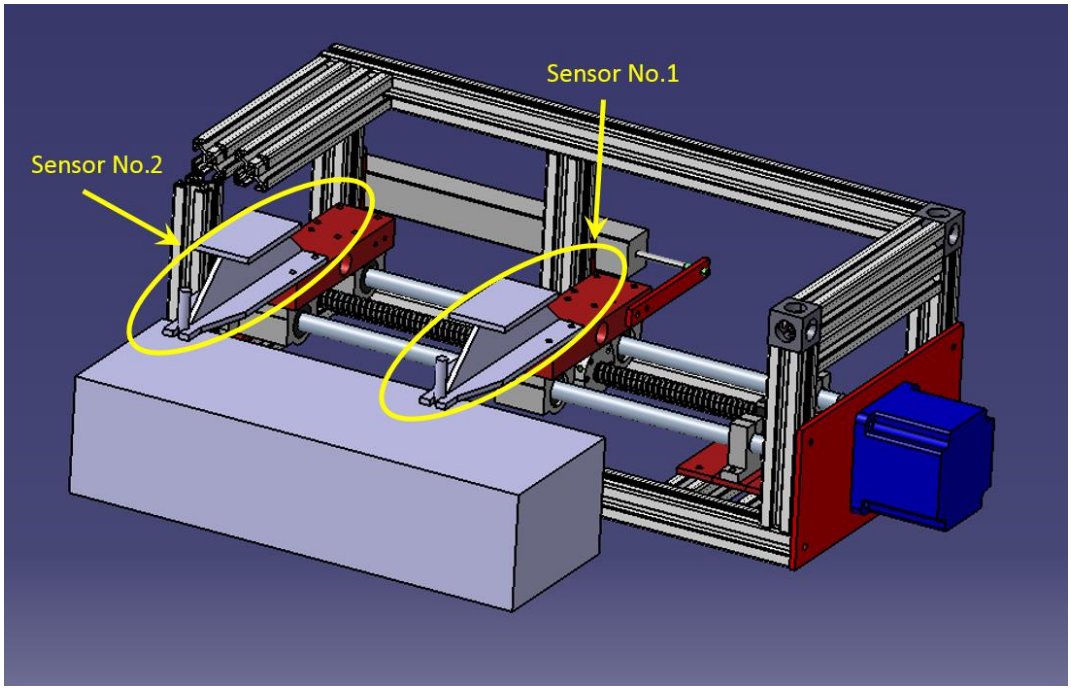

Figure 5-58 Capacitance Sensor No.1 and No.2

Then complete the steps of data acquisition as the following sequence on **Table 5-11**:

Table 5-11 Data Acquisition Process

		working period					
Linear motion (stepper motor)		acceleration	constant speed				deceleration
Vibration (accelerometer)			the vibration signal from rolling table				
Deviation (capacitance			no wear	100mm wear zone		no wear	
vibration reference			the vibration signal from stable table				
deviation reference			stable table capacitance probe signal				
position (linear sensor)		monitoring the whole moving process					
temperature (RTD)	pre-heating						

The following pictures from Figure 5-59 to Figure 5-60 are the experiment rig on the marble base:

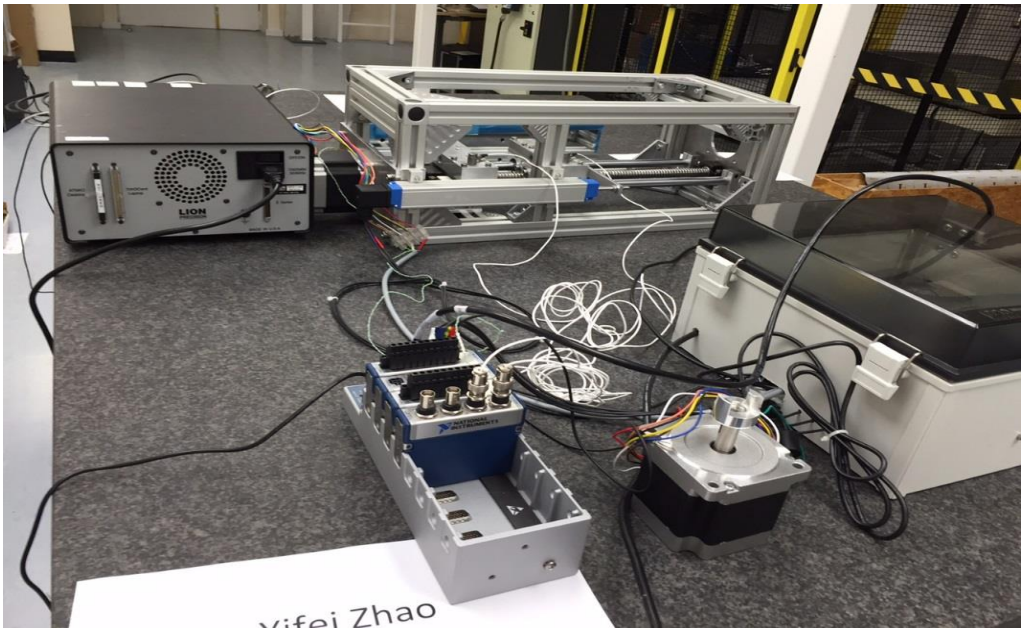

Figure 5-59 The whole rig system after completing the assembly

Figure 5-60 Shafts from No.1 to Nop.4 as the test examples

6 VALIDATION RESULT DISCUSSION

As illustrated in the experiment designing part, the whole test can be separated into two parts: the repeatability test and wear test. As can be seen in the Figure **6-1**, the repeatability test, the 4 sample shafts from No.1 to No.4 are all pristine. On the contrary, in the wear test, each of the shafts has a 20mm long wear region along the whole 100mm measuring range. In each part of the test, to each of the sample, there are five times of the test in the same condition. The following graph shows the test process:

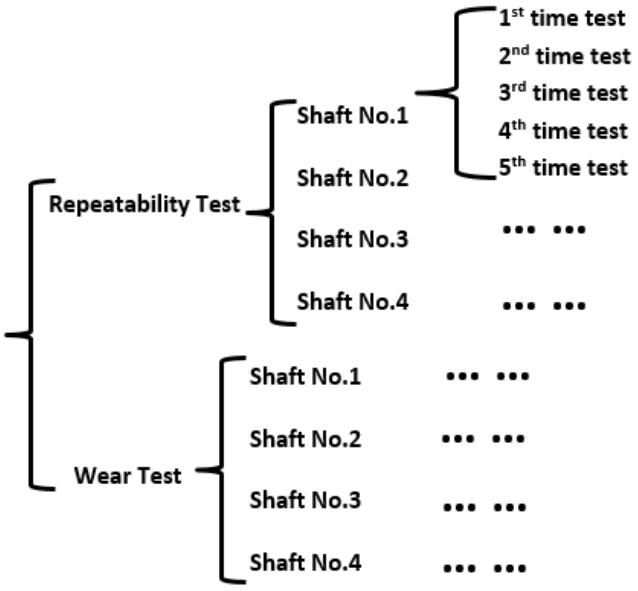

Figure 6-1 The experimental group

6.1 Original Data Processing and Analysis

The original data has the figure as is shown in the picture below, **Figure 6-2**. Because the data acquisition starts in advance, the running of the motor starts with a locking signal. Therefore, the useful signal starts with the first high altitude at point A and ends with the last one at point B.

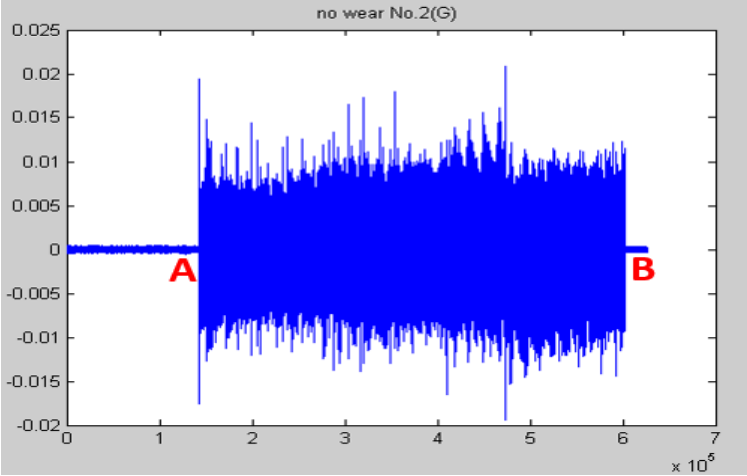

Figure 6-2 The original data whole length

The original data processing work prior at the data calculation is useful data section adopting, between point A and B. To guarantee the accordance of the data, each of the test data file shall be completed with the work, and delete non-useful data sections.

6.2 System Repeatability Test

The importance of the repeatability test is guaranteeing whether the test result is stable and reliable enough. The approach is testing how results of a measurement vary when the measurement is repeated under the same conditions and within a short period.

6.2.1 Vibration Monitoring Repeatability Test

Vibration test is all about the data from accelerometers. The repeatability test is based on the Shaft No.1. Working steps are illustrated as following.

6.2.1.1 Data Average Calculation

Defining the output of accelerometer static is a_1, accelerometer dynamic is a_2, the difference which represents the signal after getting all the disturbance filtered is:

$$difference1(n) = |a_1(n) - a_2(n)| \quad (6.1)$$

The following **Figure 6-3** is the signal of accelerometer static (green line), capacitance probe dynamic (red line) and the difference d:

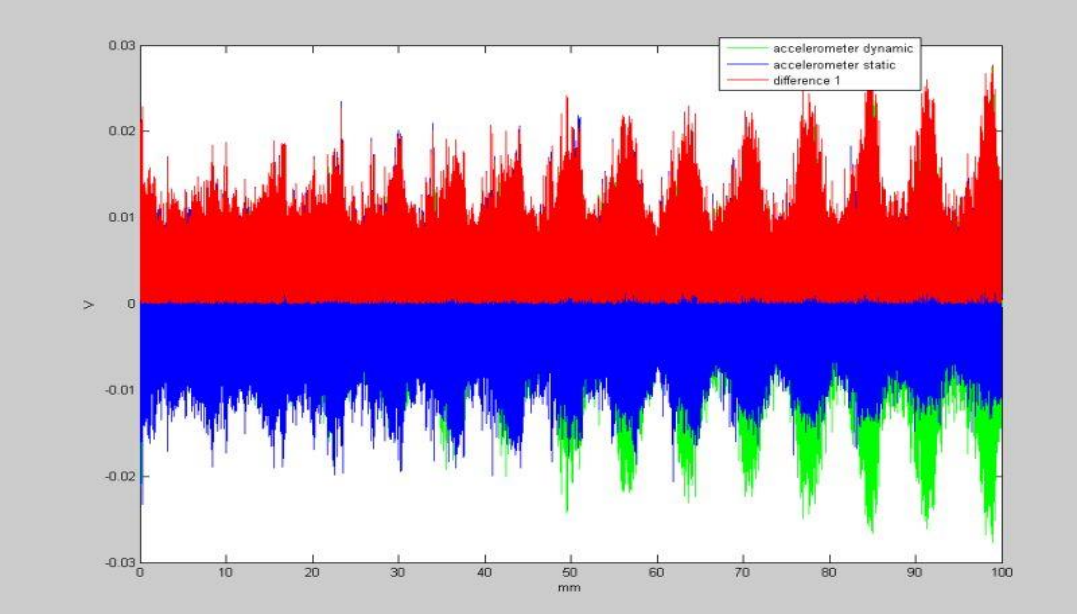

Figure 6-3 Accelerometer Dynamic, Static and the Difference Signals

Then calculate the average of difference:

$$a_v(n) = \sqrt{\frac{d_1^2(n)+d_2^2(n)+d_3^2(n)+d_4^2(n)+d_5^2(n)}{5}} \quad (6.2)$$

The figure below **Figure 6-4** shows the result of the difference average:

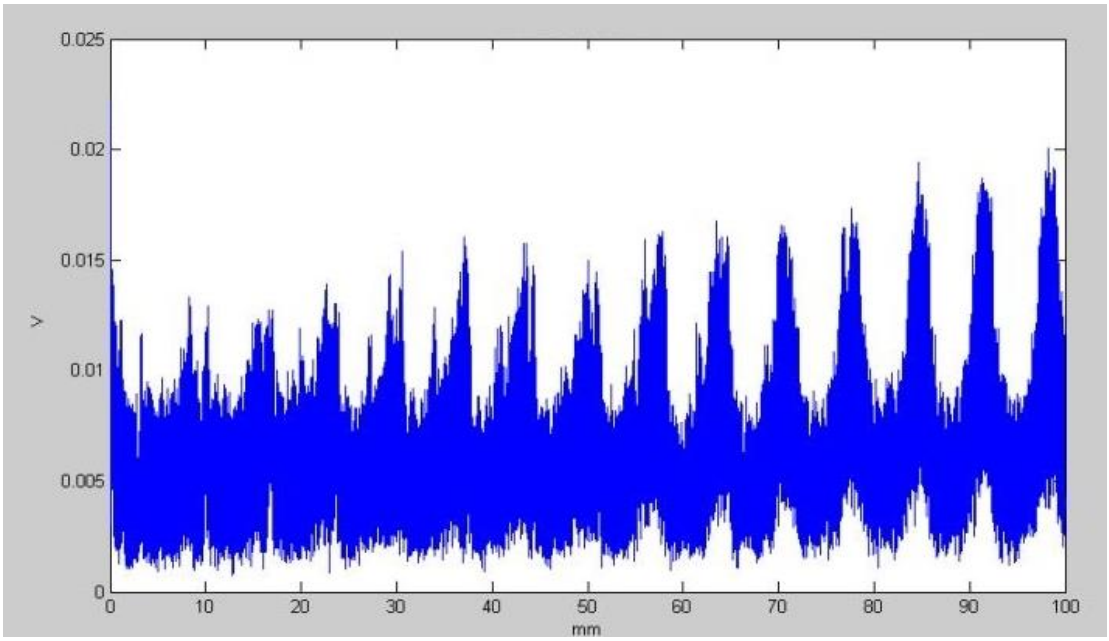

Figure 6-4 Result of the Difference on Average

6.2.1.2 Data Variation Calculation

Step1：calculate the difference of accelerometers between each result and the average:

Difference between d_i and a_v is:

$$a_d(\mathrm{n}) == \sqrt{\frac{\sum_{i=1}^{N}(d_N(n)-a_v(n))^2}{N}} \tag{6.3}$$

In this case, the N is 5. The figure below **Figure 6-5** shows the difference between d_i and a_v, the highest difference is 0.0044V:

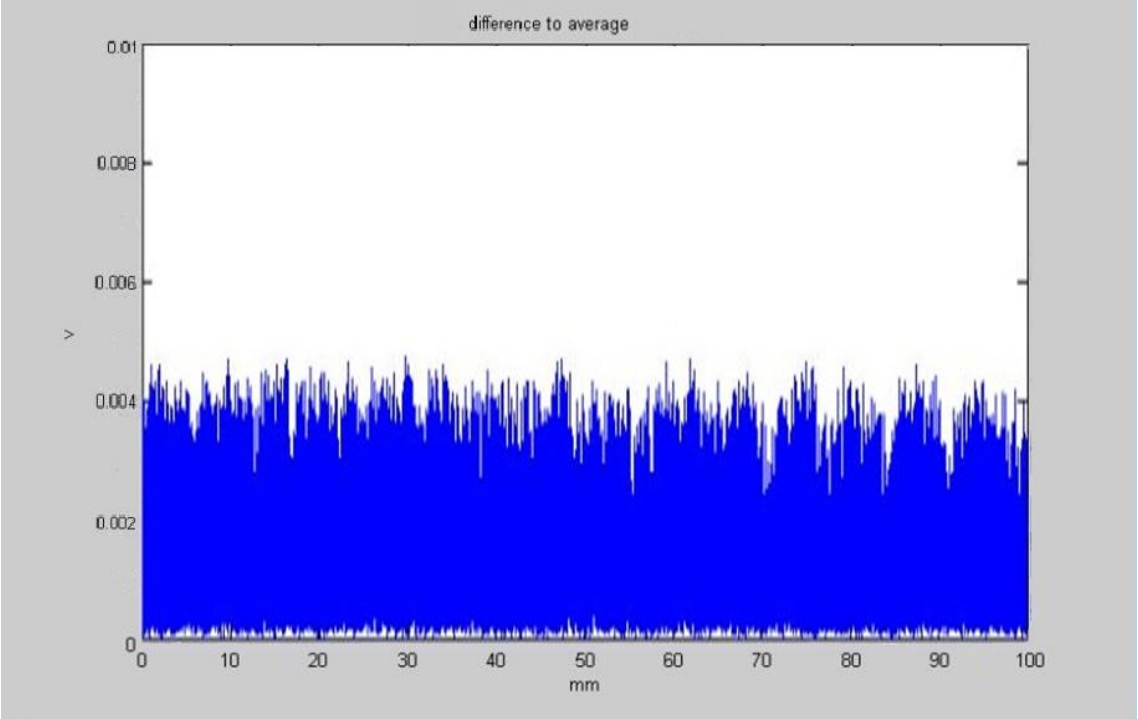

Figure 6-5 Percentage of Difference between d_i and $\mathbf{a_v}$

6.2.2 Smooth Curve Monitoring Repeatability Test

Smooth curve test is all about the data from capacitance probes. The repeatability test is based on the Shaft No.1. Working steps are illustrated as following.

6.2.2.1 Data Average Calculation

Taking a_1 as output of capacitance probe Static, a_2 as output of capacitance probe dynamic, the difference is:

$$d(n) = a_1(n) - a_2(n) \tag{6.8}$$

The following **Figure 6-6**is the signal of capacitance probe static (green line), capacitance probe dynamic (red line) and the difference d:

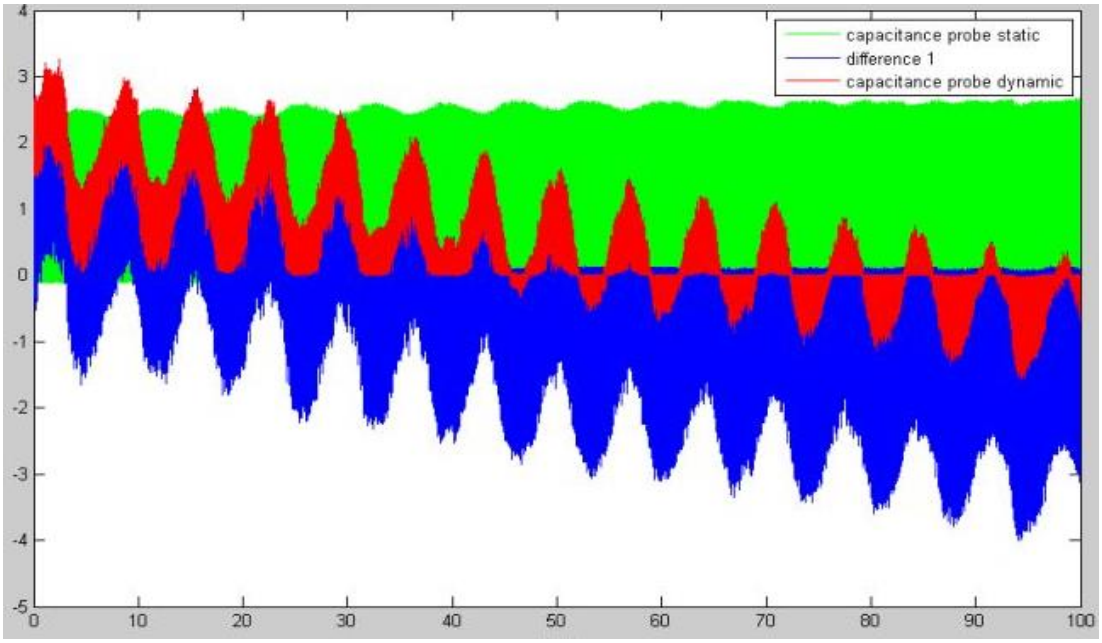

Figure 6-6 The signal of two capacitance probe sensors and the difference (Unit of the X axis is mm, unit to the Y axis is Voltage)

Then, define d_1 as the result of the first test, therefore, d_2 as the result of the second test, d_3 as the result of the third test, d_4 as the result of the fourth test, d_5 as the result of the fifth test.

The average of the 5 groups' difference is:

$$a_v(n) = \sqrt{\frac{d_1^2(n)+d_2^2(n)+d_3^2(n)+d_4^2(n)+d_5^2(n)}{5}} \tag{6.9}$$

The figure below **Figure 6-7** shows the result of the difference average

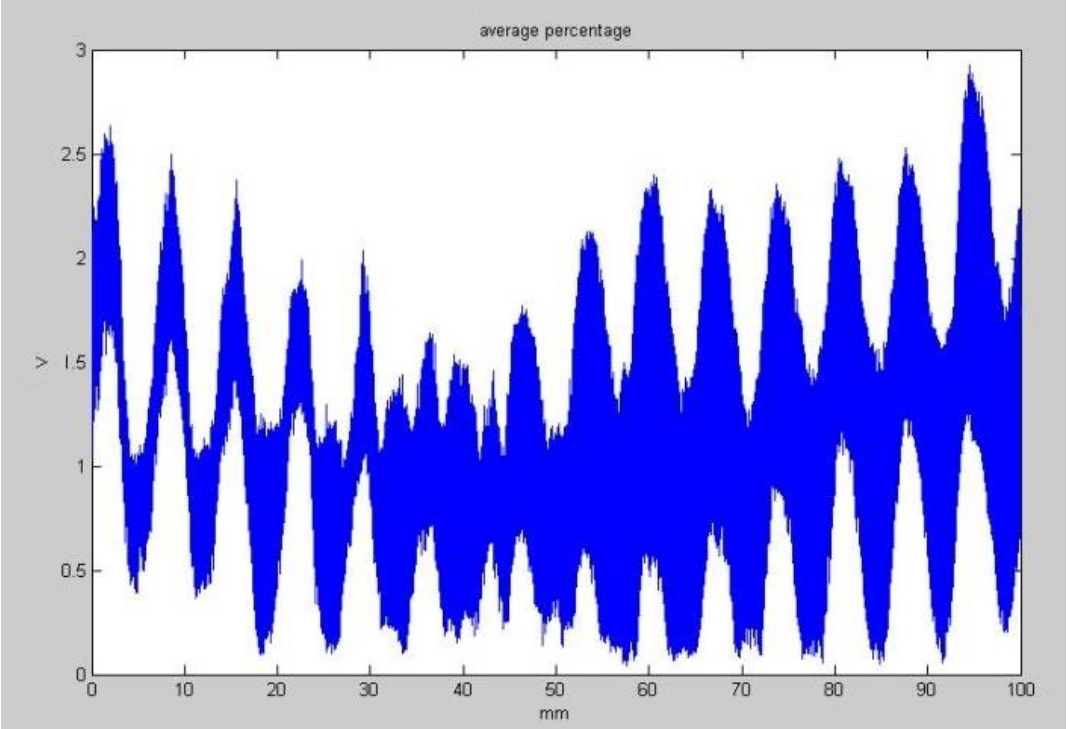

Figure 6-7 Average of difference

6.2.2.2 Data Variation Calculation

Step1：calculate the difference of capacitance probes between each result and the average:

Difference between $\mathrm{d_i}$ and $\mathrm{a_v}$:

$$a_v(n) = \sqrt{\frac{\sum_{i=1}^{N}(d_N(n) - a_v(n))^2}{N}} \tag{6.10}$$

The Figure 6-8 below shows the difference between $\mathrm{d_i}$ and $\mathrm{a_v}$, the highest difference is 0.41V:

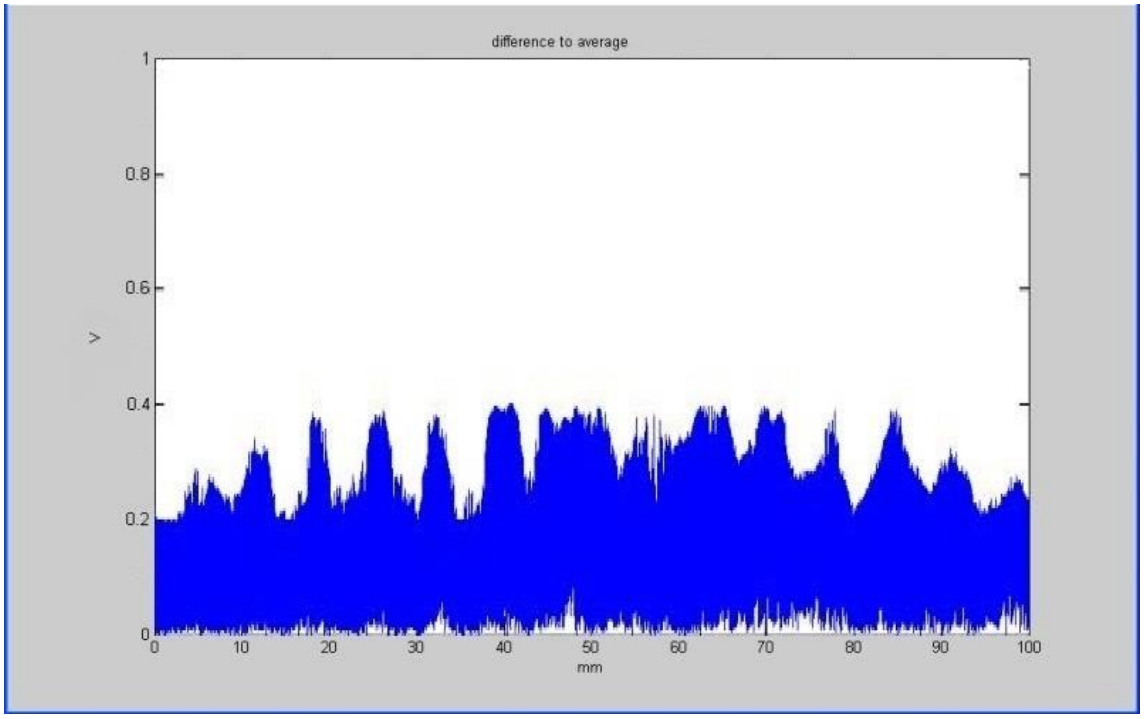

Figure 6-8 difference to the average

6.2.3 Conclusion of Repeatability Test

6.2.3.1 Vibration Monitoring System

According to the test of accelerometers' repeatability, the average of variation is 0.004V which means the variance of the repeating test results is 0.004V. Resources bring to the result could be the following:

(1) The stiffness of the assembly of sensors on tables: The accelerometer is well equipped with wax in the experiment but might still have an influence to the experiment result.

(2) The rigidity of the moving table: As is analysed in the designing part, the moving table has the looseness on Z direction of$0.009mm$, the looseness might contribute to the variance.

(3) The ball bearing: the balls in the bearing shall not move when the table is static, but might have the impact during the moving behaviour. In this case, it is still possible that part of the variance is caused by it. Further experiment on this case shall be applied to prove this.

6.2.3.2 Smooth Curve Monitoring System

Resources bringing to the variance of the result can be the following:

(1) The stiffness of the stand arm: As can be seen in figures, the stand arm for the sensor is not stiff enough and vibrates in the Z section during the whole moving process. In this case, the vibration frequency is consistent because the speed and the start-end points are settled by Arduino program. However, whether the phase of the vibration coordinating to the particular position still needs validation through a further test. Therefore, there is possibility that the variance is partially caused by such reason.

(2) The rigidity of the moving table: As is analysed in the designing part, the moving table has the looseness on Z direction of $0.009mm$, the looseness might contribute to the variance.

(3) Deviation of sensor assembly on X or Y direction: As mentioned in the uncertainty analysis part, Since the stand arm assembly hole has the drilling tolerance of 0.2mm, there is an error from the deviation of the sensor probe caused by this.

Above all, the result of repeatability test is promising. It is convinced that the further conclusion from wear data calculation is reliable to some extent.

6.3 Wear In-process Monitoring Test

After validation to the repeatability and solving the original data, the wear is deliberately fabricated on the particular length as mentioned in the experiment designing part.

In this section, in order to test the in-process monitoring approach, the wear made on shaft No.1 to No.3 with different depth is tested by the system. The No.4 shaft is pristine and the wear is made on the ball bearing, to test the vibration signal.

According to the in-process monitoring hypothesis, the calculated data which contains wear signal is minored with the previous data (while there is no wear on the shaft, taken as referencing data) to acquire the final data of the wear on each symptom.

6.3.1 Synchronising In-process Test

Before the wear test, the static test is represented solely to identify the static feature of the system on disturbance receiving. Taking the accelerometer as the example, the test is made while the sensor is turned on but the motor is not running, simultaneously, making disturbance signal on the frame during the measuring. The purpose is to check if those two sensors receive the signal on the same sampling frequency and there is no phase difference which impacts the result.

As can be seen from the result in **Figure 6-9**, those blue dots are signals from the static accelerometer, red ones are from the dynamic one.

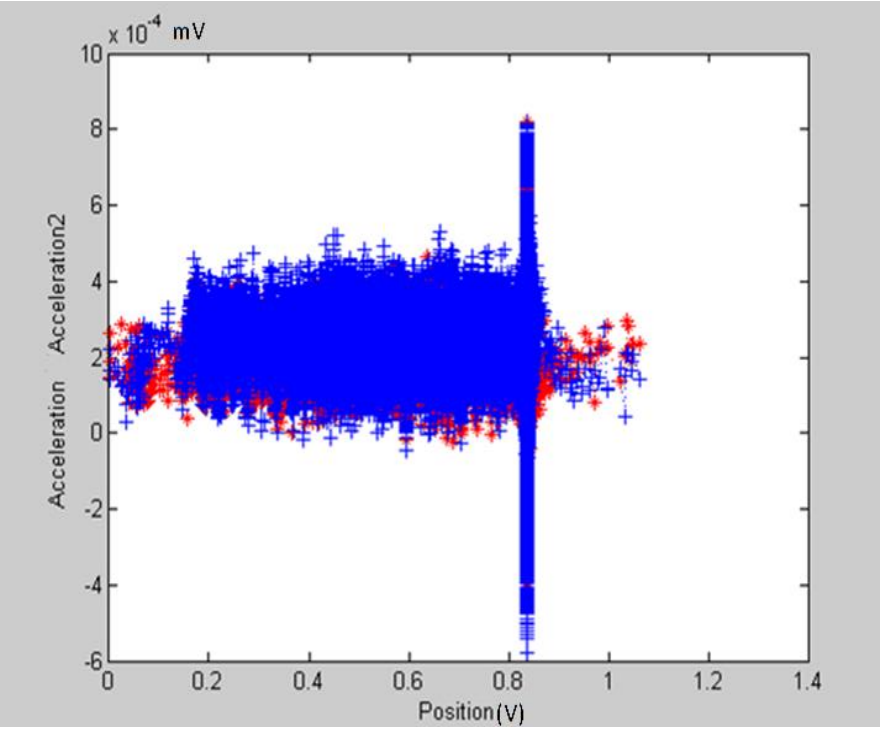

Figure 6-9 Signals from two sensors in the same sampling frequency

In the **Figure 6-10**, the percentage of the difference U_Y among those two signals (a_1 is the signal from static accelerometer and a_2 is from dynamic one) are shown, the calculation formula is:

$$U_Y = \frac{\sqrt{|(a_1)^2-(a_2)^2|}}{\sqrt{\frac{(a_1)^2+(a_2)^2}{2}}} \times 100\% \quad (6.15)$$

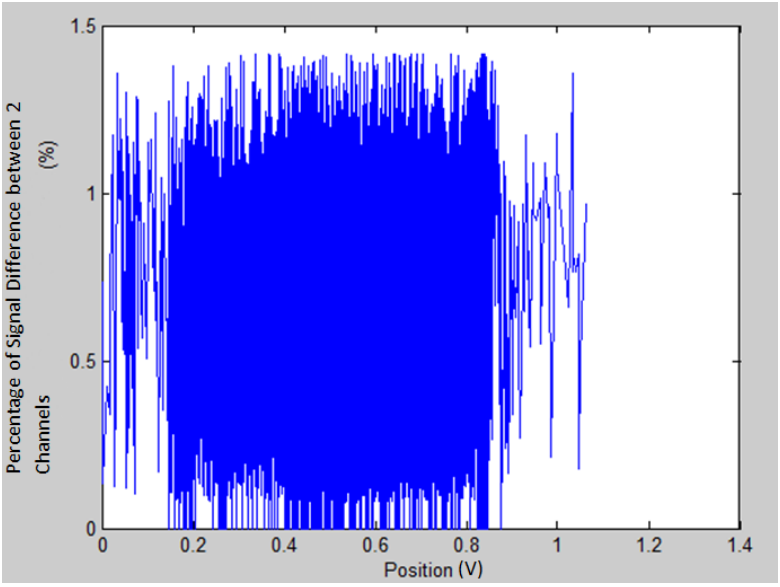

Figure 6-10 Percentage of the static and dynamic sensors' difference

6.3.2 Wear Symptom (1): Non-smooth Behaviour Monitoring Test

Wear Data Processing and Wear Observation

Since the repeatability of No.1 shaft is not reliable, the data of No.1 is abandoned.

Step 1: calculate the root-mean-square of accelerometer static from No.2to No.5 files:

Taking the 5 times measured data from shaft No.2 which the wear has made, as example, assuming each value of the accelerometer static is a_{sc1}, a_{sc2}, a_{sc3}, a_{sc4}, a_{sc5}, thenthe average of the value isa_{scv2}:

$$a_{scv2} = \sqrt{\frac{a_{sc1}^2+a_{sc2}^2+a_{sc3}^2+a_{sc4}^2+a_{sc5}^2}{5}} \tag{6.16}$$

Assuming each value of the accelerometer dynamic is a_{dc1}, a_{dc2}, a_{dc3}, a_{dc4}, a_{dc5},then the average of the value $a_{dcv2}$is:

$$a_{dcv2} = \sqrt{\frac{a_{dc1}^2+a_{dc2}^2+a_{dc3}^2+a_{dc4}^2+a_{dc5}^2}{5}} \tag{6.17}$$

Step 2: Same solution to the data of No.2 shaft without wear, the average of accelerometer static and dynamic are (in the following formula, a_{scv2n} is the

average of the 5 times accelerometer static data, from $a_{sc1n}$to a_{sc5n}; , a_{dcv2n} is the average of the 5 times accelerometer dynamic data, from $a_{dc1n}$to a_{dc5n}):

$$a_{scv2n} = \sqrt{\frac{a_{sc1n}^2+a_{sc2n}^2+a_{sc3n}^2+a_{sc4n}^2+a_{sc5n}^2}{5}} \quad (6.18)$$

$$a_{dcv2n} = \sqrt{\frac{a_{dc1n}^2+a_{dc2n}^2+a_{dc3n}^2+a_{dc4n}^2+a_{dc5n}^2}{5}} \quad (6.19)$$

Step 3: calculate the result without the noise to No.2 shaft, a_{wc2}:

$$a_{wc2} = a_{dcv2} - a_{scv2} \quad (6.20)$$

Step 4: calculate the result to No.2 shaft without the noise and wear (data from the repeatability & reproducibility file)

$$a_{nwc2} = a_{dcv2n} - a_{scv2n} \quad (6.21)$$

Step 5: calculate the result of wear changes U_{wc2} (as provided in **Figure 6-11**):

$$U_{wc2=}a_{wc2} - a_{nwc2} \quad (6.22)$$

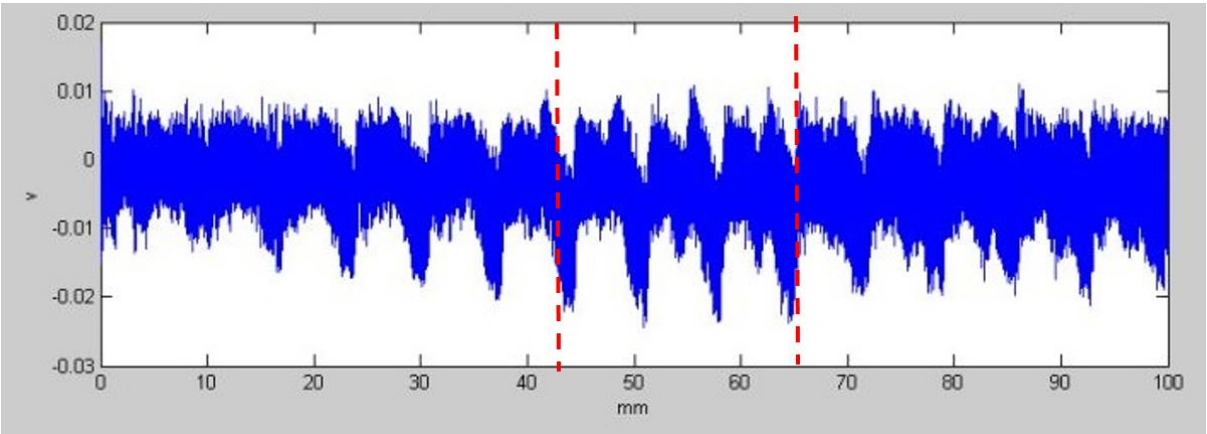

Figure 6-11 Wear Changes U_{wc2}

Step 6: repeat the calculation from step1 to step5 on shaft No.3 data, then calculate the result of wear change U_{wc3} (as provided in **Figure 6-12**):

$$U_{wc3=}a_{wc3} - a_{nwc3} \quad (6.23)$$

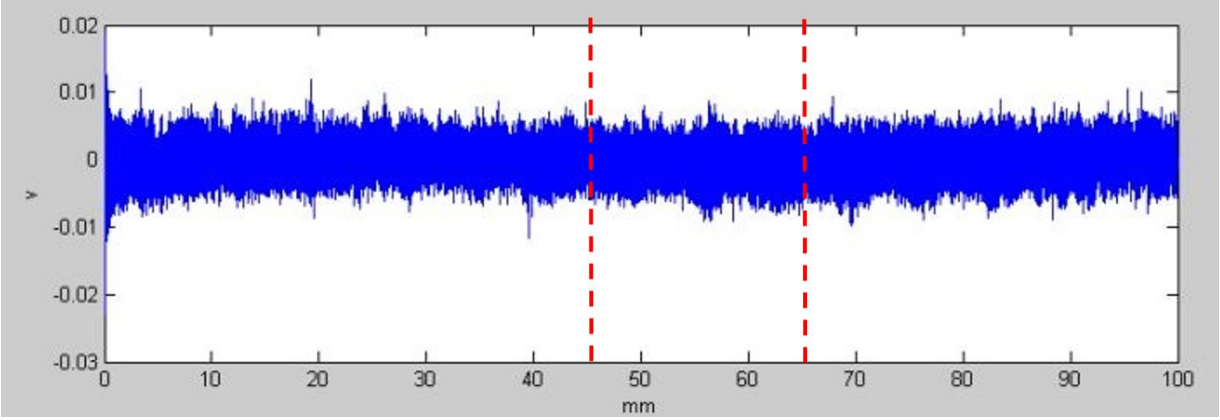

Figure 6-12 Wear Changes U_{wc3}

6.3.3 Wear Symptom (2): Smooth Curve Increase Monitoring Test

Step 1: calculate the root-mean-square of capacitance probe static from No.2to No.5 files:

Taking the five times measured data from shaft No.2 which the wear has made, as example, assuming each value of the capacitance probe static is a_{sp1}, a_{sp2}, a_{sp3}, a_{sp4}, a_{sp5}, thenthe average of the value is a_{scv2}:

$$a_{sp2} = \sqrt{\frac{a_{sp1}^2+a_{sp2}^2+a_{sp3}^2+a_{sp4}^2+a_{sp5}^2}{5}} \tag{6.24}$$

Assuming each value of the capacitance probe dynamic is a_{dp1}, a_{dp2}, a_{dp3}, a_{dp4}, a_{dp5}, then the average of the value $a_{dpv2}$is:

$$a_{dpv2} = \sqrt{\frac{a_{dp1}^2+a_{dp2}^2+a_{dp3}^2+a_{dp4}^2+a_{dp5}^2}{5}} \tag{6.25}$$

Step 2: Same solution to the data of No.2 shaft without wear, the average of capacitance probe static and dynamic are (in the following formula, a_{spv1n} is the average of the 5 times capacitance probe static data, from $a_{sp1n}$to a_{sp5n}; , a_{dpv1n} is the average of the 5 times capacitance probe dynamic data, from $a_{dp1n}$to a_{dp5n}):

$$a_{spv2n} = \sqrt{\frac{a_{sp1n}^2+a_{sp2n}^2+a_{sp3n}^2+a_{sp4n}^2+a_{sp5n}^2}{5}} \tag{6.26}$$

$$a_{dpv2n} = \sqrt{\frac{a_{dp1n}^2+a_{dp2n}^2+a_{dp3n}^2+a_{dp4n}^2+a_{dp5n}^2}{5}} \tag{6.27}$$

Step 3: calculate the result without the noise to No.2 shaft, a_{wp2}:

$$a_{wp2} = a_{dpv2} - a_{spv2} \tag{6.28}$$

Step 4: calculate the result to No.2 shaft without the noise and wear (data in the repeatability & reproducibility file)

$$a_{nwp2} = a_{dpv2n} - a_{spv2n} \tag{6.29}$$

Step 5: calculate the result of wear changes U_{wp2}(as shown in the following Figure 6-13:

$$U_{wp2=}a_{wp2} - a_{nwp2} \tag{6.30}$$

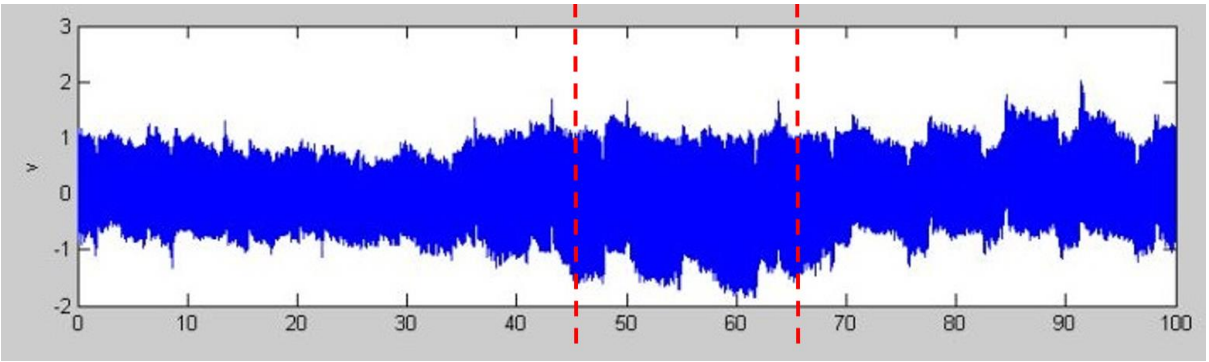

Figure 6-13 Wear Changes U_{wp2}

Step 6: repeat the calculation from step1 to step5 on shaft No.3 data, then calculate the result of wear change U_{wp3}(as shown in the following Figure 6-14:

$$U_{wp3=}a_{wp3} - a_{nwp3} \tag{6.31}$$

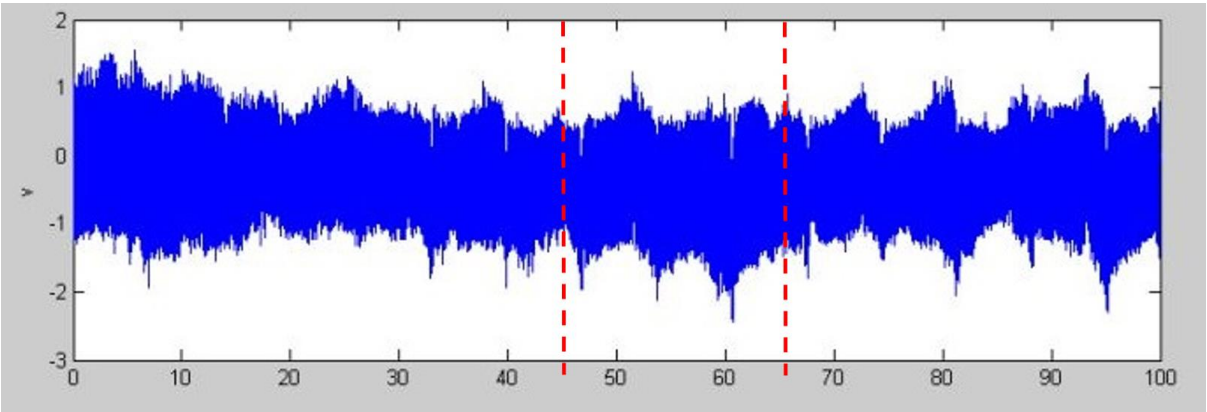

Figure 6-14 Wear Changes U_{wp3}

6.3.4 Wear Symptom (3): Small Range Vibration Monitoring Test

Taking the accelerometer data from shaft No.4, repeat the work in 6.3.2.1 to calculate the result of wear from bearing balls, then the result of wear change $\mathrm{U_{wp4}}$ (as shown in the following **Figure 6-15**:

$$U_{wp4=}a_{wp4} - a_{nwp4} \tag{6.32}$$

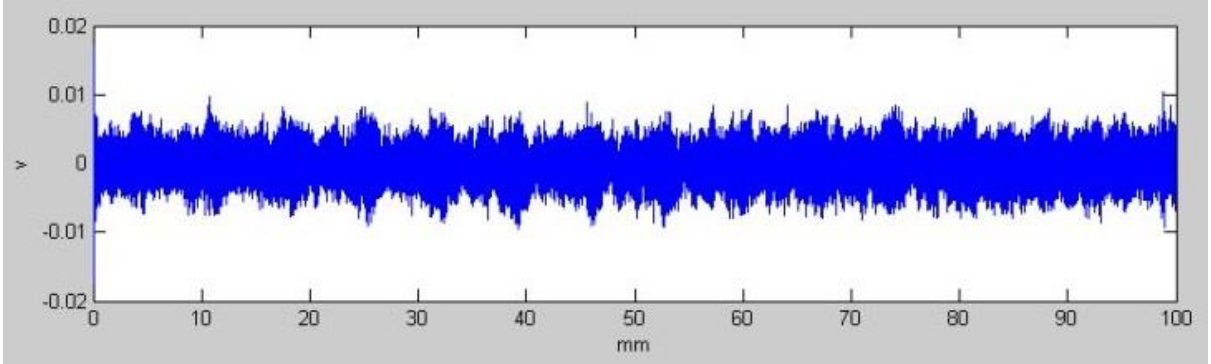

Figure 6-15 Wear Changes $\mathrm{U_{wp4}}$

6.3.5 In-process Monitoring Performance Conclusion

Whether the approach of in-process monitoring is applicable, mainly depends on two parameters:

1. the change of data on wear section is observable;
2. the changing amplitude is in accordance with the wear depth, after transferring;

The following is the conclusion of the hypothesis.

6.3.5.1 Static Performance

According to the result of static monitoring performance, there are two things can be concluded:

1. There is no phase difference that can impact the data accuracy in the settled sampling frequency, referring to the response of the pair of sensors to outer disturbance.
2. The difference between the static and dynamic signal is no more than 1.5% of the average, which means the noise and disturbance offset solution is reliable.

Above all, the static monitoring test result is supportive of the in-process monitoring approach.

6.3.5.2 Wear Symptoms (1) Monitoring Performance

In the experiment design part, the 20mm wear section is in the middle of running area (40 to 60 mm section). The expected symptom is vibration signal increases in the particular area.

In the result, it is observable that shaft No.2 has signal amplitude increase in the wear section. However, in the result of shaft No.3, there is no signal change can be observed at all, the surface of the shaft performs better comparing with the pristine condition.

The reason could be the utilisation of high grit emery paper: The emery paper selected in the experiment can reach to 3000 grit, which is even smoother than pristine shaft surface. It is similar to the running process of CNC machine newly applied.

Meanwhile, the acquired result needs to have a further study, to get more information about wear degree.

6.3.5.3 Wear Symptoms (2) Monitoring Performance

As can be seen from the result, both No.2 and No.3 shafts' signal amplification can be observed. On shaft No.2, the signal increases from -0.8 to -1.8, the difference 1V which transfers to depth is 25.4μm. On shaft No.3, the signal increase from -1.5 to -2.2, the difference 0.7V which transfers to depth is 17.8μm.

Therefore, the calculated result shows that the monitoring solution is applicable and can observe the wear as expected. The accuracy of the monitoring result requires further improvement.

6.3.5.4 Wear Symptoms (3) Monitoring Performance

The data from the test on shaft No.4 does not show clear frequency change caused by the wear on bearing balls. The reason can be:

1. the wear of ball bearing has no, or limited, impact on the performance of the CNC machine guiderail;
2. the high frequency caused by the wear has low amplitude and cannot be observed in the time domain;

Therefore, whether there is the existence of high frequency signal caused by the wear of bearing balls, still needs a further test.

7 CONCLUSION

In this part, the conclusion to the calculation result illustrated in the data analysis part is represented. The whole thesis provides complete design and experiment process for the validation of the guiderail wear in-process monitoring system

7.1 The Categorisation to the CNC Machine Guiderail wear

In the thesis, according to the literature review, the five major types of the wear happening on the CNC machine is illustrated and the major one called friction fatigue wear is selected as the study object in the whole thesis. The mechanism, effect and especially the symptom of the wear are all analysed and systematically concluded.

7.2 Requirement of the Project

After the analysis to the choose type of wear, friction fatigue wear, the requirement based on the symptom is represented. The requirement content includes the following factors which are importance to the further designing:

1. level of accuracy the monitoring system shall reach (among each particular type of the sensor)
2. draft scale of the experiment rig
3. physical requirement to sensors
4. DAQ approach and sampling frequency
5. Driving system parameter calculation
6. Importance to the uncertainty analysis
7. Novelty of the thesis: In-process monitoring approach

7.3 Designing of the Rig and the Experiment Process

7.4 Contribution to New Knowledge: In-process Monitoring Approach

According to the literature review and proper designing, the definition to the “in-process”, the solution of realisation and component selection are all specifically

illustrated in the thesis. It also includes the consideration of sensor, systematic calculation on the sensor parameter, further data calculation. Above all, the uncertainty brought into the result is systematically calculated .

As can be concluded from the result discussion, the in-process wear monitoring solution gets more optimistic result from accelerometers. The change of the signal altitude can be observed clearly and the position signal is corresponded to the position of the wear on the test shaft. Then, according to such approach, the depth of the wear can be transferred and calculated referring to the data of the result.

8 DIRECTION OF FUTURE WORK

As concluded from the previous design, the past two symptoms of the three can be monitored by the system in such an in-process solution. However, the repeating vibration caused by bearing balls' wear is not able to be observed in such approach and might need further study on both the symptom and the monitoring solution. The following aspects are the plan of future work on the theory.

8.1 Improvement of Repeatability

The repeatability of the test tells that the repeatability is over that 10% each time and if unexpected thing happens, it may reach to over 100%. Therefore, the improvement on test repeatability is crucial.

8.2 Test of Reproducibility

Another important case in evaluating the performance of the system is reproducibility which means how stable the system works in different conditions. The test needs to be:

1) Reproduced in difference areas;
2) Reproduced by different operators,
3) Reconstructing the components;
4) Reproduced with the revising of parameters

The aim is to prove that the result of the experiment is reproducible and credible.

8.3 Improvement to the range of application

After complete verification of the hypothesis, the applicability of the product is another factor that shall consider. It shall be verified by each type of CNC machine widely used in the industry and also applied on each typical guiderail with different wear types.

8.3.1 Applicability to different types of CNC machine

The following are types of CNC machine which the monitoring system shall be applied on:

1) gantry milling machine;
2) floor milling machine;
3) C-frame milling machine;
4) box milling machine;
5) turret milling machine;
6) bed milling machine;

8.3.2 Applicability to different types of guiderail

The following are types of guiderails widely applied in the CNC machine besides the round guiderail:

By working mechanism:

1) sliding contact guiderail;
2) aerostatic linear guiderail;
3) hydrostatic linear guiderail;

By component cross-section shape:

1) triangle guiderail;
2) rectangular guiderail;
3) dovetail guiderail;
4) multiplex guiderail.

8.3.3 Applicability to other types of machine wear

The following are the other types of wear which can be tested with the in-process hypothesis:

1) grinding abrasion;
2) corrosive wear;
3) rusty wear;
4) fretting fatigue wear.

The next step of the wear monitoring study shall focus on testing if the methodology applies those different types of wear. It is the key point to approve that if the hypothesis is applicable. The approach of the test would be following:

1) study and conclude the phenomena, effect and symptoms of the wear;
2) Select the proper solution in the experiment to monitor the wear symptom and capture the signal;
3) Use the in-process monitoring solution to adopt the signal to carry out the result for approving.

REFERENCES

Heisel, U. Koscsák, G. Stehle, T (2004). Thermally induced positioning errors of feed drives by example of a ball screw. 55(1) 423–426.A12

Angus, H, T. (1957/58) The Wear of Cast Iron Machine Tool Slides,Shearsand Guideways. Wear VOL. 1.

Besharati, SR. Dabbagh, V. Amini, H. (2016), Multi-objective selection and structural optimization of the gantry in a gantry machine tool for improving static, dynamic, and weight and cost performance. *Concurrent Engineering: Research and Applications* Vol. 24(1) 83–93

Bosetti, P. Bruschi, S. (2010) In-line Monitoring of Cut Surfaces in Interrupted Machine Operations. Int J Mater Form Vol. 3 Suppl 1:487– 490

Brocard, M. Farcy, A. Le Maître, P. (2014) RF characterization of the substrate coupling noise between TSV and active devices in 3D integrated circuits. Microelectronic Engineering, 130:74-81

Bronckers, S. Geert, V. der P, Vandersteen, G, and Rolain, Y. (2010) Substrate Noise Coupling Mechanisms in Lightly Doped CMOS Transistors. IEEE TRANSACTIONS ON INSTRUMENTATION AND MEASUREMENT, VOL. 59, NO. 6.

BS ISO 230-2: (2014). Test code for machine tools Part 2: Determination of accuracy and repeatability of positioning of numerically controlled axes. BSI Standards.

BSI Standards Limited, (2014). BS ISO 230-2:2014 Test code for machine tools. Determination of accuracy and repeatability of positioning of numerically controlled axes. *BSI Standards Limited.*

BSI Standards Limited. (2012). BS 4656-4:1971 Specification for the accuracy of machine tools and methods of test. Milling machines, bed type, horizontal or vertical spindle. BSI Standards Limited

Danford, Matthew D. CNC Package For Knee Mills (2007), *Modern Machine Shop*., Vol. 79 Issue 12, p260-262. 2p. 2

Deng, Y. Jin, X. Zhang, Z. (2015) A macro–micro compensation method for straightness motion error and positioning error of an improved linear stage. *Int J Adv Manuf Technol* 80:1799–1806

Eric, N. Simons. (1972) Metal Wear- A Brief Outline. *Frederick Muller Limited*.

Fan, K., Chen, H., & Kuo, T. (2012). Prediction of machining accuracy degradation of machine tools. *Precision Engineering*, Vol 36:2, pp. 288-298.

Fitch, B. (2013). Anatomy of Wear Debris. *Machinery Lubrication*

Giourntas, L. Hodgkiess, T. Galloway, A.M. (2015) Enhanced approach of assessing the corrosive wear of engineering materials under impingement. Wear 338-339155–163

Girardin, F., D. Remond and J.F. Rigal, (2010). Tool wear detection in milling: An original approach with a non dedicated sensor. *Mech. Syst. Signal*. Pr., 24: 1907-1920.

Gorasia, J. (2009) Structural Design of a Desktop CNC Mill. *Mechanics of Solids and Structures Spring*.

Y, Hongxiang. X, Mengchen. Z, Jie (2015) In-situ Roundness measurement and Correction for Pin Journals in Oscillating Grinding Machines. *Mechanical Systems and Signal Processing* 50-51548–562

Hung, J. P. (2009) Load Effect on the Vibration Characteristics of a Stage with Rolling Guides. *Journal of Mechanical Science and Technology* 23 89~99

Kamalzadeh, A. Daniel, J, Gordon. (2010) Erkorkmaz, K. Robust compensation of elastic deformations in ball screw drives. *International journal of Machine Tools & Manufacture* 50 559–574

Kong, L.B. Cheung, C.F. (2012) Prediction of surface generation in ultra-precision raster milling of optical freeform surfaces using an Integrated Kinematics Error Model. *Advances in Engineering Software*., Vol. 45 Issue 1, p124-136.

Leonardo, D, V.Stredná,P & škola, S. (2011),CNC MODULE. *Secondary Mechanical Engineering School*.

Lin, Y., Wang, S., & Wu, K. (2003). The wear behaviour of machine tool guideways clad with W-Ni, W-Co and W-Cu using gas tungsten arc welding. Surface and Coatings Technology, Vol 172:2-3, pp. 158-165.

Lion Precision. (2015) Capacitive Sensor Operation and Optimization.

Lou, S.J. Chen, J.C. (1997). In-process surface recognition of a CNC milling machine using the fuzzy nets method. *Computers & Industrial Engineering*. Vol. 33 Issue 3/4, p401

Luo, Y., (2004). Parametric tool wear estimation solution of HSC appropriate machining*. Int. J. Adv. Manuf. Technol*., 23: 546-552.

Majda, P. (2012) Modeling of geometric errors of linear guideway and their influence on joint kinematic error in machine tools. *Precision Engineering* 36 369– 378

Nallasamy, P., Saravanakumar, N., Nagendran, S., Suriya, E., & Yashwant, D. (2015). Tribological investigations on MoS2-based nanolubricant for machine tool slideways. *J Engineering Tribology*, Vol. 229(5), pp. 559–567.

Nanfara, F. Uccello, T. Murphy, D. (2002), The CNC workshop, Prentice-Hall.

Qianjian, G, Shanshan, Y and Lei, H.(2014) Research on Tool Wear Monitoring Method based on Project Pursuit Regression for a CNC Machine Tool. Res. *J. App. Sci. Eng. Technol*., 7(3): 438-441.

Rabinowicz, E. (1965)Friction and Wear of Materials. *New York: John Wiley & Sons*.

Ratnam, M.M. and Shahabi, H.H. (2008) On-line monitoring of tool wear in turning operation in the presence of tool misalignment. *Int. J. Adv. Manuf. Technol*., 38: 718-727.

Slocum, A. Fundamentals of Design Error Budget. (2012) *Massachusetts Institute of Technology*.

Sparham, M. Sarhan, A. A. D & N. A. Mardi & M. Hamdi. (2014) Designing and manufacturing an automated lubrication control system in CNC machine tool guideways for more precise machining and less oil consumption. *Int J Adv Manuf Technol* 70:1081–1090

STAR CNC Machine Tool Corp. (2011). Large-Capacity Multi-Turret for Complex Jobs, Star CNC Machine Tool Corp., Booth 1118. *Production Machining.* Vol. 11 Issue 5, p52-52. 1/4p. .

Sutar, M, D. Deshmukh, B B. (2013) Linear Motion Guideways – A Recent Technology for Higher Accuracy and Precision Motion of Machine Tool *International Journal of Innovations in Engineering and Technology (IJIET)* Vol. 3 Issue 1

T, Yanqing. Z, Lianhong & H, Yahui (2015) A Wear Model of Plane Sliding Pairs Based on Fatigue Contact Analysis of Asperities, Tribology transactions, 58:1, 148-157, DOI: 10.1080/10402004.2014.956907

Tan, Y., Zhang, L., & Hu, Y. (2015). A Wear Model of Plane Sliding Pairs Based on Fatigue Contact Analysis of Asperities. *Tribology Transactions*, Vol 58:1, pp. 148-157

Technical Documentation. (2010), HURON company.

U, Heisel. G, Koscsak. T, Stehle, (2006) Thermography-based investigation into Thermally Induced Positioning Errors of Feed Drives By Example of a Ball Screw*. CIRP Annals - Manufacturing Technology 55(1):423-426*

Vacharanukul, K. Mekid, S. (2008) New real-time non-contact probe using Gaussian convolution smooth technique for in-process inspection. *In Sensors & Actuators: A. Physical*. 141(1):20-28.

Vi´afara, C.C, Castro, M.I. V´elez, J.M, Toro, A. (2005) Unlubricated sliding wear of pearlitic and bainitic steels. *Wear* 259 405–411

Waterhouse, R, B. (1972). Fretting Corrosion. *Pergamon Press*.

Wei, H. Li, Y & Lee, Y.(2010) Interfacial Fracture Analysis of a Semicircular Cylindrical Guide Rail. *Mechanics Based Design of Structures and Machines*, 38: 190–203

Wu, F. Qiao, L. Xu, Y. (2012) Deformation Compensation of Ram Components of Super-heavy-duty CNC Floor Type Boring and Milling Machine. *Journal of Aeronautics* 25(2):269-275.

Wu, J, S. Changa, J, C, Hungb J, P. (2009). The effect of contact interface on dynamic characteristics of composite structures. *Journal of Mechanical Science and Technology*. 23 89~99